Institut für Physik

Arbeitsgruppe Nichtlineare Dynamik

Population dynamics in theory and experiment:

An investigation of species interactions

on different scales of complexity

Dissertation
zur Erlangung des akademischen Grades
"*doctor rerum naturalium*"
(Dr. rer. nat.)
im Fach Physik / Nichtlineare Dynamik

eingereicht an der
Mathematisch-Naturwissenschaftlichen Fakultät
der Universität Potsdam

von
Lars Rudolf

Potsdam, den 14.August 2008

Contents

Chapter 1

General Introduction

1.1 Background

Undoubtedly the growing population causes an increasing human impact on the environment. As a result, anthropogenic habitat change or destruction, overexploitation, climate change, and bio-invasions influence ecosystem functioning and cause the largest species mass extinction in the history of earth. However, we are embedded in this web of life and therefore dependent on our environment. Thus, any environmental change may cause critical economical and social problems. Furthermore, there is a feed back of the web of life to the abiotic environment and the influence of ecological systems, e.g. on the atmospheric carbon dioxide or the albedo, may cause subsequent changes. Thus, in the past decades, there has been an increasing concern about the impact upon human dependency on the ecological environment. The understanding of the processes and the underlying dynamics is one of the most pressing question faced by humanity (Levin , 1999).
The ecological environment is highly diverse and complex. Therefore understanding of its processes and dynamics is non-trivial. On large scales one can find a multitude of different populations interacting in a complex web. The population dynamics on such webs can be stationary, oscillatory or chaotic, while the interactions can be cooperative, competitive or predative. The interactions themselves are a result of the interplay between individuals and, therefore, even the understanding and description of a single interaction between two species is typically not trivial. Finally, also on the individual level the complex physiological and behavioural processes are often not fully understood and still object of ongoing research. The non-trivial nature of our ecological environment on the one hand and the necessity to understand the consequences of the environmental change, on the other hand, are motives

for an increasing scientific interest, at all scales of observation. Also, the understanding of the ecological environment on different levels of abstraction will be the focus of that work.

1.2   Fundamental notions in Ecology

One-species population growth

Although the environmental problems strongly encouraged the research in the last decades, the ambition to understand our ecological environment is much older. One of the first known mathematical descriptions of a single population growth was recorded by Fibonacci (1202). In this theoretical work he assumed for a idealised rabbit population, an increasing growth, which produces an increasing sequence of population numbers in time, today known as "Fibonaccis numbers". Later, in a comprehensive study about population growth, Malthus, T.R. (1826) states a general exponential nature of population growth, which corresponds to a doubling of the population number in a finite time. Indeed, exponential growth is a good model for population dynamics on short time scales. However eventually limiting factors set in and cause a divergence from the exponential trajectory. To model saturation effects, Verhulst (1838) extended the exponential growth model by a carrying capacity, which is the number of individuals that a system can support. This, so-called logistic equation, predicts exponential growth for sufficiently small populations, but leads to an asymptotic convergence to a fixed carrying capacity for larger populations. This basic model, is a good first-order approximation of many growth processes; a common, accepted standard model in ecology; and often the first basic component in more complex models.

Horizontal species interaction - Competition

Explaining the dynamic, processes and consequences of species interactions is one central goal in ecology and especially the competition between species for resources or niches is a topic of ongoing scientific debates. Already Naegeli (1874) and Grinnell (1904, 1917) described competing species and the possibility of a competitive exclusion of species. To formalize species competition, Volterra (1928) extended the logistic equation by species interaction terms and showed mathematical the competitive exclusion of one species by another. Gause (1934) provided evidence for a competitive exclusion of species in experiments and stated that two similar species cannot indefinitely survive

on just one limiting resource. A more general formulation of this observation states, that the number of species that coexist indefinitely, cannot exceed the number of niches in a system (Levin , 1970). This is one of the fundamental concepts in ecology: "The competitive-exclusion principle" (Hardin , 1960). Even if the competitive-exclusion principle is one of the most striking theorems in ecology, it is rarely observed in nature and many biological communities seem to violate it. One famous example is the paradox of plankton (Hutchinson , 1961). Typically in aquatic ecosystems a large number of different phytoplankton species coexist on a small number of available resources. A significant amount of research was done to understand this phenomenon. Several studies hypothesise, that for phytoplankton external factors, like selective predation, spatial heterogeneity or environmental fluctuations, may explain the paradox of plankton (Richerson et al. , 1970; Levins , 1979; Sommer , 1985; Padisak et al. , 1993). Other authors hypothesised that inherent system properties may allow a coexistence of more species than limiting resources. In a theoretical investigation Armstrong & McGehee (1980) were able to construct examples of two species coexisting on one resource. Extending this approach, Huisman & Weissing (1999) showed, by standard models of competitive exclusion, that competitive interactions which generate oscillations and chaos may allow the coexistence of many species on a handful of resources. Nevertheless, even if this approach give possibility of coexistence of more species then resources, and therefore a possible explanation for the paradox of plankton, this mechanism has never been observed in nature. Thus, despite intense research there is still no satisfactory and broadly accepted solution to the paradox of plankton.

Specific characteristics of competition in aquatic ecosystems

Environmental conditions are one major factor which decide the outcome of species competition. In aquatic ecosystems commonly the environment exhibits little variation on the horizontal axis, while one finds strong gradients in the vertical direction. Especially growth limitation by light, supplied from above, and nutrients, often supplied from below, are one fundamental mechanism for the phytoplankton dynamics, governing the outcome of competition. The growth limitation by light often leads to a phytoplankton maximum in the upper layers of the water body. However, in nutrient poor waters, the lack of nutrient in the upper layers, may force the phytoplankton distribution towards deeper layers. The resulting, so-called deep chlorophyll maximum, is a common phenomenon in aquatic ecosystems and has a strong impact

on phytoplankton competition. Usually it is assumed, that the realisation of either a deep or an upper chlorophyll maximum is solely determined by the environmental conditions. However, recent field investigations (Venrick , 1993; Holm-Hansen & Hewes , 2004) pointed out, that both patterns can appear under similar conditions. Another component in aquatic ecosystems with influence on species competition is a so called upper mixed layer. Here, external mechanical forces, e.g. wind, impede the stratification of the water body close to surface, which results in a highly mixed layer of a certain depth. The spatial varying environment and its influence on phytoplankton dynamics and competition were studied in a series of modelling investigations (Huisman & Weissing , 1995, 1999; Klausmeier & Litchman , 2001; Diehl , 2002; Fennel & Boss , 2003; Hodges & Rudnick , 2004; Huisman et al. , 2006). Starting from these works one part of this thesis investigate the appearance of upper or deep chlorophyll maxima under the influence of an upper mixed layer and discuss their effects on phytoplankton competition.

Vertical species interaction - Predation

Beside competition, predation is certainly the most studied type of species interaction. The corresponding notion of predator-prey cycles is among the most fundamental phenomena in ecology. First mathematical description of the predator-prey concept were proposed independently by Lodka (1925) and Volterra (1926). Already these first basic modelling approaches showed self-sustained population cycles. One striking example for such population cycles is the Canadian hare-lynx cycle (Elton , 1942; Blasius et al. , 1999). Here, the oscillations tends to follow a tight rhythm with a period of about 10 years for more than hundred years. Understanding and explaining the causes of population cycles has been a central issue in ecology and over the past decades an extensive list of possible mechanisms have been cataloged (Berryman , 2002; Turchin , 2003). However, it is known that free-running oscillations in biological systems may break down after certain time, and besides the comprehensive theoretical study of predator-prey cycles, there is no experimental or field study which provides evidence for self-sustained predator-prey cycles for more than 20 cycles. In contrast to theoretical findings, predator-prey cycles in nature or experiments are often masked by noise and non-stationary dynamics and a distinction of predator-prey cycles from noise induced fluctuations may be not trivial. Therefore, a part of this thesis focus on an experimental study of predator-prey cycles and a time series analysis of the measured signals.
The notion of predator-prey cycles is related to another another fundamental concept in ecology, the so called paradox of enrichment. First noted

by Huffaker et al. (1963); Rosenzweig (1971), it states, that enrichment of available resources can have a destabilizing effect on population dynamics (Gilpin , 1972; Rosenzweig , 1977; May , 1987; Abrams & Roth , 1994; Rosenzweig , 1995). Thereby, steady states may becomes oscillatory and further enrichment may cause a rapid increase of the cycle amplitudes until extinction occurs (Cunningham & Nisbet , 1983; Pascual & Caswell , 1997). Nevertheless, even though the paradox of enrichment is well studied and understood in theory, there have bean few confirmations for "paradox" behaviour in real systems (Luckinbill , 1974; Tilman & Wedin , 1991), and a couple of experimental studies showed opposite results (McAllister et al. , 1972; McCauley & Murdoch , 1990; Kirk , 1998). Thus, the paradox of enrichment is another phenomena in ecology, which is well understood in theory, but becomes contradict by observational findings.

Multi species systems - food webs

Competition or predation among two species are key factors for the understanding of ecological interactions and the research of such simplified systems is an adequate and well established approach for the understanding of population dynamics. However, as species interact with a multitude of different species and are embedded in a diverse and complex web of interactions, the population dynamics in real food webs may differ from these findings. Therefore, the investigation of multiple interacting species and in particular food web stability is a major topic in population ecology. Ecological intuition as well as the first theoretical approaches (McArthur , 1955; Elton , 1958) predicted a high stability for complex webs, but since the seminal works of Robert May (May , 1971, 1972), in which he showed, that large, densely connected webs are in general unstable, there is an ongoing debate about the food web diversity and stability (King & Pimm , 1983; Cohen & Newman , 1985; McCann , 1998, 2000; Montoya et al. , 2002; Jansen & Kokkoris , 2003; Kondoh , 2003; Emmerson & Raffaelli , 2004; Navarrete & Berlow , 2006). To resolve this contradiction, it is necessary to find the special properties of real food webs, which give them there unusual stability. Most of the recent work on food web stability has focused on numerical modelling (Jansen & Kokkoris , 2003; Kondoh , 2003; Jonsson et al. , 2006; Uchida et al. , 2007; Garcia-Domingo & Saldaña , 2008). However, in these studies, numerical constraints limits the size of the food webs, whereas real ecosystems are commonly much larger and may therefore differ in its dynamics. Moreover, also the number of possible realisations of different food webs is limited in these approaches, which in turn strongly limits the parameter space that is studied. Recently generalised modelling, a novel numerical approach for the

analysis of the stability of families of non-linear rate equations resolve these constraints (Gross & Feudel , 2006). To extend the recent findings and to contribute to the understanding of the ecological environment on that scale of abstraction, in this thesis the generalized modelling approach is used for a comprehensive search for stability properties in food webs of different size and structure.

1.3 Survey of the included manuscripts

There are a couple of fundamental concepts provided from theoretical ecology, with no or weak support from field studies or experimental results. And despite intense research, there are still many open questions. To solve these problems, further field observations or laboratory experiments are necessary. As such measured signals often suffer from external perturbations and background noise, methods of time series analysis are necessary for their interpretation. These methods can thus provide additional insights into the dynamics. Also, further theoretical research is necessary, to improve ecological concepts and to close the gap between theory and observational findings. On this account, the three papers, included in this thesis, contribute to the understanding of population dynamics and species interaction on different scales of abstraction with an experimental study, a time series analysis and different theoretical investigations.

I. Long-term cyclic persistence and phase signature in an experimental predator-prey community

The focus of this manuscript are long term predator-prey oscillations in an experimental system. In order to study this predator-prey interactions for a preferably long time chemostat experiments were initiated. For the analysis and evaluation of the measured signals we use well-established wavelet methods. They provide time and scale decomposed information of the inherent cycles and provide insights into the correlation between the measured signals. Furthermore, using the wavelet method we calculate phase differences between the measured signals and give a phase difference fingerprint of our experimental predator-prey system. Finally, basic well established models are used to create surrogate predator-prey time series. This signals are analysed with the same method, to provide phase difference fingerprints of common predator-prey systems for a comparison with the measured signals.

Classification of the personal contribution:

The time series analysis of the measured time series was done by me.
The chemostat experiment were done in collaboration with Guntram Weithoff, Bernd Blasius and Ursula Gaedke.
The discussion and classification of the results were done in collaboration with Bernd Blasius, Guntram Weithoff, Gregor Fussman and Ursula Gaedke.

II. Bistability in the Distribution and Composition of Phytoplankton in a Water Column with Upper Mixed Layer

In this manuscript we studied the influence of an upper mixed layer on the phytoplankton distribution and competition. For this purpose, we implement an advection-reaction-diffusion model, which simulates the phytoplankton over a vertical water column under the influence of different mixing regimes and two limiting resources: light and a nutrient, provided from above and below respectively. One focus of that paper is the possibility and understanding of such bistable distributions, introduced by an upper mixed layer. The bistability will be shown in a single-species system and then further investigated in a multi-species system. The second focus of this work is the understanding of phytoplankton competition and coexistence under the given conditions. For this purpose, we simulate an ensemble of different competition scenarios of steady and oscillatory phytoplankton dynamics. Furthermore, we present a novel graphical approach for deducing the competition outcome.

Classification of the personal contribution:

The analysis, evaluation, discussion and classification of the results were done in collaboration with Alexey Ryabov and Bernd Blasius
The implementation of the model was done by Alexey Ryabov.

III. Importance of linking patterns and weak links for food web stability.

This manuscript focus on the analysis of food web stability. For this purpose, we use generalised modelling (Gross & Feudel , 2006), a novel numerical approach for the analysis of stability in families of non-linear rate equations, to analyse several billions instances of food webs of up to 50 species with non-linear interactions. This ensemble of food web topologies is generated by the niche model (Williams & Martinez , 2000), an algorithm which generates random food webs. In this way, we explore the stability of food webs in a large parameter space and analyse its dependence on topological properties and model parameters.

Classification of the personal contribution:

The implementation and numerical analysis were done by me.
The theoretical analysis was done in collaboration with Thilo Gross
The discussion and classification of the results were done in collaboration with Thilo Gross, Ulf Dieckmann and Simon Levin

Chapter 2

Articles

Long-term cyclic persistence and phase signature in an experimental predator-prey community

Lars Rudolf, Guntram Weithoff, Ursula Gaedke, Gregor Fussmann
and Bernd Blasius

to be submitted

Predator-prey cycles have fascinated ecologists for long times and rank among the most fundamental concepts in ecology. Not only are cycles predicted by the simplest ecological models but they also allow predator and prey populations to coexist indefinitely, despite the exploitative character of their interaction. While cycling populations never become extinct in theory, it remains an open question for how long cyclic dynamics can be self-sustained in simple, live communities. Field or laboratory observations have been restricted to a few cycle periods and experimental studies indicate that oscillations may be short-lived in the absence of external stabilizing factors. Here we present chemostat experiments with a prey, *Monoraphidium minutum*, and a predator, *Brachionus calyciflorus* in which population densities and life stage characteristics were measured under constant environmental conditions. We report a predator-prey time series of unprecedented length, with sustained oscillations for more than 50 cycles. Multivariate wavelet analysis of this and a second, slightly shorter time series reveal continuous oscillations in all measured signals during the whole experimental time. However the cycles undergo sudden shifts between two different dynamic regimes: regularly oscillating episodes with a clear, nearly constant, predator-prey phase lag are intersected by short time intervals of cycles without any significant phase relationship. The mutual phase differences between all measured time series can be compactly encoded in a single polar phase histogram, providing a fingerprint for the temporal succession of the community. Our results, which are supported by numerical simulations, establish the phase signature as a robust measure for identifying species interactions in dynamical systems and demonstrate the potential for infinite coexistence of predator and prey populations in a cyclic dynamic regime.

For a long time population biologists have been fascinated by the appearance of regular cycles in animal populations where population numbers are not stationary but undergo recurrent changes from one cycle to the next. Oscillating

population numbers are observed in a large range of communities in field data (Turchin , 2003) and in the laboratory (McCauley et al. , 1999; Ellner et al. , 2001; Fussmann et al. , 2000; Yoshida et al. , 2003). A survey of 700 long term animal population time-series concluded that one-third of all investigated time series shows cyclic dynamics (Kendall et al. , 1998). A prominent example istthe Canadian hare-lynx cycle (Elton , 1942; Blasius et al. , 1999). Understanding and explaining the causes of population cycles has been a central issue in ecology and over the past decades an extensive list of possible mechanisms have been cataloged (Berryman , 2002; Turchin , 2003). Cycles may originate either from external, periodically changing factors or they may be generated by delayed negative feedback related to the internal structure of the system, such as age structure or maternal effects. However, the most prominent mechanism for explaining cyclic dynamics is by "+/-" trophic interactions between populations of exploiter and exploited organisms, as may be realized, for example in the form of predator-prey, consumer-resource or host-parasite relationships. A mechanistic underpinning is provided by mathematical models, which give evidence that predator-prey systems are inherently prone to generate oscillations. Based on this congruence between field observations and ecological theory the notion of predator-prey cycles ranges among the most fundamental concepts in ecology.

Surprisingly, however, when going to actual population surveys, it is not clear how much of this is backed-up by direct observation of population processes. The lack of knowledge is partially due to the enormous length of animal population cycles, with periods of about ten years in North America and three to four years in Northern Europe (Berryman , 2002; Turchin , 2003). This clearly set strict limits on the number of observable cycles. The longest recorded free-running predator-prey time series have a length of about ten periods, whereas controlled manipulations have been restricted to short-term experiments lasting just one or two cycles. As another difficulty, any specific population of interest will be embedded in a complex environment of physical and ecological interactions, which often obscure the dominant mechanism which is driving the cycle.

To circumvent these problems, ecologists have resorted to laboratory investigations, where long-running experiments can be realised under strictly controlled conditions (Utida , 1957; Nichelson , 1957; McCauley et al. , 1999; Fussmann et al. , 2000; Ellner et al. , 2001; Becks et al. , 2005). In a recent study a complex plankton food web was cultured in a laboratory mesocosm for prolonged times of more than eight years (Beninca et al. , 2008). In these experiments intricate temporal structures, including chaotic dynamics, where observed, which however makes it difficult to identify simple predator prey signatures. In opposite, there has been a long tradition of experimental

studies trying to realise long-lasting oscillations in simple communities. In a seminal investigation by Utida (1957) population numbers of azuki been weevil *Callasobruchus chinensis* and its larval parasite *Heterospilus prosopidis* were recorded for a time span of about 20 cycles (Utida , 1957). However it was found that oscillations could not be sustained for the whole duration of the experiment. Instead "with the progress of the experiment the fluctuations diminished in violence and approached a relatively stable level or steady state" (Utida , 1957). This observation is paradigmatic for many other recent experimental studies, where it was observed that the cycles in closed laboratory predator-prey systems are short-lived and the populations reach extinction in experimental time scales (Nichelson , 1957; Holoyak & Lawler , 1996; Ellner et al. , 2001).

All these findings suggest that predator-prey systems inherently are not robust and may need stabilization by external factors such as spatial extension, outside immigration or external environmental perturbations (Holoyak & Lawler , 1996; Ellner et al. , 2001; McKane & Newman , 2005), and the question arises as to how long cyclic behavior can be sustained in simple predator-prey communities without the rhythm being re-initiated by the environment. To our knowledge such an upper limit of cycles, or any upper bound for such a limit, is not known while, on the other hand, there is no evidence, either from field observation or from experiment, that free running predator-prey oscillations can persist for more than about ten cycles. Here we report results about long-term experiments with an aquatic predator-prey food chain. Following Fussmann et al. (2000) in our experiments planktonic rotifers, *Brachionus calyciflorus* were cultured together with their prey, the unicellular green algae, *Monoraphidium minutum*, in a chemostat under constant environmental conditions. We report an exceptionally long predator-prey time series where sustained oscillations were maintained for the whole duration of the experiment (total number of measurements equals $N = 373$ days), lasting over 50 cycles and so five-fold extending the previously known maximal oscillation duration (Fig.1a). The experiments were reproduced with very similar results for a time span of > 20 cycles (see Fig.1 supplement). Note that in contrast to other recent experiments, in our system the oscillations could be maintained without spatial structure, immigration or external signals.

Since the measured signals show large variability we apply phase analysis. Phase analysis, to study predator-prey oscillations was introduced in Blasius et al. (1999) and relies on the fact that the regulatory dependence between state variables is often encoded in their phase relationship, while the amplitudes may be highly erratic and uncorrelated. It was shown that the wavelet method (Daubechies , 1992; Kaiser , 1994; Lau & Wen , 1995; Torrence &
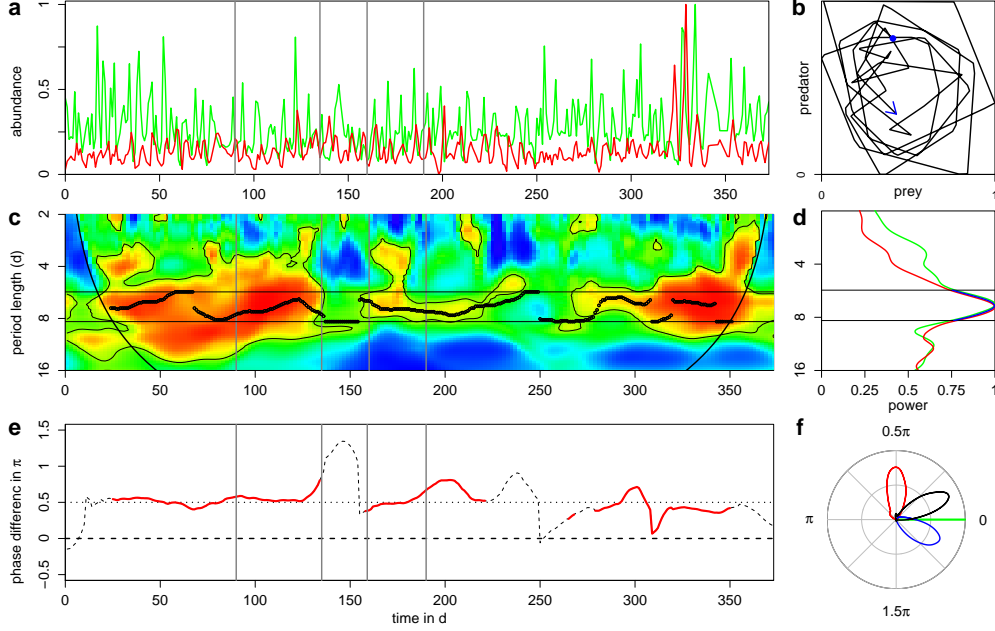
Figure 1: Analysis of the predator-prey time series. a.) Normalized time series of the predator, *Brachionus calyciflorus*, (red) and the prey, *Monoraphidium minutum*, (green). b.) Phase portrait of the prey-predator time series between days 90 and 135 (after smooth filtering). c.) Wavelet coherency (WCO) between the predator and prey signals, using a color coding from 0 (blue) to maximum (red). Significant areas are enclosed by thin solid line. The two horizontal lines indicate the frequency band $[s_1, s_2]$ and circles show the instantaneous oscillation period $\tilde{s}(t)$. Further indicated is the cone of influence. d.) Global wavelet power spectrum $P(s)$ for the predator (red) and the prey (green). e.) Phase difference $\theta(t)$ between predator and prey, significant relation between both signals is marked in red. f.) Circular distribution of the mutual phase difference to prey (indicated in green) for the predator (red), the predator egg-ratio (blue) and the abundance of egg bearing predators (black). For a better visualization we show the spline curve and applied a smooth filtering. The solid vertical lines indicate the time spans which are enlarged in Fig. 2.

Compo , 1998) is an especially powerful tool for extracting optimally resolved phase information from epidemiological and ecological time series (Grenfell et all. , 2001; Cazelles et al. , 2008; Keitt , 2008) and allows to quantify transient associations between two non-stationary time signals (Bandrivskyy et al. , 2003; Maraun & Kurths , 2004; Cazelles et al. , 2008). Applying wavelet analysis to our experimental time series (see methods) reveals continuous oscillations for both signals, during the whole experimental time, with a various amplitude and a slightly fluctuating frequency (Fig.5 supplement). Note the sharp maximum of the global wavelet power spectrum with a period length at $T = 6.9$ days in both experiments.

Even though the experiment was not perturbed by external influences the observed time series undergo marked differences in character. Thus, despite the persistent cyclic behaviour we are able to identify sharp transitions between time intervals of different dynamic regimes. For most of the time we observe oscillations with a clear, nearly constant, phase relationship, where the predator densities follow the prey availability with a phase lag of about $\pi/2$, in accord to what should be expected for classical predator-prey systems. In this regime, wavelet coherency confirms statistically significant coherent oscillations between both signals in a frequency band around the main oscillation frequency (Fig.1c). These times of regular oscillations are intersected by regimes, where the well-defined phase relationship between the measured signals is suddenly lost, only to be re-initiated shortly after without external influence. This shift between alternating dynamic regimes is exemplified in Fig.2 which shows an enlarged view on the signals in a typical time interval. One can clearly distinguish three sections with different dynamic behaviour (separated in the figure by vertical lines). The first time interval starting at day 90 shows a clear predator-prey cycle with a regular period length and a constant phase lag between prey and predator densities. These regular cycles are also reflected in the counterclockwise motion in the prey-predator phase plane (Fig.1b). However this regime of regular oscillations is suddenly intersected by a more disturbed time interval (in the range from day 135-160) where the dynamics becomes irregular. Even though the cycles do not break down and both prey and predators continue to oscillate in abundance, the period length becomes highly variable and the phase relationship between prey and predator is lost (see also phase portraits in Fig.6 supplement). Nevertheless, without external intervention, driven solely by the inherent dynamics of the system, the predator-prey signature is suddenly re-established around day 160.

The predator-prey phase difference over time (Fig.1e) and its distribution (Fig.1f) give further insight into the underlying dynamics. We find that in the time spans where the oscillations in both signals are significantly corre-
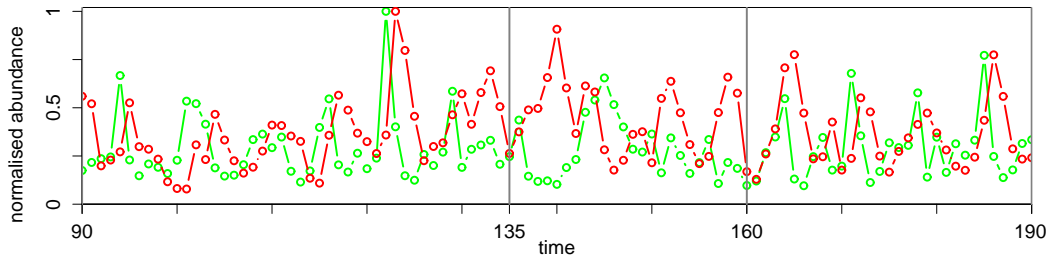
Figure 2: Enlarged view of the predator (red) and prey (green) time series in a time interval of 100 days. Vertical solid lines indicate time spans with different dynamic regimes: (day 90-135) clear predator-prey cylce with a constant phase shift of $\theta = \pi/2$, (day 135-160) out-of-phase oscillations, (day 160-190) spontaneous reinitiation of the regular phase-locked oscillations.

lated (marked as red, see methods), the phase difference between predator and prey is locked to a value around $\pi/2$ (see Fig.1e). The complex order parameter Eq.(7) has absolute value $R = 0.93$ and a mean phase $\bar{\theta} = 0.51\pi$. In contrast, during periods of no significant correlation (time spans of significant correlation are interrupted from day 135 to day 160 and from day 220 to day 270) the phases slightly decouple. Repeating the analysis for the measured density of egg-bearing predators and predator egg-ratio (i.e. the average number of eggs per female which provides a measure for the fertility of the population), we find again cycles which are correlated to the prey availability. The abundance of egg-bearing predators follows the prey cycles with a phase difference of $\bar{\theta} = 0.17\pi$ (absolute value of complex order parameter $R = 0.90$), whereas the egg ratio precedes the prey signal, resulting in a negative phase difference of about $\bar{\theta} = -0.14\pi$ (absolute value of complex order parameter $R = 0.90$).

Using this approach the mutual phase differences between all measured time series of our experimental community can be quantified and can be compactly visualized in a polar phase histogram (Fig.1f), which easily allows to read-off the temporal succession of the community during the cycle. The phase distributions remain largely unchanged for different values of the wavelet parameter ω_0 and for different wavelet functions. Further, as we find a similar phase signature for a second, shorter, experimental time series (see Fig.1 supplement), we assume the signature to be representative for our experimental system. Note that in the shorter time series the predator-prey relationship is hardly visible, whereas the phase fingerprint remains nearly unchanged in both time series - a fact, which underlines the robustness of the fingerprint. While most of the phase differences agree very well to what should be expected from ecological theory, phase relation may not be obvious at first

glance. For example we find that the predator egg-ratio precedes the phase of prey availability, which can only be understood by taking the predator life cycle into account (see below). This demonstrates that the angular phase histogram provides a characteristic fingerprint for the community structure of a given system.

Numerical simulations (see Supplement) support the phase signature and help to understand the origin for the counterintuitive phase distribution of the egg-ratio. Simulation with a non-stage-structured model revealed a consistent predator prey phase difference around 0.5π, however in contrast to the experimental data no phase lag between prey density and egg-ratio (Fig.3b). Simulations with a stage structured model reveal the impact of juvenile predators, which are unable to bear eggs, on the phase difference signature. Using the stage structured model we obtain a perfect agreement between the phase signatures of experimental and simulated data (Fig.3c). As the egg production is directly connected to food availability, one would expect a fast reaction of the egg-ratio to changes in prey availability, which would mean a small positive phase difference as they are found in the simulations without stage-structure. However, juvenile predators, unable to produce eggs, can have an important impact as they lead to an early breakdown of the egg-ratio maximum, caused by the multitude of non-egg-bearing juveniles during the prey maximum, and, therefore a negative phase difference between egg ratio and prey, in the range of -0.12π to 0 (see Fig.2 supplement).

Nonstationary dynamics on larger time scales were obtained by long time averaging of the wavelet coefficients, which reveals large fluctuations in the period length and oscillation amplitude on a time scale of about 50 days. These findings bear some similarity to the results by Utida (1957) who observed that fluctuations were damped after some periods, but "in the course of many generation this damping occurs repeatedly" and "After the populations passed through several tens of generations in a state of steady density, relatively violent oscillations suddenly recurred and were damped in their turn". These results lead to a dynamic view of ecological cycles, exhibiting different dynamic patterns at different time scales. Even though oscillations persist over the full length of the experiment (50 cycles), at an intermediate time scale of about 10 cycles the system undergoes sudden shifts between regimes where the oscillations of predator and prey are strongly phase locked and other, more perturbed, regimes where this phase-relationship is lost. Remarkably, the transition between these dynamics seems to arise spontaneous without external influence (self-sustained reorganization of the system). On a smaller time scale in the order of the period length of the system we observe stochastic changes in the amplitude from one cycle to the next, even
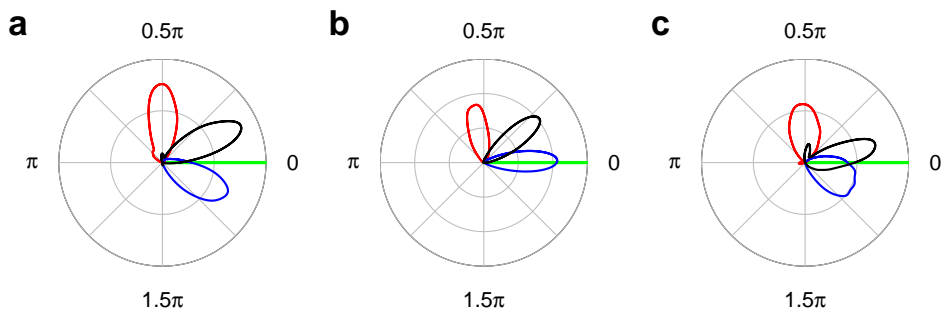
Figure 3: Comparison of laboratory and model phase signatures. Plotted is the circular distribution of phase differences to the prey (green) for the predator (red), predator egg-ratio (blue) and egg bearing predators (black). (a) Experimental results. The predator follows the prey with a phase difference of $\pi/2$, egg bearing animals are slightly delayed to prey availability, whereas predator egg ratio precedes prey abundance. (b) Simulations of a basic predator prey model reproduce quantitatively the time delay of predator and egg bearing predator abundance to prey availability, but fail to reproduce the phase of the egg ratio. (c) A model including juvenile predator live stages is able to reproduce the negative phase difference between egg-ratio to prey availability.

though the phase largely remains constant (Blasius et al. , 1999). Finally, on a time scale smaller than the period length of the system the oscillations are superimposed by stochastic perturbations.

We can only speculate about the origin of the sudden regime shifts in the dynamics. Even though the experiments were carried out under strictly constant conditions, we cannot exclude the possibility of small external perturbation (e.g., shifts in room temperature or light intensity) or other influences from maintenance, possibly even in a periodic (e.g. weekly) fashion, which might interfere with the ecological dynamics. bIt is also possible that rapid prey or predator evolution has influenced the ecological dynamics and contributed to the observed regime shifts (Yoshida et al. , 2003, 2007). However, we can think of no simple explanation how evolutionary change would lead to the observed pattern where predator and prey repeatedly abandon defined phase relationships and recur to them at later instances.

Our fast-reproducing algal-rotifer system allowed us to study community dynamics for more than 50 cycles. At the same time, we collected data on the age-structure of the predator population which helped us to perform a more revealing analysis of the dynamics than is possible for unstructured microbial populations. We showed that the experimental predator-prey cycles become manifest as a regular phase-locked succession, a pattern we were able to visualize as a community fingerprint. This allows to obtain valuable insights into the factors underlying the origin of the oscillations. Our approach clearly proofs the phase signature as a robust measure for identifying species interactions, community structure, and the regulatory dependencies between cyclic state variables in general.

Methods

Experiments.

A chemostat was set-up with a parthenogenetic, filter-feeding rotifer *Brachionus calyciflorus* as the predator and the unicellular alga *Monoraphidium minutum* as the prey under constant temperature ($23°C$) and permanent illumination. The chemostat vessel had a volume of 1.5 l and the experimental volume was 0.8 l. The chemostat was incoluated from stock cultures with *M. minutum* and after the algae had established, *B. calyciflorus* was added on day 10. The chemostat had a constant inflow of sterile medium with a rate of 0.55 per day using a peristaltic pump. The medium was a modified WC-medium after Guillard & Lorenzen (1972) with a reduced nitrogen content of 80 μmol l^{-1} nitrate as the limiting resource. A subsample of 8 ml

was taken daily to determine the abundance of both predator and prey. The algae were analysed with an electronic particle counter (Schärfe, Reutlingen, Germany), the animals were counted using an inverted microscope at 100-fold magnification (TSO-Thalheim, Pulsnitz, Germany). For the animals, the reproductive status was recorded i.e. the total number of subitaneous eggs and the number of egg-bearing females. No mictic females or males were observed throughout the experiment. The ratio of the total number of eggs and the number of females is the egg ratio which is a measure of the reproductive output of the population. The number of egg-bearing females is an indicator for the resumption of reproduction after a period of food limitation (the minimum of the prey abundance within a cycle).

Continuous wavelet transformation (CWT).

The wavelet transform $W(s,t)$ is calculated as the convolution

$$W(s,t) = \frac{1}{\sqrt{s}} \int \mathrm{d}t' \, x(t') \, \psi^* \left(\frac{t'-t}{s} \right),$$

(1)

('$*$' denotes the complex conjugate) of the signal $x(t)$ with a localized wavelet function $\psi(\tau)$ centered at time t and dilated by the factor s, here always taken from 256 uniform steps on a logarithmic scale. After decomposing the complex valued CWT into amplitude and phase $W(s,t) = |W(s,t)| \, \mathrm{e}^{\mathrm{i}\phi(s,t)}$ intuitively it can be understood as the extend $|W(s,t)|$ to which the signal $x(t)$ at local time t resembles an oscillation with period length s and phase $\phi(s,t)$.

We use the Morlet wavelet $\psi(\tau) = \pi^{-1/4} e^{i\omega_0 \tau} e^{-\tau^2/2}$ with $\omega_0 = 6$ so that the scale parameter can simply be interpreted as the period length of the oscillation (Torrence & Compo , 1998). Edge effects are minimized by applying zero padding to the next highest integer power of two. We always indicate the cone of influence, which marks the zone in the CWT which is effected by edge effect (Cazelles et al. , 2008; Maraun & Kurths , 2004; Torrence & Compo , 1998). Since the CWT, as a map from a one-dimensional signal to a two-dimensional time-scale representation, does not produce any new information, the wavelet coefficients are highly redundant, leading to the appearance of smooth patterns, that may suggest structures which are just coincidences. The width of the cone of influence provides a rough approximation to the minimal extension of a feature at a given scale in order to represent genuine cyclical behavior.

The local wavelet power spectrum (WPS) at time t and scale s is given as $WPS(s,t) = W(s,t) \, W^*(s,t)$. The global wavelet powerspectrum, defined

as the time average of the WPS

$$P(s) = \langle WPS(s,t) \rangle, \tag{2}$$

and measures the averaged variance of the signal at scale s (Cazelles et al. , 2008).

Bivariate wavelet analysis.

To quantify the statistical relationship between two nonstationary signals $x(t)$ and $y(t)$, the wavelet cross spectrum (WCS) is defined as the product of the corresponding wavelet transforms

$$WCS^{x,y}(s,t) = W^x(s,t)\, W^y(s,t)^*. \tag{3}$$

After decomposition into amplitude and phase $WCS(s,t) = A(s,t)\, \mathrm{e}^{\mathrm{i}\Delta\phi(s,t)}$ the phase describes the delay $\Delta\phi(s,t) = \phi^x(s,t) - \phi^y(s,t)$ between the two signals at time t and scale s, whereas the amplitude $A(s,t)$ expresses the covarying power of two processes.
The WCS is not specific because it exhibits high values when either a true covariance exists or one of the spectra exhibits a high value. A scale and time resolved measure for the interrelation between the two signals is given by the normalized wavelet coherency (WCO)

$$WCO(s,t) = \frac{|\langle WCS(s,t)\rangle|}{\langle W^x(s,t)\rangle^{1/2}\, \langle W^y(s,t)\rangle^{1/2}} \tag{4}$$

where "$\langle\rangle$" denotes a smoothing operator in the scale-time plane (Torrence & Compo , 1998; Maraun & Kurths , 2004; Cazelles et al. , 2008). Here, smoothing in scale direction was obtained by averaging over a constant window of 0.5 octaves on a logarithmic scale. For smoothing in time direction we used a scale-dependent window of size $6s + 1$, corresponding to three periods in each direction (Maraun & Kurths , 2004).
Following Maraun & Kurths (2004), to assess the statistical significance, we simulated 10000 realizations of two independent Gaussian white noise processes, and assume two signals to be significant correlated, for such time and frequency values, where the WCO-correlation coefficient is above a significance level of 0.917 corresponding to a 95% critical value.

Phase signature of community succession.

Assume that two signals $x(t)$ and $y(t)$ oscillate with a common but non-stationary period length $\tilde{s}(t)$. Here we define $\tilde{s}(t)$ as the scale at time t

having the maximal wavelet cross spectrum over all scales in a prefixed band $[s_1, s_2]$ (Bandrivskyy et al. , 2003)

$$\tilde{s}(t) = \max_{s_1 < s < s_2} WCS(s, t). \tag{5}$$

The upper and lower frequency band boarders s_1 and s_2 are taken according to values where the wavelet power $P(s)$ is reduced to a factor of 0.95. These values $s(t)$ define a line of the strongest co-oscillating components. Inserting this line in the WCS we obtain the phase difference $\theta(t)$ between the two signals at every time instance

$$\theta^{x,y}(t) = \phi^x(\tilde{s}(t), t) - \phi^y(\tilde{s}(t), t). \tag{6}$$

For statistical analysis only such values are taken into account which are located inside the cone of influence and inside the statistically significant areas in the WCO (indicated as red lines in Fig.1e).
The significance can be computed with the complex order parameter

$$Re^{i\bar{\theta}} = \frac{1}{N} \sum_k e^{i\theta_k}. \tag{7}$$

Here the angle $\bar{\theta}$ indicates the mean phase difference between the two signals and the absolute value $0 \leq R \leq 1$ measures the strength of the peak. The angular deviation of the distribution is defined as $\sigma = \sqrt{2(1 - R)}$. To verify if the distribution has a mean distribution can be verified with the Rayleigh test. We calculate $z = NR^2$, where N is the number of data points.

Simulation analysis.

Our model is given as a system of nonlinear differential equations (see supplementary information for model equations and parameter values). The model is based on a standard chemostat model (Fussmann et al. , 2000) and describes the state variables: limiting nutrients, algal abundance and either rotifer abundance or, as an extension, various rotifer life stages.
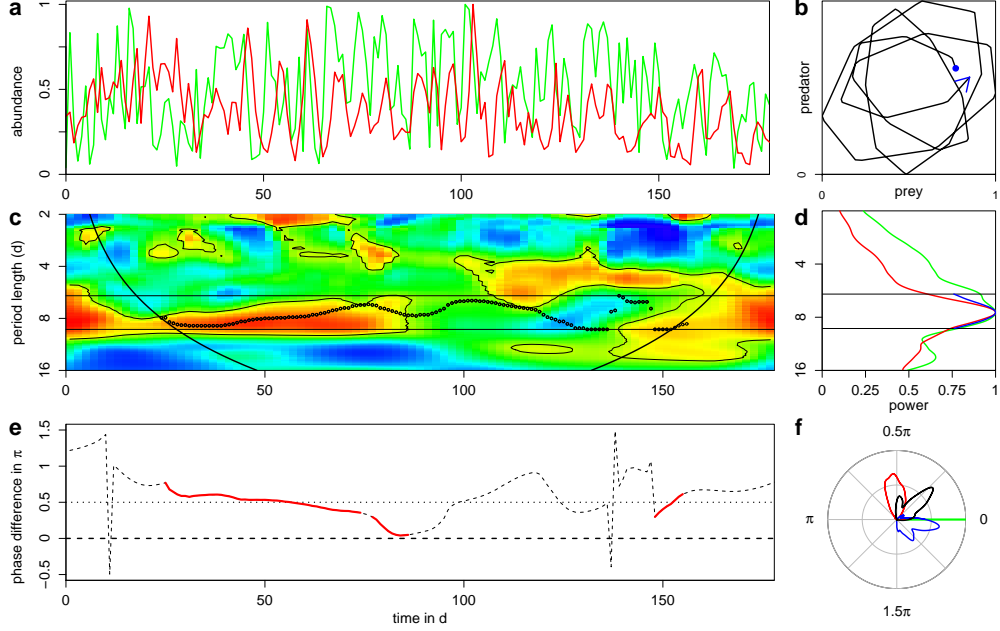
Supplementary Information

Figure 1: **Analysis of an equivalent shorter 178 days experimentally measured time series.**
Experiments have been carried out as in the longer experiment (see Fig.1 in main text). **a,** Normalized time series of the predator (red) and the prey (green). **b,** Prey-predator phase portrait of a selected time interval with clear oscillations. **c,** Wavelet coherency (WCO), with a color coding from 0 (blue) to 1 (red). Significant areas are enclosed in thin solid lines. Further shown is the cone of influence (thick solid line). **d,** Normalized mean of the wavelet power spectrum (WPS) for the predator (red) and the prey (green). **e,** Phase difference between predator and prey, significant relation between both signals is marked red. **f,** Circular distribution of the mutual phase difference to prey (indicated in green) for the predator (red), the predator egg-ratio (blue) and the abundance of egg bearing predators (black). Complex order parameters for the distributions of the phase to the prey density are: predator ($R = 0.87$, $\bar{\theta} = 0.49\pi \pm 0.16\pi$), egg-ratio ($R = 0.83$, $\bar{\theta} = -0.08\pi \pm 0.18\pi$), egg-bearing animals ($R = 0.94$, $\bar{\theta} = 0.27\pi \pm 0.11\pi$). For a better visualization we show the spline curve and applied a smooth filtering. The findings are comparable to that of the longer 373d time series, however as shorter time series are more influenced by stochastic disturbances the phase difference distributions are broader and more unclear.
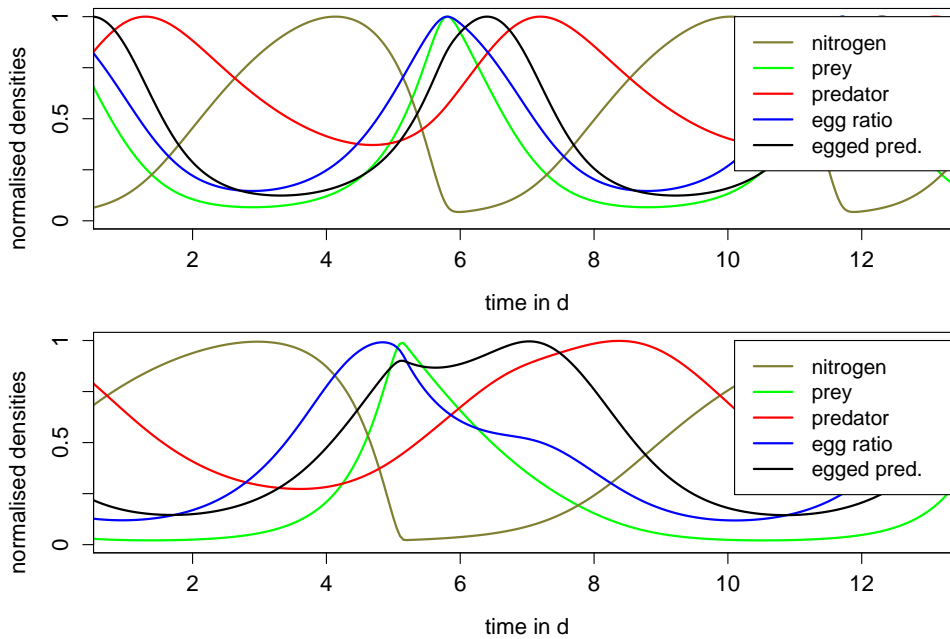
Figure 2: **Simulated time series without noise reveal the influence of juvenile predator life stages on the phase relationship between the time series.**
Plotted are the normalized densities (between 0 and 1) of the simulated time series in the deterministic model without any stochastic influence.
Top: Simulation results in the basic model, without predator live stages. While the predator and the egg bearing predators follow the prey signal with a certain delay, the predator egg-ratio coincides with the prey signal.
Bottom: Simulation results in the extended model with 21 juvenile and one adult predator life stage. While the predator and the egg bearing predators follow the prey signal with a certain delay, the predator egg-ratio precedes the prey signal.
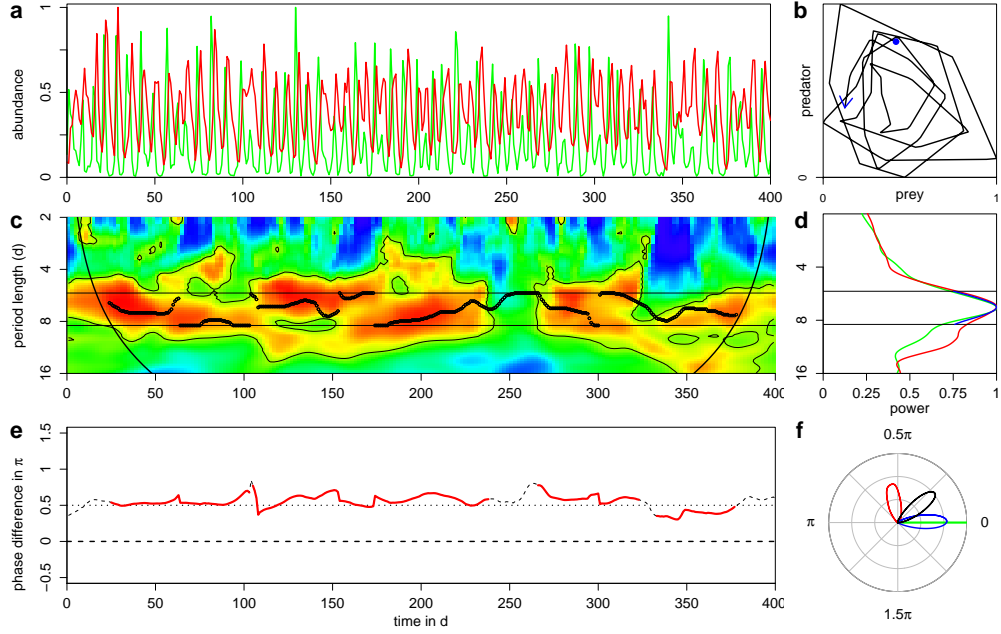
Figure 3: **Phase analysis of stochastic simulation without predator live stages.**

Results are shown for the numerical simulations in the basic model without predator live stages under the influence of stochasticity. Results were highly robust against the type of noise which was implemented in the numerical simulations. Here we show results were additive white noise of strength $\sqrt{C}$ and $\sqrt{A}$ was introduced into the equations for the algae and the adult predators, respectively. Additionally measurement noise was simulated by multiplying each simulated density by a random number drawn from a uniform distribution in the range $[0.5, 1.5]$.

a, Simulated time series of the predator (red) and the prey (green) for 400 days. **b,** Wavelet coherency (WCO) between the predator and prey signals, with a colour coding from 0 (blue) to maximum (red). Significant areas are enclosed by thin solid line. The two horizontal lines indicate the frequency band $[s_1, s_2]$ and circles show the instantaneous oscillation period $\tilde{s}(t)$. Further indicated is the cone of influence. **c,** Normalized mean of the wavelet power spectrum (WPS) for the predator (red) and the prey (green). **d,** Phase difference between predator and prey, significant relation between both signals is marked red. **e,** Circular distribution of the mutual phase difference to prey (indicated in green) for the predator (red), the predator egg-ratio (blue) and the abundance of egg bearing predators (black). For a better visualization we show the spline curve and applied a smooth filtering.
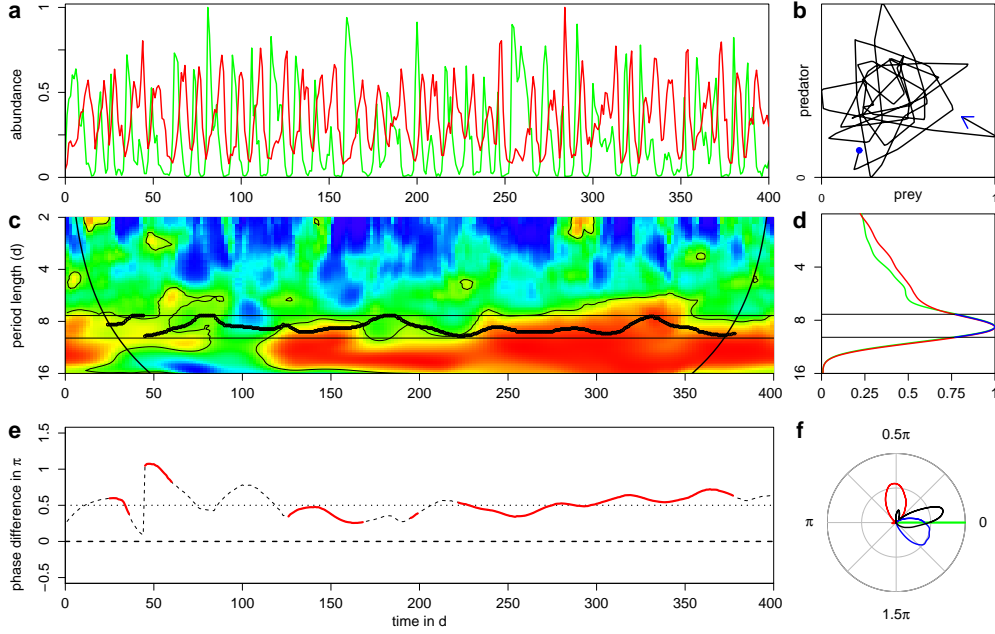
Figure 4: **Phase analysis of stochastic simulation with predator live stages.**
Wavelet analysis of numerical simulations in the extended model with 21 predator juvenile live stages under the influence of stochasticity. Noise was introduced as in the previous figure. **a,** Simulated time series of the predator (red) and the prey (green) for 400 days. **b,** Wavelet coherency (WCO) between the predator and prey signals, with a colour coding from 0 (blue) to maximum (red). Significant areas are enclosed by thin solid line. The two horizontal lines indicate the frequency band $[s_1, s_2]$ and circles show the instantaneous oscillation period $\tilde{s}(t)$. Further indicated is the cone of influence. **c,** Normalized mean of the wavelet power spectrum (WPS) for the predator (red) and the prey (green). **d,** Phase difference between predator and prey, significant relation between both signals is marked red. **e,** Circular distribution of the mutual phase difference to prey (indicated in green) for the predator (red), the predator egg-ratio (blue) and the abundance of egg bearing predators (black). For a better visualization we show the spline curve and applied a smooth filtering.
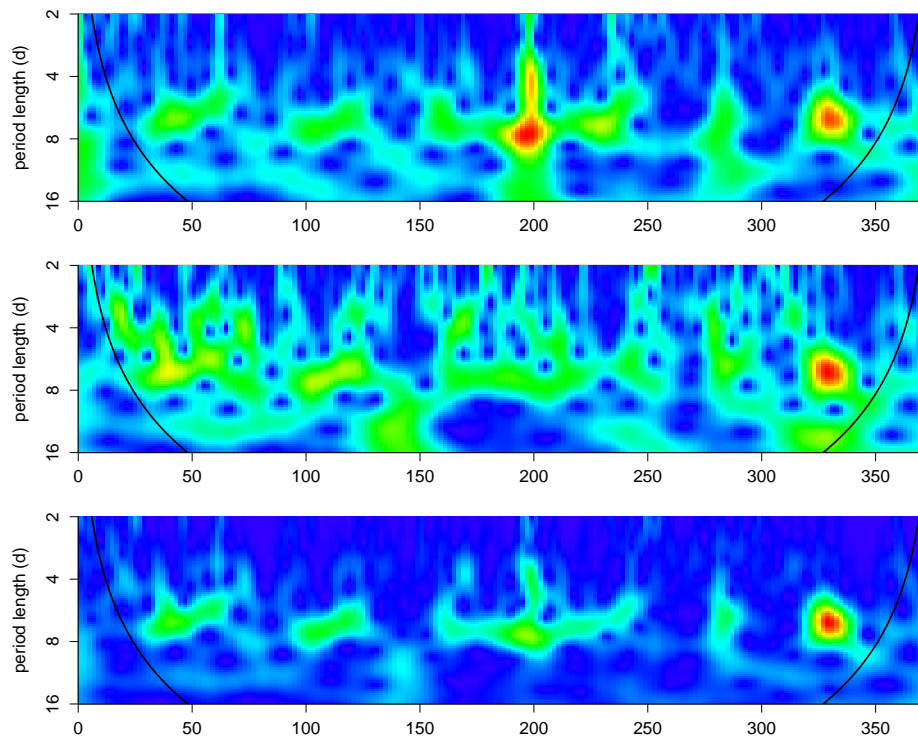
Figure 5: **Additional wavelet plots of the long measured time series.**
Plotted are the local wavelet power-spectrum (WPS) for the predator (**top**)
and prey (**middle**) signals in color-coding.
bottom: the corresponding wavelet cross-spectrum (WCS) between both
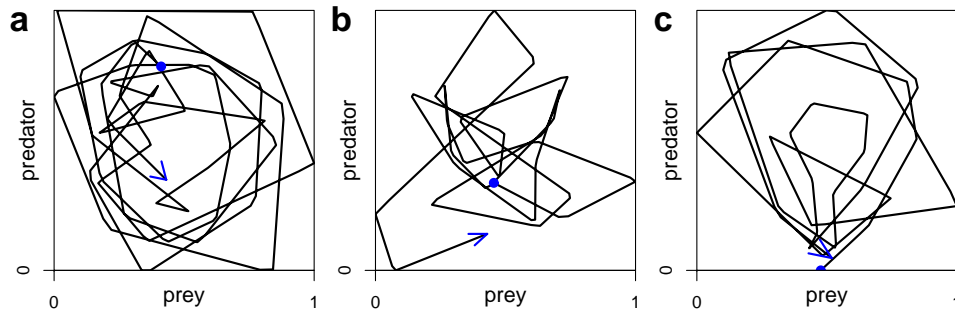time series.

Figure 6: **Phase portraits in different dynamic regimes.**
Plotted are the phase portraits in the prey-predator phase plane of the long
measured predator-prey, corresponding to the three time windows with dif-
ferent dynamic outcome in Fig. 2 (main text), showing **a** regular cycles (day
90-135); **b** disturbed cycles (day 135-160); **c** reorganized cycles (day 160-190).

Simulation analysis

Numerical simulations of the experiment have been performed in a standard chemostat model using two different model versions:

- the **basic model** consists of the state variables Nitrogen N, the consumer *Monraphidium minutum* M and its predator *Brachionus calyciflorus* B (in the basic model simulated without live stages)

$$\begin{aligned}
\frac{dN}{dt} &= \delta(N_i - N) - F_M(N)M \\
\frac{dM}{dt} &= F_M(N)M - \frac{1}{\epsilon}F_B(M)B - \delta M \\
\frac{dB}{dt} &= F_B(M)B - (\delta + m)B.
\end{aligned}$$

$$(1)$$

- the **extended model** additionally consists of L juvenile predator life stages J_i $(i = 1 \ldots L)$ and one adult predator live stage A (so that $B = A + \sum_{i=1}^{L} J_i$)

$$\begin{aligned}
\frac{dN}{dt} &= \delta(N_i - N) - F_M(N)M \\
\frac{dM}{dt} &= F_M(N)M - \frac{1}{\epsilon}F_B(M)(\sum_{i=1}^{L} J_i + A) - \delta M \\
\frac{dJ_1}{dt} &= F_B(M)A - (\delta + m + a)J_1 \\
\frac{dJ_n}{dt} &= a\,\beta J_{n-1} - (\delta + m + a)J_n \\
\frac{dA}{dt} &= a\,\beta J_L - (\delta + m)A\,.
\end{aligned}$$

$$(2)$$

In both model versions algal nutrient uptake and predation are modeled with Monod functions

$$F_M(N) = \frac{r_M N}{K_M + N} \qquad\qquad F_B(M) = \frac{r_B M}{K_B + M}\,. \qquad (3)$$

The number of egg bearing animals E was considered to be proportional to the growth rate (in the basic model we set $A = B$)

$$E = F_B(M) \cdot A \qquad (4)$$

and the predator egg-ratio ρ was calculated as the ratio between egg bearing animals and total predator density, yielding

$$\rho = F_B(M) \cdot \frac{A}{B}. \qquad (5)$$

Variables:

- N - nutrient (Nitrogen) (mol N l^{-1})

- M - prey (*Monoraphidium m.*) (mol N l^{-1})

- B - predator (*Brachionus c.*) (mol N l^{-1})

- A - adult predators (mol N l^{-1})

- J_n - predator in juvenile stage n (mol N l^{-1})

- E - egg bearing animals (mol N l^{-1})

- ρ - predator egg ratio

Parameters:

- a - transition rate between successive live stages (10 d^{-1})

- β - biomass ratio between two successive live stages (1.08)

- δ - flow rate (0.55 d^{-1})

- ϵ - predator assimilation efficiency (0.25)

- K_B - half saturation constant predator growth (30 mol N l^{-1})

- K_M - half saturation constant prey growth (4.3 mol N l^{-1})

- L - number of juvenile life stages (21 or 7)

- m - predator mortality (0.055 d^{-1})

- N_i - Nitrogen in inflow (80 mol N l^{-1})

- r_B - maximum predator growth rate (2.25 d^{-1})

- r_M - maximum prey growth rate (3.3 d^{-1})

Bistability in the Distribution and Composition of Phytoplankton in a Water Column with Upper Mixed Layer

Alexei B. Ryabov, Lars Rudolf and Bernd Blasius

to be submitted

Limitation of phytoplankton growth by light and nutrients commonly leads to either surface or deep chlorophyll maxima. Usually it is assumed that the realization of these two configurations is determined by the environmental conditions. However some recent field investigations pointed out that both patterns can appear under similar conditions. Here we analyze the influence of an upper mixed layer (UML) in an advection-reaction-diffusion model for the growth of a phytoplankton community in a vertical water column. The model predicts two alternative density configurations and may be bistable (realized configurations depends on initial conditions) or metastable (transition between solutions takes many years). In both regimes the system is very sensitive to disturbances which can induce long-lasting shifts in the system's state. A system of two competing species exhibits bistability in the spatial distribution and in the competition outcome. We present a novel graphical approach for deducing the competition outcome. Moreover, we identify a subtle competitive exclusion effect when oscillatory states in the lower layers are replaced by steady solutions in the UML. Our findings proof the UML to be a major factor controlling the spatial organization and species composition of the whole water column.

Introduction

The survival and competition of species in an heterogeneous environment has been a fascinating question for many ecologists (see e.g. Holmes et al. 1994; Tilman and Kareiva 1997; Huisman et al. 1999c; Neuhauser 2001). In many systems the spatial diversity of natural populations originates mainly from some underlying abiotic heterogeneity of the environment. If growth conditions vary between different locations then this spatial variation should be reflected in the density distribution of natural populations. After the seminal papers by Skellam (1951) and by Kierstead and Slobodkin (1953),

the dynamics of such systems have often been analyzed in terms of favorable and unfavorable patches (see e.g. Okubo and Levin 2001; Cantrell and Cosner 2001; Birch et al. 2007). This approach assumes that space can be divided into regions of positive and negative net growth, between those the organisms are transported by diffusion and advection. Although realistic in many situations, these suggestions, however, do not hold in some resource-consumer systems, in which the size, the form, and even the location of the species habitat may vary, reflecting external and internal perturbations.

The dynamics of phytoplankton profiles in an incompletely mixed water column represents an important example of such systems (see e.g. Radach and Maier-Reimer 1975; Jamart et al. 1977; Shigesada and Okubo 1981; Varela et al. 1992; Klausmeier and Litchman 2001; Yoshiyama and Nakajima 2002; Hodges and Rudnick 2004; Huisman et al. 2006; Beckmann and Hense 2007). Growth of phytoplankton cells is usually limited by light, supplied from the surface, and by nutrients, diffusing from the bottom. Thereby, the light limitation leads to a surface phytoplankton maximum, whereas lower nutrient concentrations at the bottom favors phytoplankton build-up in deeper layers (Venrick 1973, 1993). If the chlorophyll:biomass ratio does not change with depth, this maxima coincide with deep chlorophyll maxima (DCM), which are a widespread phenomenon and constitute one of the most striking characteristics of nutrient poor waters in ocean ecosystems and freshwater lakes (Steele and Yentsch 1960; Anderson 1969; Abbott et al. 1984; Cullen 1982; Holm-Hansen and Hewes 2004; Raven and Falkowski 1999; Tittel et al. 2003).

Moreover, most light limited species may have a positive production rate close to the surface, whereas the higher nutrient requirements results in the subsurface productivity (see e.g. Venrick 1993). This means that a production layer is species specific. Furthermore, as the biomass of each species shades light and consumes nutrients, this location will depend on the current abundance of a phytoplankton species, on the invasion of another species, etc. Even though this mobility of the favorable layer may lead to new types of dynamics (Yoshiyama and Nakajima 2002; Huisman et al. 2006) and new aspects of the species competition (Britton and Timm 1993), this problem still has not received sufficient attention in the literature.

What is more, this topic has a great ecological importance, as phytoplankton form the basis of aquatic food webs and provide an essential part of the Earth's oxygen. They are also the major component of the biological carbon pump, a mechanism exporting the greenhouse gas CO_2 into the oceans' deep layers (Falkowski et al. 2000). Climate models predict that the ongoing global warming may result in the higher water stratification (Bopp et al. 2001; Sarmiento 2004), thereby affecting the main component of the ocean's

metabolism.

Theoretical models have been a useful approach to describe and understand the dynamics of nutrient limited phytoplankton growth in constant and seasonally driven environments (Huppert et al. 2002, 2004). The dynamics, competition and structuring within a vertical water column have been investigated in a series of modeling investigations (Shigesada and Okubo 1981; Huisman and Weissing 1995; Huisman et al. 1999c; Klausmeier and Litchman 2001; Diehl 2002; Hodges and Rudnick 2004; Huisman et al. 2006; Beckmann and Hense 2007). It was shown that a given set of parameters may lead to either a surface or a deep chlorophyll maximum, whereby the location of the maximum is entirely determined by the environmental conditions. These model results are in agreement with many field studies (e.g., Aristegui et al. 2003; Matondkar et al. 2005; Weston et al. 2005). However, in a few recent investigations (Venrick 1993; Holm-Hansen and Hewes 2004), either a maximum in the upper mixed layer (UML) or a maximum below it were observed under almost the same conditions.

An upper mixed layer commonly occurs in oceans and lakes due to mechanical perturbation of the surface waters (e.g., wind, waves, storms), and is characterized by the strong turbulent mixing in contrast to the rather slow diffusion transport in the deeper layers. The depths of a UML can vary from 10 m to 200 m or more (Deuser 1987; Venrick 1993; Law et al. 2000).

A UML is one of the major components influencing the aquatic environment close to the surface. Firstly, it provides almost uniform distributions of resources (with except of light) and biomass. Secondly, sinking phytoplankton species require a sufficiently high diffusivity to prevent the population washout from a favorable area, whereas a deep UML may result in the extinction of light limited species (Huisman et al. 1999b). Nevertheless, previous theoretical approaches showed that a UML has vanishing effects on the dynamics of phytoplankton if the self-shading of phytoplankton biomass (Fennel and Boss 2003; Hodges and Rudnick 2004) or the heterogeneity of the nutrient distribution (Huisman et al. 1999c) are negligible.

However, taking into account both the light and the nutrient heterogeneity, Yoshiyama and Nakajima (2002, 2006) demonstrate that in a range of parameters the phytoplankton profiles exhibit bistability, characterized by the placement of phytoplankton maxima in either the deep or the upper layers. Thereby, depending on the initial conditions, the production layer may have two different stable locations. This model however has some restrictions. In particular, Yoshiyama and Nakajima (2002) assume that a water column is divided into an infinitely mixed UML and poorly mixed lower layers, with a very small diffusivity across the separating boundary layer (thermocline), that leads to vertical phytoplankton patterns with a sharp edge at the ther-

mocline. Moreover, the competition of species, possibility of the oscillatory solutions and other important questions about the role of the UML still remain open.

To progress this investigation and to address these questions we propose a mathematical model for the growth of a nutrient and light limited phytoplankton community in a vertical incompletely mixed water column with a UML. We find that a UML ameliorates the growth conditions close to the surface. Even though the spatial extension of the UML may be quite small compared to the rest of the water body, this can have drastic effects because organisms close to the surface occlude light and prevent growth in all deeper layers. In this way the presence or absence of a UML turns out to be a major factor controlling the vertical distribution and competition outcome in the whole water column. Most notably, the spatial density profile can become bistable with vertical maxima either close to the surface or in deep layers. Further the UML can strongly modify the competition outcome between different phytoplankton species by providing a vertical niche for species which are better adapted to the conditions close to the surface. Moreover, in this section, we show that a light limited species can obtain a competitive advantage if the diffusivity in the deep layers is reduced below a critical value. In this case the species composition is determined by the dynamic state, and the oscillatory states in the deep layers are displaced by steady solutions in the UML. To analyze these effects, we present a graphical approach which allows to deduce the competition outcome from the equilibrium pattern of each species alone .

Model

The appearance of a vertical phytoplankton profile is a complex process subjected to many factors, such as the availability of light and nutrients, the concentration of carbon, temperature of water, upwelling, downwelling, grazing, seasonal changes, etc. However, in many regions of the world's ocean only two factors are crucial. First, the reduction of the light intensity with depth makes deep layers unfavorable for photosynthetic phytoplankton species. Second, an opposing gradient of nutrients can often maintain the positive net production rate only in deep subsurface layers.

It is evident that the phytoplankton profile is determined by resource distributions. However, the biomass consumes nutrients, shades light and is remineralized back into a nutrient pool. Thereby the biomass, in turn, influences the resource profiles, and a favorable layer for phytoplankton appears as a result of the consistent dynamics of all components.

For simplicity, consider the dynamics of only one species in a vertical water column of depth Z_B (the multispecies model see in Supplementary Information). Let $P(z,t)$ denote the density of the species at time t and depth z. Assume that there are only two limiting factors: the concentration of a nutrient, $N(z,t)$ and the light intensity, $I(z,t)$. Coupling of the nutrient and the phytoplankton dynamics leads us to the system of two reaction-diffusion equations (Radach and Maier-Reimer 1975; Jamart et al. 1977; Klausmeier and Litchman 2001; Fennel and Boss 2003; Hodges and Rudnick 2004; Huisman et al. 2006; Beckmann and Hense 2007)

$$
\begin{aligned}
\frac{\partial P_i}{\partial t} &= \text{growth} - \text{loss} - \text{sinking} + \text{mixing} \\
&= \mu_i P_i - m P_i - v \frac{\partial P_i}{\partial z} + \frac{\partial}{\partial z}\left[D_z \frac{\partial P_i}{\partial z} \right]
\end{aligned}
\tag{1}
$$

$$
\begin{aligned}
\frac{\partial N}{\partial t} &= -\text{uptake} + \text{recycling} + \text{mixing} \\
&= -\alpha \sum_{i=1}^{n} \mu_i P_i + \varepsilon \alpha m \sum_{i=1}^{n} P_i + \frac{\partial}{\partial z}\left[D_z \frac{\partial N}{\partial z} \right]
\end{aligned}
\tag{2}
$$

where $\mu(N,I)$ is the local growth rate, m is the mortality rate, v is the phytoplankton sinking velocity, D_z is the depth dependent turbulent diffusivity, α is the nutrient content of a phytoplankton cell, and ε is the phytoplankton recycling coefficient.

Equations (1) and (2) are coupled by means of the growth rate $\mu(N,I)$ which depends on the local resource availability and also controls the nutrient uptake. Assuming that the limitation of growth follows the Michaelis-Mentel kinetics (e.g. Turpin 1988) and both resources are essential (von Liebig's law of minimum), we obtain

$$
\mu(N,I) = \mu_{\max} \min\left(\frac{N}{H_N + N}, \frac{I}{H_I + I} \right) ,
\tag{3}
$$

where $\mu_{\max}$ is the maximum growth rate, H_N and H_I are the corresponding half saturation constants. Varying H_N and H_I we can model, for instance, a species which is better adapted for the light (a smaller H_I) or for the nutrient (a smaller H_N) competition.

Light dissipates with depth as it is absorbed by the biomass, water, clay particles and many other absorbing substances. Assume that the light intensity decreases exponentially according to Lamber-Beer's law (see e.g. Shigesada and Okubo 1981, Kirk 1994)

$$
I(z) = I_{in} \exp\left[-K_{bg} z - k \int_0^z \sum_{i=1}^{n} P_i(\xi,t) d\xi \right] ,
\tag{4}
$$

where I_{in} is the incident light intensity, K_{bg} is the turbidity of the water without biomass, and k is the light absorption coefficient a phytoplankton cell.

To describe the water column stratification, we assume a high diffusivity, D_U, in the upper layer and a much smaller mixing, D_D, in the layers below the UML. A gradual transient from one area to another (see supplementary information for the detailed description).

To specify the boundary conditions for equations (1) and (2), we assume that the biomass and the nutrient cannot diffuse across the surface of the water column, the bottom is also impenetrable for the biomass, and a supply in the sediment maintains a constant nutrient concentration, N_B, at the bottom.

In a deep incompletely mixed water column (see Table 1 for the parameters) the diffusive time scale $\tau_D = (Z_B - Z_{mix})^2/2D_D \simeq 10 - 30$ years is much larger than the biological time scale $\tau_B = \mu_0^{-1} \simeq 1$ day. Thus the nutrient dynamics (in the deep, free of the biomass layers) is a quasistationary process in comparison with the development of phytoplankton profiles. To minimize the influence of the biomass, we assumed initially a small concentration of phytoplankton ($P(z,0) < 1$ cell m^{-3}), whereas for the nutrient we used two different initial profiles, describing a nutrient saturated water column ($N(z,0) = N_B$) and a nutrient poor upper layer ($N(z,0) = 0$ if $z \leq Z_{mix}$). Checking the stability of solutions, in each case we simulated dynamics for 50,000 system days (approximately 130 years). Further details of the model and of the numerical scheme are presented in the supplementary informations.

The single species model

We first concentrate on the dynamics of a single species population and describe the formation of a DCM in a water column without a UML. Suppose that we start with an initially nutrient rich system ($N(z,t) = N_B$). Thereby the nutrient limitation is negligible and we observe the rapid formation of a transient phytoplankton maximum close to the surface (Fig. 1A). This phytoplankton profile $P(z,t)$ is, however, not stable. With the depletion of the nutrient in the surface layer the production layer, i.e. the layer where $\mu(N,I) \geq m$, shifts downwards, until the systems reaches a stable equilibrium (Fig. 1B), in which the upward flux of nutrient compensates the nutrient consumption and the further sinking of the production layer is balanced by the light limitation (Klausmeier and Litchman 2001).

Note that the spatio-temporal evolution of the concentration profile $P(z,t)$ depends on the growth conditions at all vertical positions. Due to self-shading
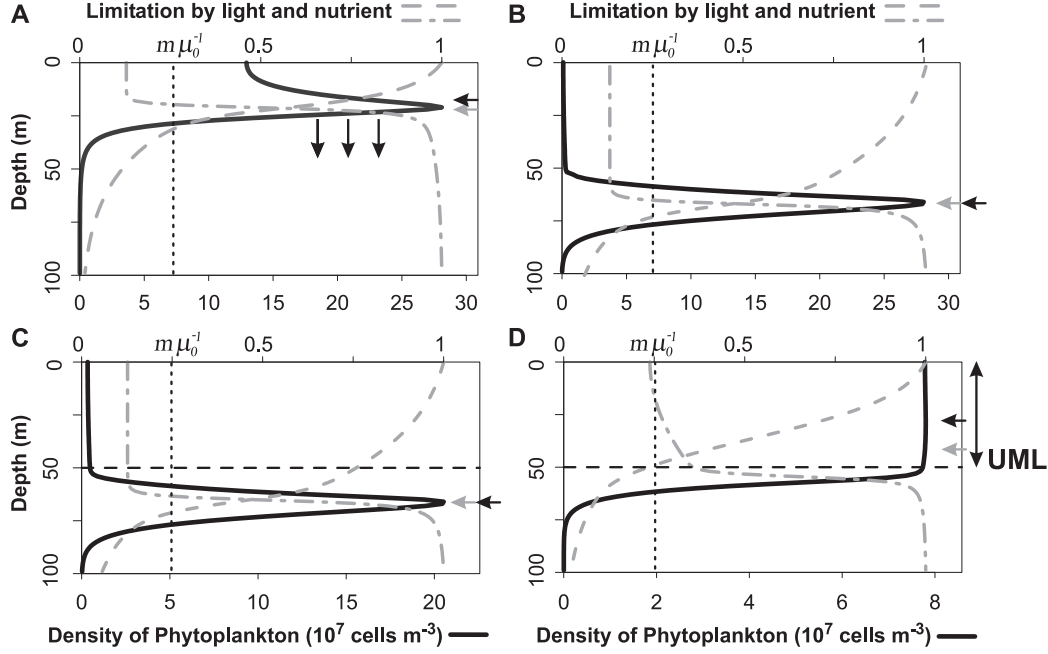
Figure 1: Typical vertical phytoplankton profiles $P(z)$ and the normalized growth rate $\mu(N, I)/\mu_{max}$ in the single species model. Without a UML, a non-stable phytoplankton maximum (A) evolves to the stable state (B). Under the same conditions in a system with a UML, we observe two alternative stable configurations: a phytoplankton profile with a maximum in the deep layers (C) and with a maximum in the UML (D). Black and gray arrows show the centers of biomass and net production, respectively.

and the water turbidity the light intensity $I(z, t)$ is reduced in deeper layers that increases the limitation by light in the deep layers. Contrarily, the nutrient concentration $N(z, t)$ is close to zero within the bulk of phytoplankton biomass and above it, and increases almost linearly with depth below the phytoplankton peak (Fig. 1, see also Fig. 2 and Fig. 3 in the supplementary information) for the resource distributions). This shaping of the spatial dependence of the growth limiting factors self-consistently depends on the full phytoplankton density profile $P(z, t)$, a fact which makes the problem very hard to understand without mathematical simulation.

A rough insight into the time evolution of $P(z, t)$ can be gained by considering the centers of biomass $Z_m = \int zPdz/\int Pdz$ and of phytoplankton net production $Z_g = \int zgPdz/\int gPdz$ (black and gray arrows in Fig. 1, respectively), where $g(z)$ is the net phytoplankton production rate which includes

reproduction, mortality, sinking and diffusivity. In an incompletely mixed water column without a UML the position of the center of mass, Z_m, follows that of Z_g. Thereby the phytoplankton production around Z_g shifts the mass center Z_m, changing the local nutrient consumption and the light absorption, that in turn is able to shift the growth center Z_g. In this feedback-loop, the system finally reaches an equilibrium configuration where both centers coincide, $Z_g = Z_m$, giving rise to a DCM (Fig. 1B).

Now suppose that there is a strong mixing in the upper layer. If the bulk biomass is located sufficiently deep, then the mixing in the upper layer has practically no effect and an identical DCM can persist (Fig. 1C) independent of whether or not a UML is present. Here, we always assume that the depth of the UML is smaller than the compensation depth (a depth at which $\mu(I) = m$ in the absence of biomass, see e.g. Sverdrup 1953, Huisman et al. 1999b).

In contrast, if the phytoplankton biomass is initially located close to the surface, it will be almost uniformly distributed within the UML. The position of Z_m is then fixed approximately in the middle of the UML and is almost uncoupled from Z_g (Fig. 1D). Therefore a gradual shift of the center of mass into the deep layers is no longer possible and the transition to a DCM can only take place if the light intensity below the UML is sufficiently large to provide positive net growth in the deep layers – otherwise the phytoplankton remains trapped in the UML. We denote this stable configuration of a nearly uniform phytoplankton profile in the UML as an upper chlorophyll maximum (UCM, note that all acronyms are listed in Table 2). Thereby, Figs. 1C and 1D show that with a UML, depending on the initial conditions, the system can undergo two very different spatial configurations of either a deep or an upper phytoplankton maximum.

Fig. 2 depicts the typical spatio-temporal evolution of the phytoplankton density. Without a UML (Fig. 2A), an initial phytoplankton maximum at the surface slowly moves downward until the distribution converges to a stable DCM equilibrium. However, as is shown in Fig. 2B, DCM's are not necessarily stable states. Huisman et al. (2006) showed that at very small diffusivity, D_D, the sinking of biomass may destabilize the deep chlorophyll maxima and the density profile shows sustained regular or chaotic oscillations of biomass. Moreover, if the diffusivity is lower than the minimal diffusivity

$$D_{min} = \frac{v^2}{4(\mu(N_B, I_{in}) - m)} \qquad (5)$$

the sinking phytoplankton biomass cannot survive (Riley 1949; Shigesada and Okubo 1981). As will be shown below, these factors can play a crucial role in a system with an UML.
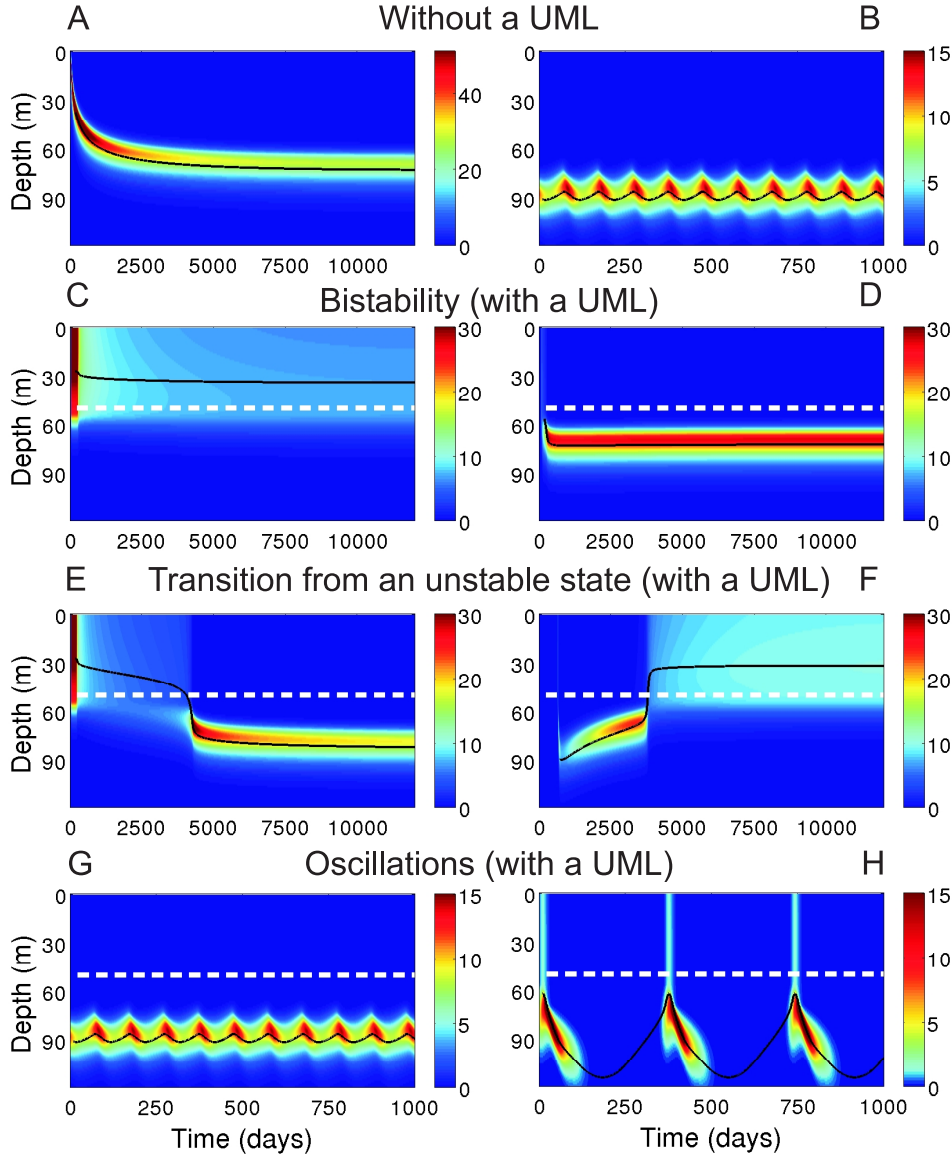
Figure 2: Time evolution of phytoplankton density, $P(z,t)$, in color-coding ($\times 10^7$ cells m^{-3}) for different values of D_D and initial conditions, in a system without a UML (A-B) and in the presence of a UML (C-H). Black lines track the evolution of the center of biomass, Z_m, white dashed lines show the depth of the UML. (A) Gradual evolution of a DCM, $D_D = 0.3$ cm^2/s. (B) Oscillations of the biomass for very small mixing, $D_D = 0.12$ cm^2/s. Bistability: depending on the initial conditions a stable UCM (C) or a stable DCM (D) is formed (value of D_D as in A). For any initial conditions (E) only a DCM is stable, $D_D = 0.2$ cm^2/s, or (F) only a UCM is stable, $D_D = 0.4$ cm^2/s, however the transient process may last a long time. Oscillations of the biomass (G) are not affected by a UML, $D_D = 0.12$ cm^2/s, and (H) induced by a UML, $D_D = 0.04$ cm^2/s.

While only two types of globally attracting solutions (Figs. 2A and 2B) hold for a system without a UML, in the presence of a UML the dynamics may be bistable. Under the same parameters as in Fig. 2A, an initially nutrient saturated water column gives rise to a stable UCM (Fig. 2C), whereas an initially nutrient depleted water column leads to a DCM (Fig. 2D). In the one species model, we observe bistability only in a certain parameter region in which a DCM is not affected by the upper layer and a UCM contains enough biomass to limit growth in the deep layers. The diffusivity D_D is a suitable bifurcation parameter as it controls the nutrient flux from the bottom and an increase of D_D rises the level of the DCM (Klausmeier and Litchman 2001). Thus decreasing D_D in comparison with Fig. 2C and 2D, we obtain a stable or an oscillatory DCM (Figs. 2E and 2G, respectively), whereas for larger values of D_D only upper maxima are stable (Fig. 2F).

Consider the transition from an unstable upper maximum to a stable DCM (Fig. 2E). Here the water column is initially nutrient saturated that gives rise to a uniform phytoplankton profile in the UML. While, as mentioned above, the center of biomass Z_m is trapped inside the UML, with ongoing nutrient depletion the phytoplankton density is slowly declining. This configuration can be sustained for a long time, which has the order of the diffusive time scale $\tau_B = (Z_B - Z_{mix})^2/(2D_D)$. For instance, in deep waters this transition will last several years. However, as soon as the biomass in the UML is not sufficient to shade light below it, the system undergoes a rapid transition to a DCM. This transition occurs on the biological time scale $\tau_B = \mu_0^{-1}$ and takes approximately 10-50 days for the model in our parameter range. Obviously, in a system with essential seasonal variability this transition will never be reached. Similar dynamics with two very different time scales are observed in Fig. 2F, where a DCM gradually moves upward until it reaches the bottom of the UML, Z_{mix}, and then the biomass rapidly shifts into the upper layer. The further decrease of D_D leads to the oscillatory deep maximum, which might be not affected by the UML(Fig. 2F). What is more, the UML can support these oscillations even if $D_D < D_{min}$ (Fig. 2H). Now, in the absence of biomass the nutrient can freely diffuse towards the UML, where the population can outgrow sinking as soon as the nutrient concentration has reached a critical level. However, if the biomass in the UML is not limited by light, the depletion of the nutrient shifts the prodaction layer downwards into the weakly mixed water, where the biomas slowly sinks, consuming the nutrient. Finally the population declines because of the light limitation and a new portion of the nutrient can reach the UML.

The stability of upper phytoplankton maxima depends also on the mixing intensity in the UML, D_U. Fig. 3 shows the position of the phytoplankton center of mass, Z_m, as a function of D_U, for different values of the diffusivity

in the deep layers, D_D. With the increase of D_U (with the development of the UML) three scenarios are possible. If the center of biomass is located within or slightly below the UML, then with the increase of D_U it shifts toward the UML center. In contrast, if the phytoplankton maximum settles sufficiently deep, then it is not affected by the presence of the UML. For intermediate parameters starting from some critical value of D_U the system becomes bistable. Note, that the further increase of D_U does not yield any qualitative changes.
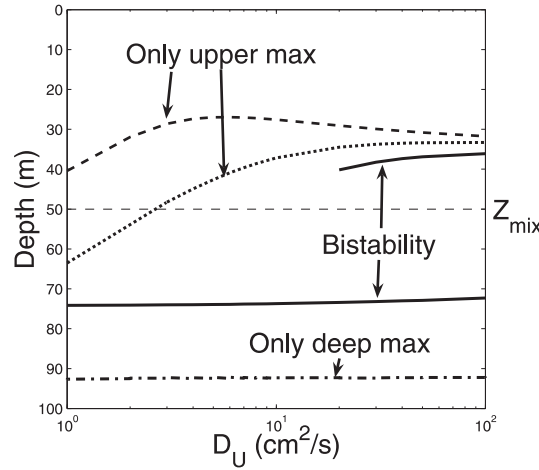

Figure 3: The depth of the center of phytoplankton biomass, Z_m, with the increase of D_U, for small to large values of the deep diffusivity D_D: 0.15 cm^2/s, only DCM (dot-dash line); 0.45 cm^2/s, bistability (solid lines); 0.6 cm^2/s and 1.0 cm^2/s, only UCM (dotted and dashed line, respectively). The thin dashed line shows the depth of the UML, Z_{mix}. $N_B = 30$ mmol m^{-3}.

To investigate the system behavior in a large range of parameters we performed simulations for 900 pairs of (N_B, I_{in}) and (N_B, D_D). The results are presented in the stability diagrams Fig. 4A and 4B. As shown in Fig. 4A, large values of I_{in} lead to a DCM and large N_B to a UCM, while for intermediate resource levels we observe a region with the bistable behavior. The bistability range is reduced for smaller values of I_{in} or N_B and disappears at a critical point ($I_{in} \approx 350$ μmol photons m^{-2} s^{-1} and $N_B \approx 25$ mmol/m^3 in Fig. 4A). These results confirm the findings of Yoshiyama and Nakajima (2002) and are presented here for a comparison with the two-species model. Fig. 4B demonstrates the bistability range in the (N_B, D_D) coordinate plane, where the bifurcation lines have an almost hyperbolic form. A UCM appears for large values of D_D and N_B, whereas small values favor a DCM. Suffi-

ciently small values of D_D result in oscillatory DCM solutions (region II), in accord to the results of Huisman et al. (2006). Note that this behavior can still be observed at $D_D < D_{min}$.

Interestingly, outside the region of bistability for large values of D_D, a smooth transition from the deep to the surface maximum is possible. In this case intermediate density profiles, with no clear separation between DCM and UCM, appear and the phytoplankton biomass is located in both parts of the water column (see Fig. 3 in supplementary information 2).

The range of stability of the upper maxima can be described by an analytical criterion (see Eq. (8) in supplementary informations 2), which is derived from the condition that the phytoplankton net production rate below the mixed layer is not positive (dash-dotted line in Figs. 4A and 4B).

The two species model

So far we have considered the vertical distribution of a single phytoplankton species. However, different mixing and inhomogeneous resource distribution lead to new aspects for the competition of species which are differently adapted to the conditions at the surface or in the deep water. In this section, we extend the model to contain two phytoplankton species which differ in their respective half saturation constants H_I and H_N in Eq. (3). More specifically, we consider the competition between a most light-limited species (I-species) characterized by a low H_N and a large H_I value and so is forced to live close to the light source, and a most nutrient-limited species (N-species) with low H_I and large H_N that will usually do better in deep water. Note that the results of the previous section hold for the N-species.

To avoid the influence of different growth, mortality, and consumption rates, we keep the other species' parameters (see Table 1 in supplementary informations) identical in both species. Thereby, in a chemostat these species would have parallel consumption vectors (Tilman 1980, 1982; Huisman and Weissing 1995). This means that in a well mixed uniform environment the success of one species or another depends only on the resource concentrations in the absence of biomass. Furthermore, in the chemostat such species cannot coexist and the outcome of their competition cannot be bistable (Tilman 1980, 1982). In a well mixed water column, where the light intensity reduces with depth, the competition of these species would be more complicated, however the same result would still hold for sufficiently clear water column (Huisman and Weissing 1995). Moreover, assuming only the light gradient in an incompletely mixed water column, one can find only a narrow region of the species coexistence (Huisman et al. 1999c). As is shown below, the presence of two
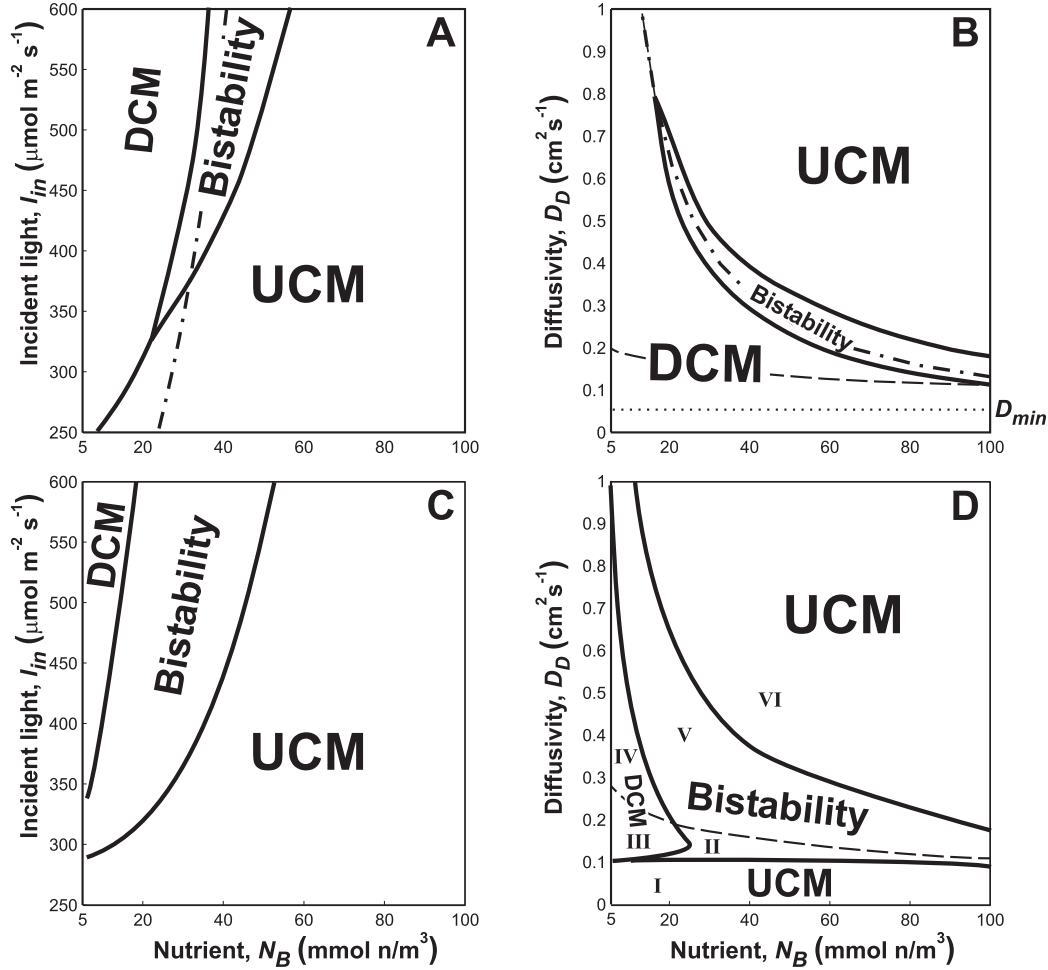
Figure 4: Stability diagram in the presence of a UML, showing the region of bistability for the N-species solely (top) and for competition between N- and I-species (bottom) in the (N_B, I_{in}) plane (left column) and the (N_B, D_D) plane (right column). The dashed line in (B) and (D) separates the regions of steady (above this line) and oscillatory (below it) DCM. The dash-dotted lines in (A) and (B) indicate the analytic border of stability of a UCM, see Eq. (8). Parameter values: (A) and (C): $D_D = 0.3$ cm^2/s; (B) and (D): $I_{in} = 600$ μmol photons m^{-2} s^{-1}.

opposing resource gradients and the variation of the diffusivity with depth may drastically alter the outcome of competition, resulting in new regions of competitive exclusion, bistability and coexistence.

Figs. 4C and 4D present the stability diagram of the bulk biomass of two com-
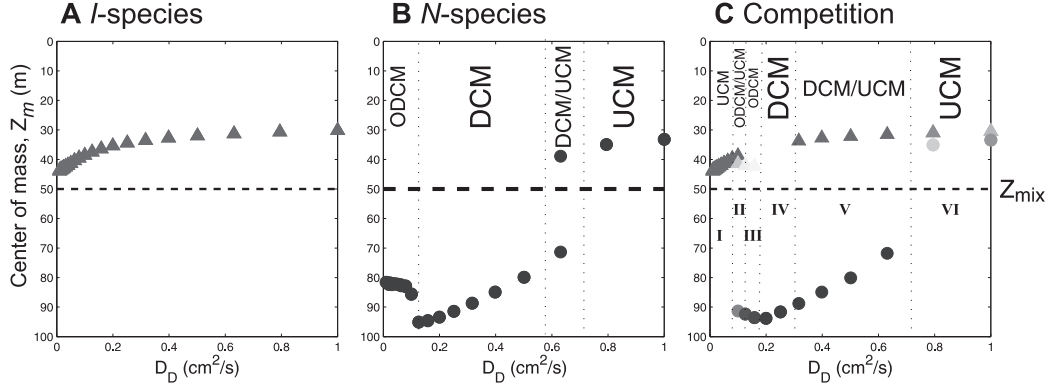
Figure 5: Vertical cross section for $N_B = 20$ mmol/m³ through the (N_B, D_D) parameter plane of Figs. 4B and D. Plotted is the location of the center of mass, Z_m, of the I-species (triangles) and the N-species (circles) in the system with a UML. (A) Monoculture of the I-species. (B) Monoculture of the N-species. (C) Two species system. In (B) and (C) several dynamic regimes (separated by vertical dotted lines) can be distinguished (see text). The competition outcome in (C) : I – I-species wins, II – bistability: either I-species wins or the species coexist due to oscillations, III – coexistence due to oscillations, IV – N-species wins, V – bistability, VI – coexistence. In the regimes of coexistence, the fraction of biomass is indicated by the intensity of gray color. The roman numerals refer to the regions in Fig. 4D. Parameters as in Fig. 4.

peting species. Basically, the overall shapes of the bifurcation lines remain identical to those of the one-species model (Figs. 4A and 4B, respectively). The most notable difference is that the bistability range has become much wider and is extended toward the smaller nutrient concentrations. In contrast, the transition line to the upper maximum remains largely unchanged, since it is mainly determined by the minimal depth of the deep maximum at which it is not affected by the UML. For our set of parameters, the deep maximum is always formed by the N-species (the upper maximum can be formed by both species) and so this boundary does not change with addition of the I-species.

New aspects arise for the small values of D_D, at which the N-species alone exhibits the oscillatory dynamics in the deep layers (Fig. 4B). The biomass of I-species reduces the light intensity in the deep layers and the destabilization occurs at higher values of D_D (the bifurcation line is the dashed line in Fig. 4B and 4D).
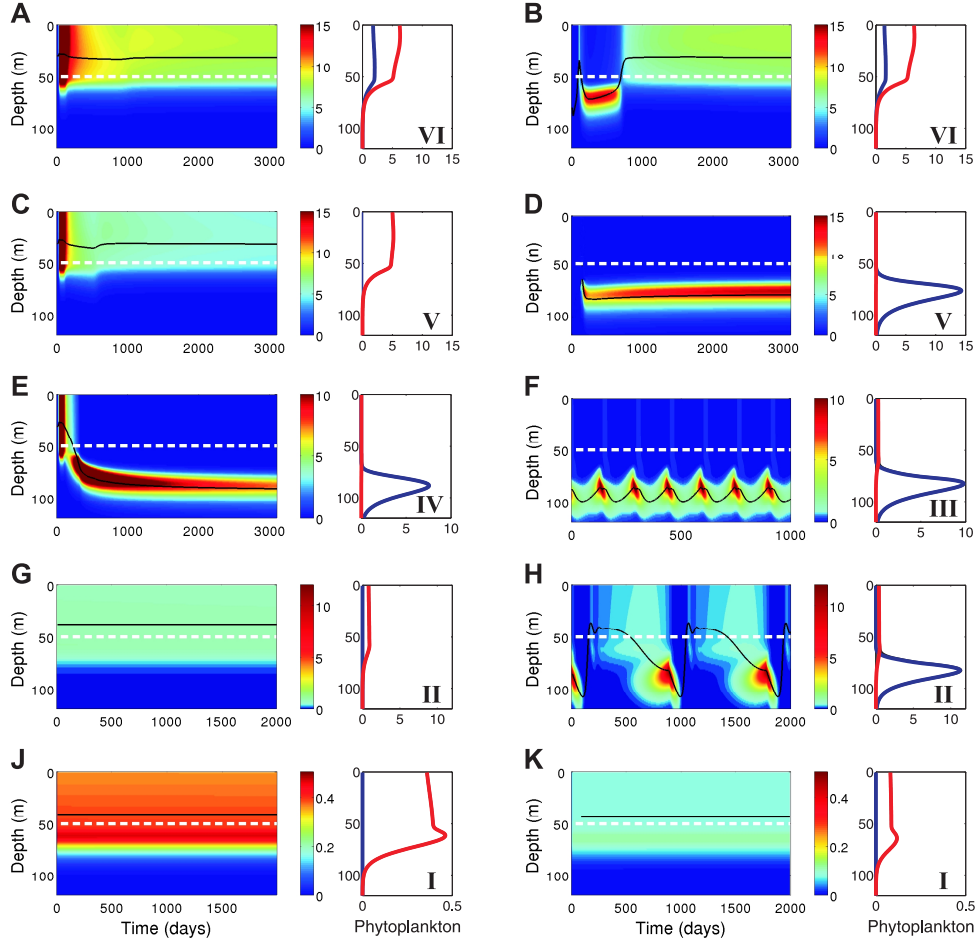
Figure 6: Time evolution of phytoplankton density and the phytoplankton density profiles in the two species model for different values of D_D and initial conditions in the presence of a UML. (A) and (B) different initial conditions lead to an upper maximum and to the same species composition, $D_D = 0.8$ cm^2/s. (C) and (D) bistability, $D_D = 0.5$ cm^2/s. (E) and (F) N-species always wins and forms a stable or an oscillatory deep maximum, $D_D = 0.2$ cm^2/s and 0.15 cm^2/s, respectively. (G) and (H) bistability between a stable UCM and an oscillatory DCM, $D_D = 0.10$ cm^2/s. (J) and (K) stable UCMs, I-species always excludes N-species, $D_D = 0.05$ cm^2/s and 0.01 cm^2/s, respectively. The roman numerals refer to the regions in Fig. 4D and Fig. 5C.

Furthermore, different location of the specific production layers and indirect competition leads to a variety of patterns. First, if the nutrient concentration is low, we observe only an oscillatory or a stationary deep maximum (region III and IV in Fig. 4D, respectively). Second, in addition to bistability between two steady solutions (region V, Fig. 4D) we observe a new kind of bistability, when either a stable upper maximum or an oscillatory deep maximum of biomass appears (region II, Fig. 4D). Third, the further reductions of D_D leads to a surprising result: a stable upper maximum formed by I-species becomes a single possible attractor in the system and outcompetes the oscillatory DCMs independently on the initial conditions (region I). Note that this transition occurs at $D_D > D_{min}$. Furthermore, I-species survives even if $D_D < D_{min}$ provided that the nutrient concentration in the upper layer is sufficiently high. Thus a strongly light limited species is able to establish a steady population in the upper mixed layer, outcompeting a less light limited species which, in the absence of the former, would form an oscillatory maximum in the deep weakly mixed layers.

These transitions and the species composition can be visualized in more detail by comparing the species locations in the single species and in the two species models. Consider the location of the center of biomass as a function of the deep diffusivity (Fig. 5). This plot adds the third dimension to the vertical cross section through Figs. 4B and 4D at $N_B = 20$ mmol/m^3. While the bulk of the I-species biomass is always located within the UML (Fig. 5A), the monoculture of N-species exhibits four dynamical regimes (Fig. 5B). First, for large values of D_D we observe stable configurations with the maximum in the upper mixed layer. Second, with decreasing values of D_D a DCM suddenly appears, resulting in a region of bistability between an upper and a deep biomass maximum. Third, with the further reduction of D_D bistability is lost and we obtain a range in which only DCMs are possible. The following reduction of D_D shifts the maximum toward the deeper layers and for low values of D_D the steady DCM solutions are replaced by oscillatory deep chlorophyll maxima (ODCM).

As is shown in Fig. 5C, the competition of two species leads to even more intricate behavior. At the high end of the D_D range both species are located in the UML and can either coexist or the N-species will competitively exclude another species if light is the only limiting factor. With the reduction of D_D, the N-species can form a DCM in the lower layers and we obtain a large bistability range between a DCM solution of the N-species and a UCM of the I-species. Thereby in this region, the bistability of phytoplankton profiles originates from the bistability in the competition outcome. Following reduction of D_D leads to competitive exclusion of the I-species and only stable DCM solutions are found. However, then the DCM loses its stability. What

is more, in this regime, the I-species obtains a time niche to establish a population in the UML, but the next rapid outburst of N-species will again lead to the dominance of the N-species. A similar regime of the species succession when the DCM is not stationary was reported by Huisman et al. (2006), here we only want to stress that the oscillatory dynamics occurs at a higher value of D_D in the presence of another species, shading light in the lower layers. With the further reduction of D_D, the period of the DCM oscillations increases and the N-species cannot outcompete an established population of the I-species in the upper layer. However, the oscillatory regime also can appear. Thereby, we observe another kind of bistability between the competitive exclusion of the N-species by the stationary upper maximum and the coexistence due to oscillations. Finally at extremely low values of D_D, the I-species always wins the competition and only a steady UCM formed by the I-species can be found. The detailed representation of the biomass dynamics and phytoplankton profiles is found in Fig. 6.

Note that the dynamics of the two-species model without the UML (see supplementary informations) is much simple. We do not observe any regions of bistability, instead the I-species is either fully outcompeted or coexists with the N-species.

Graphical approach for analysis of competition outcome

As we have shown in the previous section, production layers of differently adapted species are located at different depths. Therefor on the one hand, the strength of interspecific competition is weaker, but on the other hand, the competition becomes indirect, since the occurrence of the phytoplankton biomass at a certain depth changes total resource distributions in the water column. Furthermore, the intensive mixing in the UML is favorable for sinking phytoplankton, and as mentioned above, the emergence of a UML can alter the species composition, replacing, for instance, competitive exclusion or coexistence by bistability. Note that, the strong mixing can also play a negative role if the thermocline is located below the critical depth (Huisman et al. 1999b). To obtain an insight into the mechanisms of competition in such an environment, we suggest a graphical approach, which is based on the well known graphical method developed by Tilman (1980, 1982).

In a well mixed system, all resources and the biomass are uniformly distributed. Thus the state of the system may be presented as a point in multidimensional resource space (Fig. 7A). The concentrations of resources in
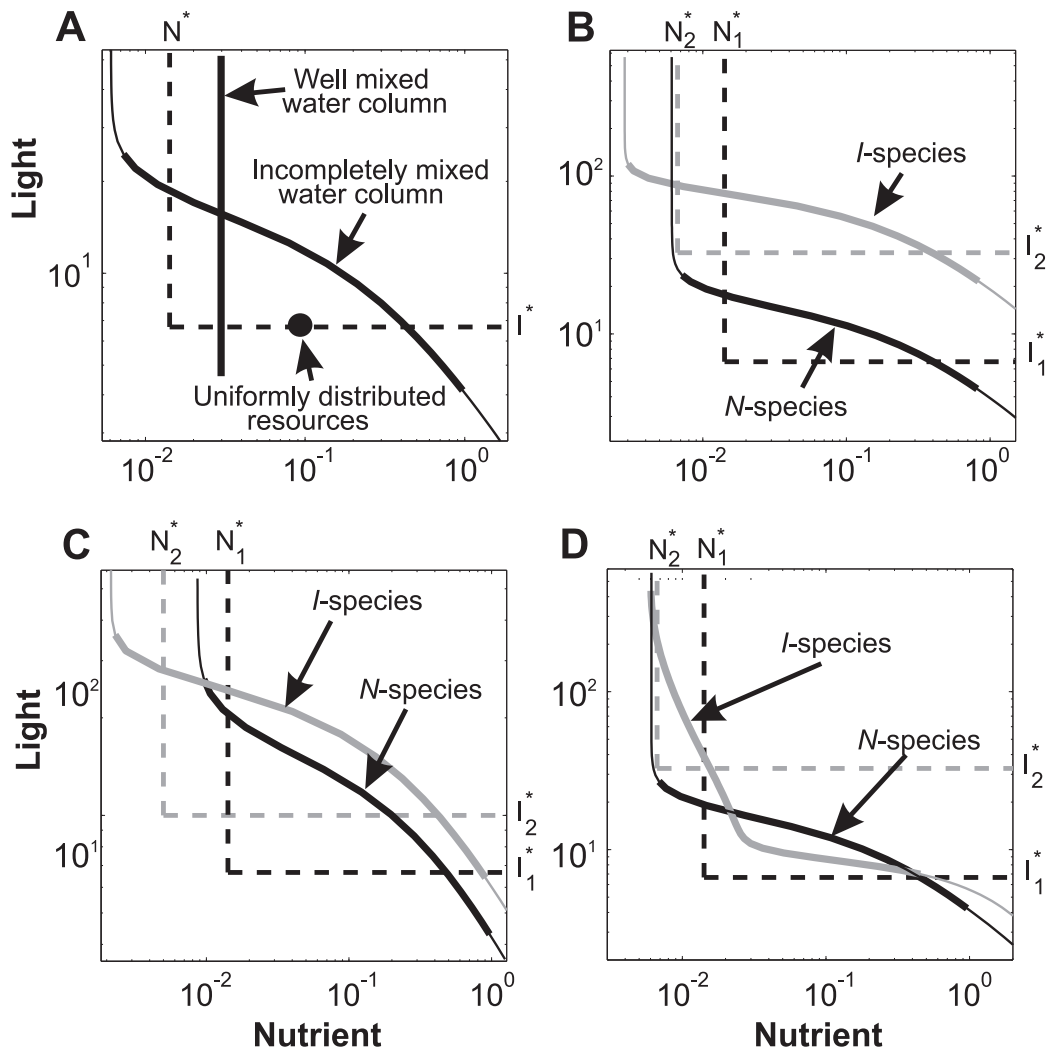
Figure 7: Zero net growth isoclines (dashed) and the system state curves (solid lines with dotted tails) in equilibrium for an incompletely mixed water column plotted for the monocultures of *N*- and *I*-species, black and gray lines, respectively. (A) Differently mixed systems. (B) Competitive exclusion (*N*-species wins) and (C) coexistence in the system without a UML. (D) Bistability under the same parameters as (B) but in the system with a UML. Due to diffusion the phytoplankton density is larger then zero everywhere in the water column, the area containing 90% of the biomass is marked as a thick line. Note the logarithmic scale of the axes.

the absence of biomass give the coordinates of the so-called supply point.

As the biomass grows and takes up resources the state point moves from the supply point along a consumption vector. The resource depletion stops when the state point hits the zero net growth isocline, characterized by a balance between growth and loss processes. These isoclines divide the resource plane into areas of positive and negative local population net growth and mark possible resource combinations in equilibrium, so that the species with the least resource requirement survives. Using Eq. (3) we can find such values $N^\star$ and $I^\star$ so that the specific growth rate equals the mortality

$$N^* = \frac{H_N}{\frac{\mu_{max}}{m} - 1} \ , \qquad I^* = \frac{H_I}{\frac{\mu_{max}}{m} - 1} \ . \qquad (6)$$

These values determine the location of the zero net growth isoclines (Fig. 7). In a spatially-extended system, where the resource values change with depth z, the competition outcome must be calculated for every vertical position. Then the state of the system is represented as a curve in the resource space, which is parametrically determined by the resource values $(N(z), I(z))$. In this sense, the state point of a homogeneous system naturally extends to a state curve in the resource space (Fig. 7A). A special case is given by a well mixed water column (Huisman and Weissing 1995). In this system the nutrients are uniformly distributed, whereas the light intensity decreases exponentially with depth and the system state curve reduces to a line segment $\{N = \text{const}, \ I_{out} \leq I \leq I_{in}\}$.

In general, however, the form of the curve is more complicated. To simplify the discussion in the following we always focus on the system state curve (SSC) in equilibrium. Fig. 7A shows the simulation outcome for the SSC in an incompletely mixed water column. Note that we use logarithmic scale to magnify the location of a SSC close to the zero net growth isoclines. The inhomogeneity and diffusive mixing does not allow the SSC to settle at the zero net growth isoclines, as would be the case for a uniform distribution of the resources. Instead the SSC extends into the area of positive (favorable patch) as well as into the area of negative population net growth (unfavorable patch). As the species density in the unfavorable patch is usually very small we indicate the range of SSCs which contains 90% of the biomass as a thick line in Figs. 7A-D.

Consider competition in a two-species system. Fig. 7B illustrates an apparent example of the competitive exclusion. The SSC of the N-species lies below the null growth isocline of I-species, whereas the I-species SSC allows the positive production of the N-species. Therefore the I-species will always be excluded as it has higher resource requirement.

However, if the SSC of one species lies above the zero null growth isocline of

its competitor, there is no unambiguous answer to the question "whether or not the latter species can invade?". On the one hand this species obtains a favorable zone, where $\mu > m$, and could invade in the limit of zero diffusivity (and zero sinking). But on the other hand, if $D > 0$, it will invade only if the patch and the growth rate are large enough to compensate for losses into unfavorable layers (see e.g. Ryabov Blasius Review 2008). More precisely the possibility of invasion will depend on the principle eigenvalues of a reaction-diffusion equation, characterizing growth of the biomass (Cantrell and Cosner 2001), a problem which unfortunately may only be solved in some simple cases. Therefore we find it more robust to analyze the intersection of the SSCs rather than their placement with respect to the isoclines.

Fig. 7C demonstrates an example of coexistence. In this figure both curves intersect in such a way, that the SSC of one species is below that of its competitor in an essential part of its favorable range and vice versa. Therefore, both species can coexist because both are superior competitors at different depths. However, if the SSC of a species would lie above that of its competitor then the former would be excluded because it requires higher resources. Analysis of SSCs becomes a useful tool for understanding the role of a UML. The intensive mixing in the upper layer changes the form of system state curves and they can intersect in more intricate ways. Take for instance the situation shown in Fig. 7D. Here we use the same set of parameters as in Fig. 7B, but in the presence of a UML. In this case the main part of the I-species biomass is located close to the surface, while the N-species still forms a DCM. Hence the presence of the UML leaves the SSC of the N-species unaffected while the SSC of the I-species becomes steeper and is shifted in direction of smaller resource values (see also supplementary informations). This fact improves the competing abilities of the I-species. On the one hand the presence of the N-species completely prevents growth of the I-species (as in the case without a UML). On the other hand now the SSC of the I-species lies below the main part of the N-species' SSC, this means that even though the N-species can exist in the presence of the I-species, its fraction should be very small and its influence of the total resource distribution is negligible. Thus the outcome of competition is bistable and depends on initial conditions.

Our investigations show that the analysis of a species' SSC provides a powerful tool for understanding the dynamical behavior and competition in a multi-species system. Especially in the important case, when the spatial size of the areas of positive net growth is equal for both species in monoculture, it is possible to precisely predict the outcome of competition. However we concede that, if the favorable patch sizes of the species are somewhat different, it may be difficult, or even impossible, to analyze the competition

relying solely upon the SSC. Nevertheless, even in this case, if the SSC of a species lies below the zero null growth isocline of the other, the results for competitive exclusion and bistability will still hold true.

Now consider the role of the phytoplankton sinking. In a water column where the diffusivity does not depend on depth, its is easy to show that the washout from a water column can be interpreted as an additional mortality rate. Substituting $P = \tilde{P}\exp\left(-vz/2D\right)$ into Eq. (1), we obtain

$$\frac{\partial \tilde{P}}{\partial t} = \mu\tilde{P} - \left(m + \frac{v^2}{2D}\right)\tilde{P} + D_z\frac{\partial^2 \tilde{P}}{\partial z^2} \ .$$

Note that $\partial_t \tilde{P}$ has the same sign as $\partial_t P$, thereby both functions grow and decline simultaneously. Introduce the new mortality

$$m' = m + \frac{v^2}{4D} \ , \tag{7}$$

and substitute it in the expression for the limiting resource values (6). Since $m' > m$, the new limiting values I'^* and N'^* in the presence of sedimentation should be larger. That results in the shift of the zero net growth isoclines towards the higher values of resources. However, in a well mixed layer the term $v^2/2D$ vanishes, leading to the lower resource requirements. Thus a UML creates more favorable conditions for the sinking phytoplankton biomass.

Finally note that a UML has only one boundary with the unfavorable environment below the euphotic zone. Whereas a deep production layer has two such boundaries, as the diffusion upward and downward from it leads to the additional losses due to either the light or the nutrient limitation. Thereby the loss rate from the UML into the hostile environment is roughly two times smaller than that in the deep layers. That also lowers the requirements for resources in the UML.

Discussion

In this article we investigated the influence of an upper mixed layer on the distribution and competition of phytoplankton species in a water column, in which inverse resource gradients (of light and a nutrient) can limit growth of the biomass. In this system the location of a production layer is not fixed, rather it depends on initial and boundary conditions and on the stage of the process. That, in the presence of differently mixed areas, leads to a plethora of phenomena, including bistability of phytoplankton profiles, changes in the competition outcome, and new critical conditions for survival of a phytoplankton population.

While previous theoretical investigations have usually focused on either a fully mixed or an incompletely mixed system, the presence of a UML requires a combination of these approaches. Including both factors Yoshiyama and Nakajima (2002, 2006) showed the existence of bistability in the spatial distribution of a phytoplankton monoculture. Our work confirms and extends this research on the following key points. Firstly, assuming a gradual change of diffusivity with depth, our modelling approach integrates the whole water column in a single framework. That, for example, allows us to investigate the influence of mixing in both the upper and the lower layers. Secondly, we analyze competition of species, differently adapted to the availability of nutrients and light. As we show, this has drastic effects because the species composition strongly correlates with the spatial patterning. And finally, our analysis includes the case of a stratified lower layer, which is important as some climate models predict the higher water stratification with the increase of temperature caused by global warming (Bopp et al. 2001; Sarmiento 2004).

Bistability of phytoplankton profiles in this system occurs due to the mobility of the production layer, which, in a range of parameters, can be steadily located either within the UML or below it. Both the consumption of nutrient and the self-shading of light are necessary conditions for this behavior. Since the biomass obstructs the upward nutrient flow, it make the upper layer unfavorable, provided that a deep maximum of phytoplankton has established. The shading of light is an opposite mechanism, which prevents growth of the biomass in the lower layers. The third necessary part is the strong mixing in the upper layer, which decouples the locations of the production layer and of the bulk biomass. That prevents drift of the population toward a deep maximum, which would occur in a system without a UML.

Three important factors make a UML more favorable for sinking phytoplankton species. Firstly, it has only one border with the unfavorable environment below it. Therefore the losses to unfavorable layers are roughly two times smaller than those in deep layers, where the unfavorable environment is located below and above the production layer. Secondly, the strong mixing in the upper layer always provides a sufficient propagation velocity, which allows for the persistence of a sinking phytoplankton population. That in particular can support a population of phytoplankton even if the diffusivity in the lower layers vanishes. Thirdly, a UML promotes a nearly uniform distribution of nutrients, that makes the nutrient consumption more efficient and gives an additional competitive advantage for a species inhabiting the UML. Finally note that a deep UML can also play a negative role, as it can lead to the the extinction of species because of the light limitation (Huisman et al. 1999b).

In our investigation, the inclusion of a UML in the single species model allows for the existence of three characteristic density profiles. If the nutrient is the most limiting factor we observe deep biomass maxima, whereas the strong light limitation leads to an upper maximum of biomass. The intermediate resource values may result in the third possible distribution with an essential part of the biomass above and below the thermocline. However, in the largest part of the transient range we observe bistability between an upper and a deep maximum, the emergence of those is determined by the initial distribution of the nutrient.

Outside the bistability range the system possesses only one attractor. However, the transition from an unstable to a stable solution may take a long time and includes two stages. During the first stage, the nutrient concentration reaches a level which allows for the formation of a stable biomass profile. This stage occurs on the slow diffusive time scale and may, for instance, last 5-10 years in deep water. Then the unstable biomass profile transfers into a stable one. The last stage develops on the relatively rapid biological time scale and lasts approximately 10-50 days. Note that this effect is observed only close to the bistability range.

Another important observation is the survival of a sinking phytoplankton population even if the diffusivity in the deep layers cannot prevent the population washout. In the absence of phytoplankton in the deep layers, the nutrient can diffuse upward into the UML, where the population can start to grow as the nutrient concentration reaches a sufficient level. However if the light limitation is not strong enough the biomass shifts into the deeper layers where it cannot outgrow the sinking and ultimately declines being limited by light. Then the cycle repeats. In this sense a strongly light limited species obtains an unexpected competitive advantage as due to the light limitation it is forced to occupy the UML and cannot shift into the deep layers. Note, however, that its biomass might be very small as it will be limited by a weak nutrient flow from the lower layers.

The effects of a UML are even more pronounced in a system that includes two competing species which are differently adapted to the light and the nutrient limitation. To analyze this situation we presented a graphical approach which enables estimation of the competition outcome, based on the equilibrium distribution of each species alone. Moreover, we found that in the range of parameters where the two species can independently form an upper or a deep maximum, the two species model demonstrates bistability both in the spatial distribution and in the competition outcome. Therefore, compared to the single-species model, the bistability range is considerably enlarged. Note that the bistability in the competition outcome was induced by the UML, in a homogeneously mixed water column we observed coexistence of these

species.

Furthermore, we have identified an interesting competitive exclusion effect, where a species can be outcompeted in dependence of its dynamical state. This occurs for low values of deep diffusivity, when the DCM abundance of the N-species becomes oscillatory, however the further reduction of diffusivity favors to the I-species occupying the UML. At the first glance this result is counterintuitive, because usually a decrease of nutrient transport results in an increased depth of the biomass maximum, that should make it even more robust against a competitor in the UML. The replacement of the oscillatory solutions can be understood by considering the mechanism underlying the oscillations. If advection (sinking) is sufficiently strong, reduced mixing leads to population washout from the patch of growth (Shigesada and Okubo 1981; Speirs and Gurney 2001; Huisman et al. 2002b, 2006; Straube and Pikovsky 2007). This allows the nutrient to freely diffuse upward and at a certain moment provides conditions for exponential growth of the biomass. However, if the mixing is weak the biomass sinks again and the cycle repeats. Now suppose that another species is present in the UML. This species can shade light, inhibiting the rapid outburst of the biomass in the lower layers. As a consequence the (non-oscillatory) UCM configuration in the UML is able to replace the oscillatory deep maximum. The importance of low values of diffusivity, in connection with the expected stratification ongoing with future climate change, was emphasized in (Huisman et al. 2006). In this sense our findings are of utmost importance for helping to predict future changes in global phytoplankton patterns.

Supplementary Information

Model details

The model parameters were chosen to describe clear ocean water (Huisman et al. 2006) and can be found in Table 1.

To describe a UML we assume that the diffusivity D_z takes a large constant value D_U in the upper layer (with the depth of $Z_{mix} = 50$ m), a much smaller constant value D_D in the deep layers, and gradually changes from D_U to D_D in a transient layer (width around 10 m, see Fig. 1). The course of the diffusivity can be written in terms of so-called Fermi function

$$D_z = D_D + \frac{D_U - D_D}{1 + e^{(z - Z_{mix})/w}} \ ,$$ (1)

where Z_{mix} is the depth of a UML and the parameter w characterizes the width of the transient layer. In all numerical experiments (with exception of Fig. 3 main paper) we chose $D_U = 50$ cm^2/s, modeling well-mixed waters in the UML, and $D_D = 0.1...1.0$ cm^2/s for the lower layers (Lewis et al. 1986; Smyth et al. 2001; Finnigan et al. 2002).
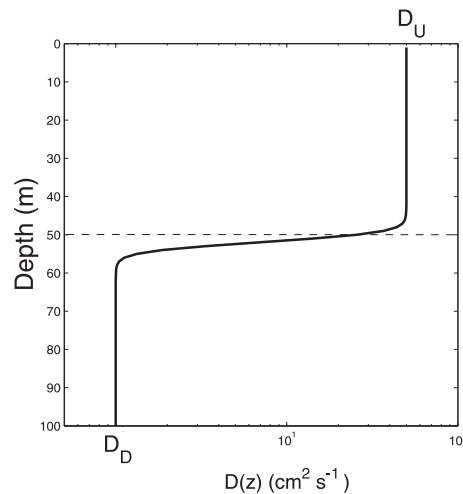

Figure 1: Assumed course of diffusivity, D_z, as a function of depth z (see equation (1)). Dashed line indicates the assumed depth Z_{mix} of the UML.

We assumed impenetrable boundaries at the surface and at the bottom for

the phytoplankton biomass

$$\left(v_i P_i - D_z \frac{\partial P_i}{\partial z} \right)\bigg|_{z=0,Z_B} = 0 \ , \tag{2}$$

and an impenetrable surface and a constant nutrient concentration at the bottom for the nutrient

$$\frac{\partial N}{\partial z}\bigg|_{z=0} = 0, \qquad N(Z_B) = N_B \ . \tag{3}$$

To avoid the influence of initial phytoplankton distributions we used a Gaussian distribution of the biomass with the maximum 1 cell m^{-3} at 70 m depth. Note that if the initial concentration is small then its specific from does not play an important role, more important is the initial nutrient distribution. Simulating bistability, we used two different initial conditions for the nutrient: i) the "nutrient depleted surface", where the initial concentration of nutrient was exactly zero above 70 m depth and increased linearly below; ii) the "nutrient saturated surface", corresponding to initially uniformly distributed nutrients in the water column.

The model was integrated using a backward difference method, based on the finite volume scheme (Pham Thi et al. 2005). For the numerical solution we have discretized all variables on a grid which consisted of 600 points. Diffusion terms were approximated by the second order central discretization scheme, the advection term was represented by the third-order upwind biased formula, integration was made via the trapezoidal rule. The resulting system of ordinary differential equations was solved by the CVODE package (http://www.netlib.org/ode). For model validation we have compared our simulation results with already published results (Huisman et al. 2006) and further verified that the results remain unchanged if we double the number of points in the grid. Furthermore, in some limiting cases it was possible to compare our simulation results with analytical solutions.

Considering only the diffusion process it is possible to estimate the relaxation time of the system $\tau_{rel} \lesssim L^2/(2D)$, where L is the characteristic size and D is the minimal diffusivity. For $L = 300$ m and $D = 0.5$ cm^2/s, we obtain $\tau_{rel} \simeq 9,000$ days $\simeq 25$ years. To make sure that our solutions are steady, in each case we simulated 50,000 system days, which corresponds to about 130 years.

Basic spatial configurations

Fig. 2 shows typical biomass and resource distributions when the single-species system is bistable. The two alternative distributions of the phyto-

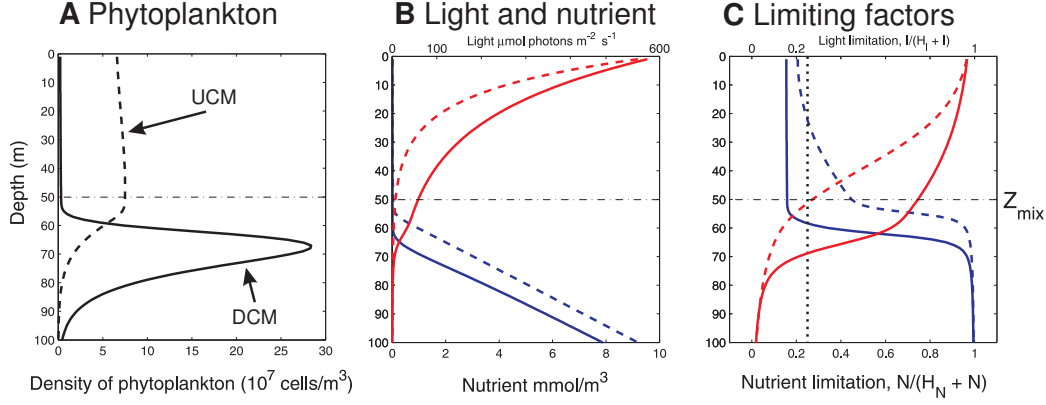**A** Phytoplankton **B** Light and nutrient **C** Limiting factors

Figure 2: (color online) Bistability in the single-species model with a UML. (A) Alternative distributions of phytoplankton biomass, a DCM (solid line) and a UCM (dashed line). (B) Corresponding distributions of the nutrient (blue) and of the light intensity (red). (C) Limitation of growth by the nutrient (blue) and light (red). Dotted black line at $x = m/\mu_{max}$ in Fig.C shows the level of the local zero net growth. The horizontal dash-dotted line indicates the boundary of the UML. Parameters see in Table 1.

plankton biomass $P(z)$ with either a deep or a surface maximum are plotted in Fig. 2A. The corresponding distributions of the nutrient $N(z)$ and light $I(z)$ are presented in Fig. 2B. Note that the nutrient concentration increases linearly with depth below the phytoplankton maximum and is almost zero above it. Fig. 2C shows the level of zero net growth (m/μ_{max}) and the limitations of the growth rate equation (3) by the nutrient and light, separately. The production layer (i.e. the layer where both limitations are higher than m/μ_{max}) is located within the UML when the system demonstrates an upper phytoplankton maximum and below it in the case of a DCM.

Outside the region of bistability a smooth transition from a deep to an upper biomass maximum is possible (Fig. 3). In this transient regime we observe another, intermediate, spatial configuration in which the production layer extends from the UML to the deep layers and the phytoplankton biomass is located in both parts of the water column. Note that in the absence of self-shading of light only such transient patterns can be observed.

Analytical derivations

Total phytoplankton biomass

We now aim for an analytical description of the growth of a species in the single-species model in a steady equilibrium state, so the left parts of the equations (1) and (2) are equal to zero, that is

$$\mu(N, I)P - mP - v\frac{\partial P}{\partial z} + \frac{\partial}{\partial z}\left[D_z\frac{\partial P}{\partial z}\right] = 0 , \tag{4}$$

$$-\alpha\mu(N, I)P + \varepsilon\alpha mP + \frac{\partial}{\partial z}\left[D_z\frac{\partial N}{\partial z}\right] = 0 . \tag{5}$$

Integration of these equations, in view of (2) and (3), yields

$$\int_0^{Z_B} \mu(N, I)P(z)dz - mW = 0,$$

$$-\alpha\int_0^{Z_B} \mu(N, I)P(z)dz + \varepsilon\alpha mW + D(Z_B)N_z(Z_B) = 0 .$$

Here, W denotes the total phytoplankton biomass in the water column

$$W = \int_0^{Z_B} P dz,$$

the notation $N_z(Z_B)$ is a shortcut for the nutrient flux at the bottom $\left.\frac{\partial N(z)}{\partial z}\right|_{z=Z_B}$ Eliminating the integral $\int_0^{Z_B} \mu(N, I)P(z)dz$ from these equations, we obtain the total biomass

$$W = \frac{D_D}{\alpha m(1 - \varepsilon)}N_z(Z_B) . \tag{6}$$

This is a general relation between the phytoplankton biomass and the nutrient flux, which can be interpreted as a conservation law in the system.
In the area free of the phytoplankton biomass, equation (5) gives

$$D(z)N_z(z) = \text{const} .$$

This equation corresponds to the stationary diffusion flow and the linear distribution of nutrients below the phytoplankton maximum (Fig. 2B).
If the total phytoplankton biomass is located within the UML, we can neglect with the remineralization occurring below the UML (the second term in equation (5)). Therefore, the nutrient flow can be estimated as

$$D(z)N_z(z) = D_D\frac{N_B - N^*}{Z_B - Z_{mix}} ,$$

where N^* is the concentration of the nutrient within the UML (see equation (6)). Substituting this in equation (6), we obtain the total phytoplankton biomass in the UML

$$W = \frac{D_D}{\alpha m(1-\varepsilon)} \frac{N_B - N^*}{Z_B - Z_{mix}} \ .$$ (7)

This estimation is in excellent agreement with the numerical results (Fig. 4 main paper) with exception of the region of high diffusivity D_D and nutrient concentration N_B, in which the growth of phytoplankton biomass is limited by light and does not depend on the nutrient concentration.

Border of the stability of a UCM

As mentioned in the text, a UCM is stable if the light intensity below a UML is smaller than the critical light intensity I^*, see equation (6). Using equation (4), we obtain

$$I_{in} \exp\left[-K_{bg}Z_{mix} - k\int_0^{Z_{mix}} P(z)dz\right] < I^* \ .$$ (8)

If the total phytoplankton biomass is located in the upper mixed layer, then equations (7) and (8) give the following criteria of stability of the upper maximum

$$\ln\left(I_{in}/I^*\right) - K_{bg}Z_{mix} < \frac{D_D(N_B - N^*)k}{\alpha m(1-\varepsilon)(Z_B - Z_{mix})} \ .$$ (9)

This line is shown in Fig. 4A and 4B in the main paper as the lower boundary of the bistability range and is in a good agreement with the numerical simulations. One might argue that we should apply the correction (Eq.(7)) to calculate the critical light intensity below the UML, as we did it considering competition of species. The reason to use equation (7) without this correction is the following. A new species can invade a system and change the resource distribution only if its net growth rate is positive, thus we need this correction to estimate the outcome of competition. However, in the single-species system an essential part of biomass is already located below the thermocline just because of sinking from the UML. Being limited by light, this part cannot also consume the nutrient. Whereas a higher light intensity increases the nutrient consumption and can initiate a positive feed back, as the nutrient consumption in the lower layers will reduce the biomass in the UML, improving the illumination of the lower layers. Thus the conditions when a DCM replaces a UML in a single-species model are weaker, than those in a

two species model. As a result the bistability range in the two-species model is extended towards the lower resource values (Figs. 4B and 4D in the main paper, respectively).

Slope of the system state curve

Integration of Eqs. (4) and (5) over z in the interval $[0; z']$ yields

$$\int_0^{z'} \mu(N, I)P(z)dz - mW(z') - vP(z') + D(z')P_z(z') = 0,$$

$$-\alpha \int_0^{z'} \mu(N, I)P(z)dz + \varepsilon\alpha mW(z') + D(z')N_z(z') = 0 .$$

where $W(z') = \int_0^{z'} P(z)dz$ denotes the total phytoplankton biomass above depth z'. The integral $\int_0^{z'} \mu(N, I)P(z)dz$ can again be excluded from these equations yielding

$$N_z(z') = \alpha \left[\frac{m(1 - \varepsilon)W(z')}{D(z')} - P_z(z') + \frac{vP(z')}{D} \right] .$$

Taking derivative of (4), we obtain

$$\left.\frac{\partial \ln I}{\partial z}\right|_{z=z'} = -K_{bg} - kP(z') .$$

In equilibrium all partial derivatives can be changed to the ordinary ones. Then the last two equations yield the following expression for the slope of the system state curves

$$\left.\frac{d \ln I}{dN}\right|_{z=z'} = \frac{-K_{bg} - kP(z')}{\alpha \left[\dfrac{m(1 - \varepsilon)W(z')}{D(z')} - P_z(z') + \dfrac{vP(z')}{D} \right]} . \tag{10}$$

Fig. 5 shows a typical view of the system state curve, when the phytoplankton maximum is located in deep layers (DCM). This curve can be divided into three parts. The fist one (above the phytoplankton biomass) is a vertical line in the (N, I)-plane. It is clear from equation (10), that in the area where $P(z)$, $P_z(z)$ and $W(z)$ equal zero

$$\frac{d \ln I}{dN} \to -\infty .$$

The lower part of the curve settles below the biomass, where $P(z)$, $P_z(z)$ are zero and $W(z) = W$. In the semilog scale (Fig. 5B) this can be seen as a limiting line with slope

$$\frac{d\ln I}{dN} = -\frac{K_{bg}D_D}{m(1-\varepsilon)W} \ .$$

The slope of the middle part of the system state curve depends on the distribution of phytoplankton biomass and diffusivity. We are especially interested to know how the intensity of mixing D_D influences the species competitive abilities. Here we restrict to the case when the mixed layer is much smaller than the critical depth (Sverdrup 1953; Huisman et al. 1999b), in other words, we neglect the water turbidity. Then, on the one hand, an increase of the diffusivity $D(z')$ decreases the gradient of biomass $P_z(z)$, therefore, it decreases both terms in the denominator of Eq. (10) and the system state curve becomes steeper. On the other hand the top left end of the curve cannot deviate too much, because its coordinates are I_{in}, which cannot be changed, and N_{out}, which can deviate only slightly, because it should be less than or equal to N^* (which is already very small). Therefore when the curve becomes steeper only its lower part can move to the left in the direction of smaller resource values – a fact which improves the species competitive abilities (see Fig. 7D in the main paper). Note that an increase of the sinking velocity leads to opposite effects, as it increases the denominator and, thereby, increases resource requirements.

System without a UML

The competition outcome between the two species in the (N_B, D_D) coordinate plane is presented more systematically in Fig. 6. In the system without a UML (Fig. 6A) coexistence is possible only at sufficiently small values of D_D and N_B, so that the I-species can use its advantage of low nutrient limitation. Even in this region only a small fraction ($< 10\%$) of the I-species may coexist with the N-species. In the presence of a UML the competition results are for better visualization divided into two plots, corresponding to the maximum of phytoplankton density below the UML (Fig. 6B) and within it (Fig. 6C). If the maximum of biomass is located below the UML (low values of N_B and D_D in Fig. 6B) the results are similar to the case without UML, however, the persisting fraction of the I-species is larger (up to 30%) since the UML improves its competing abilities. For larger values of N_B and D_D (Fig. 6C) the system becomes bistable and the I-species can win and form a UCM (compare to the border of the bistability range in Fig. 4C of

the main paper). Further, the area where only the N-species wins becomes smaller. Also an upper maximum of the I-species appears at low values of D_D instead of an oscillatory deep maximum (see previous section). Thus, the presence of a UML changes the result of competition in such a way that it is favoring the species within the UML.

Influence of the UML on the competition outcome

Fig. 7 shows several sections of the three-dimensional parameter cube for different values of D_D. The fist column shows the position of the biomass and the region of bistability, the last two columns present the species composition below the UML (middle column) and within the UML (right column). In general, the bistability range grows with decrease in the diffusivity and the part of the upper maximum decreases. But if the diffusivity becomes very small, then the system dramatically changes the behavior and only the upper chlorophyll maximum can persist. Also note, that the N-species wins the UML in the case of sufficiently large nutrient concentration within it, whereas the I-species can survive in the mixed layer only in the bistability range. This observation coincides with the field results (Venrick 1993), where N-species were found in both layers, whereas I-species were only found in the upper layer.

Table 1: Parameter values and their meaning

Symbol	Interpretation	Units	Value
Independent variables			
t	Time	h	-
z	Depth	m	-
Dependent variables			
$P(z,t)$	Population density	cells m^{-3}	
$I(z,t)$	Light intensity	μmol photons m^{-2} s^{-1}	
$N(z,t)$	Nutrient concentration	mmol nutrient m^{-3}	
Parameters			
I_{in}	Incident light intensity	μmol photons m^{-2} s^{-1}	600 (100 - 600)
K_{bg}	Background turbidity	m^{-1}	0.045
k	Absorption coefficient of a phytoplankton cell	m^2 cell^{-1}	6×10^{-10}
Z_B	Depth of the water column	m	300
Z_{mix}	Depth of the upper mixed layer	m	50
w	Characteristic width of the thermocline	m	1
D_D	Vertical turbulent diffusivity in the deep layers	cm^2 s^{-1}	0.3 (0.1 - 1)
D_U	Turbulent diffusivity in the UML	cm^2 s^{-1}	50
μ_{max}	Maximum specific growth rate	h^{-1}	0.04
H_I	Half-saturation constant of light limited growth for N- and I-species, respectively	μmol photons m^{-2} s^{-1}	20; 98
H_N	Half-saturation constant of nutrient limited growth for N- and I-species, respectively	mmol nutrient m^{-3}	0.0425; 0.015
m	Specific loss rate	h^{-1}	0.01
α	Nutrient content of phytoplankton	mmol nutrient cell^{-1}	1×10^{-9}
ε	Nutrient recycling coefficient	dimensionless	0.5
v	Sinking velocity	m h^{-1}	0.042
N_B	Nutrient concentration at Z_B	mmol nutrient m^{-3}	50 (5-100)

Table 2: Acronyms

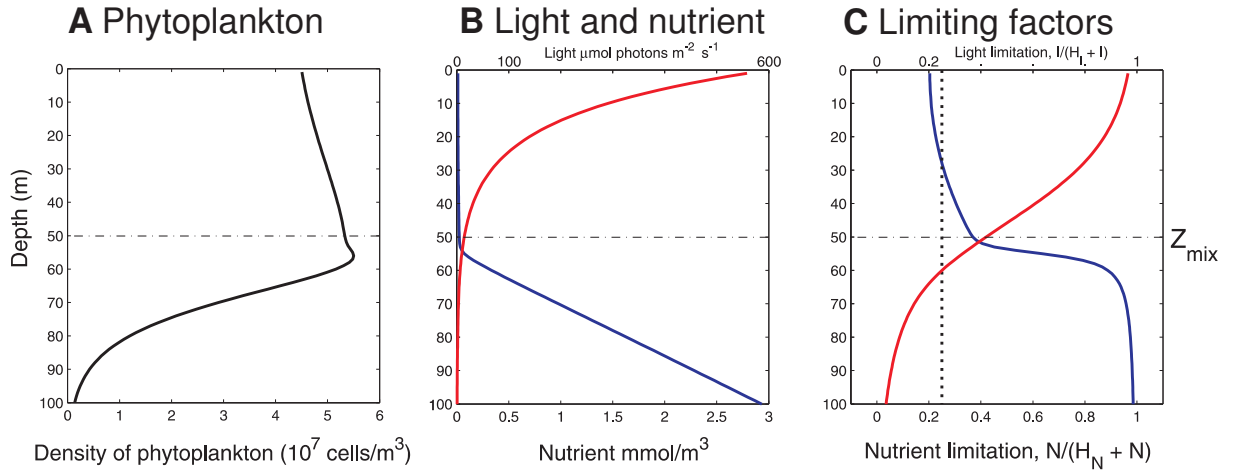| Symbol	Interpretation
DCM	Deep chlorophyll maximum
ODCM	Oscillatory or chaotic deep chlorophyll maximum
UCM	Upper chlorophyll maximum
UML	Upper mixed layer
SSC	System state curve

Figure 3: (color online) Intermediate spatial configuration. See Fig. 2 for description. Parameters: $N_B = 16$ mmol/m^3, $D_D = 0.8$ cm^2/s
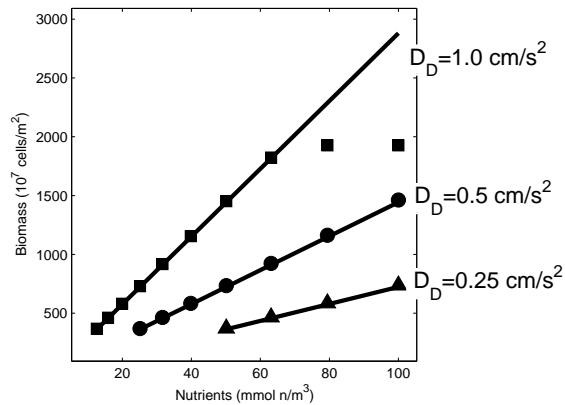

Figure 4: Total phytoplankton biomass W as a function of the bottom nutrient concentration N_B for different values of the deep turbulent diffusivity D_D. Comparison of the results from equation (7) (solid lines) with the numerical simulation (symbols).
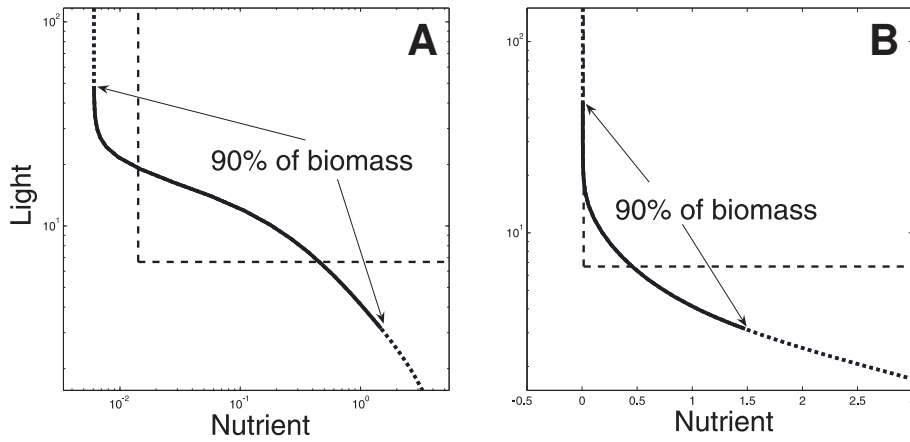
Figure 5: Two different visualizations of the system state curve of the light intensity versus the nutrient concentration, either on log-log scale (A) or using a log-linear scale (B).
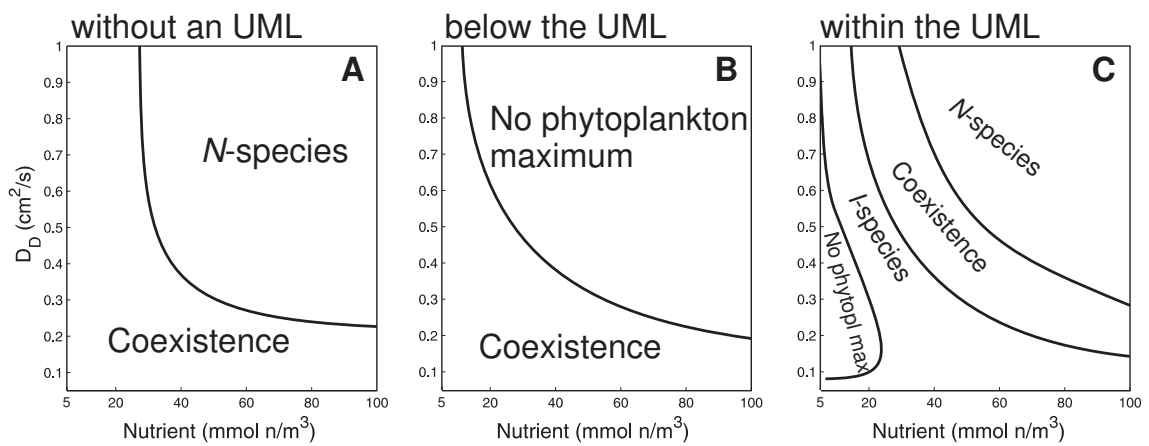

Figure 6: Competition outcome of the two-species system. (A) species composition in system without UML. (B) and (C) similar in the presence of a UML, however separated according to the contribution below the UML (B) and within the UML (C).
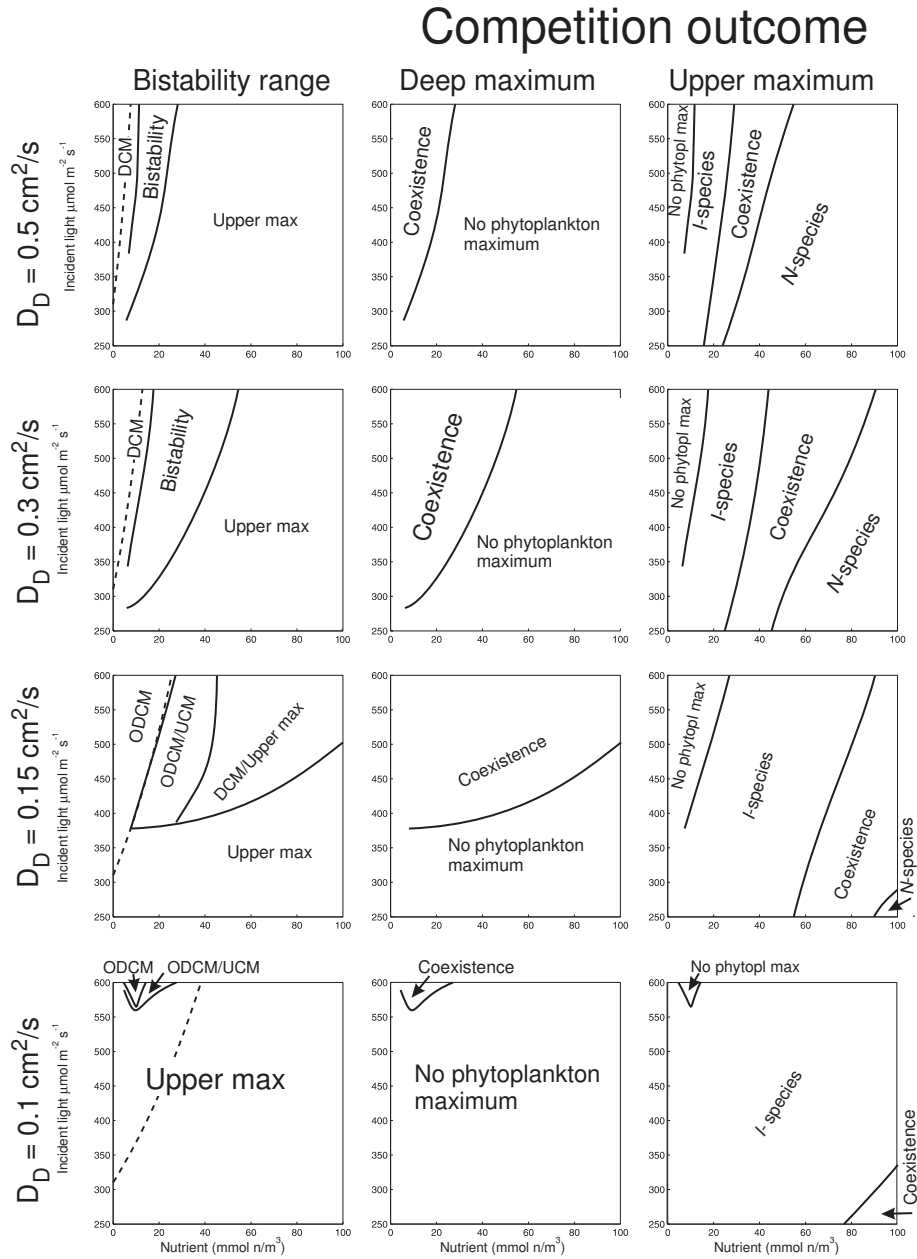
Figure 7: Bistability region(left) and the outcome competition in the lower layers (middle) and in the UML (right) of the I- and N-species for different deep diffusivities $D_D = 0.5,\ 0.3,\ 0.15,\ 0.1\ \ \mathrm{cm^2/s}$ are depicted from top to bottom. DCM and ODCM are the areas of deep and oscillatory deep maxima respectively, UCM denotes the area of upper (surface) maxima.

Importance of linking patterns and weak links for food web stability

Thilo Gross, Lars Rudolf, Ulf Dieckmann and Simon A. Levin

Since the publication of Robert May's seminal work (May , 1972) the stability of ecological food webs is a topic of intense research and hot debate (Cohen & Newman , 1985; King & Pimm , 1983; McCann , 2000, 1998; Montoya et al. , 2002; Emmerson & Raffaelli , 2004; Navarrete & Berlow , 2006; Kondoh , 2003). Contrary to many field observations, May showed that large, densely connected food webs are *in general* unstable. The only way to reconcile May's proof with observation is to find the special properties that lend natural food webs their unusual stability. It has been pointed out that the identification of such stabilizing network properties could have broad implications beyond the field of ecology (May et al. , 2008). Most recent theoretical work focuses on numerical models based on explicit rate equations (McCann , 1998; Brose et al. , 2006). These and empirical studies (Neutel et al. , 2002, 2007) have revealed that weak trophic links may play an important role for stability. However, in contrast to May's abstract random matrix model, numerical constraints limit most simulative studies to the investigation of relatively few instances (approx. 10000) of relatively small food webs (approx. 10 species). Recently, generalized modeling, a novel numerical approach for the analysis of stability in families of nonlinear rate equations, has been proposed (Gross & Feudel , 2006). Here we utilize this approach to study several billion instances of food webs of up to 50 species with nonlinear interactions. While we find a stabilizing effect of weak links in small food webs, this stabilization is absent in larger webs. Instead, we identify a universal feature in the distribution of links that is important for stability.

Generalized modeling (GM) is based on the insight that the computation of steady states is in general much more difficult than the investigation of the local dynamics around them. If a steady state is given, it is possible to compute its stability from the corresponding Jacobian matrix, which requires little information and can be done at low computational cost. Using the approach of GM the Jacobian of an arbitrary steady state can be written

as a function of a small number of *bona fide* parameters (Steuer et al. ,
2006) that capture the required information on the system and the steady
state. Thus, GM allows us to describe a system on an intermediate level of
abstraction; it offers better numerical performance than conventional models,
but more interpretability than random matrix models.

Like random matrix models, GMs focus on the local asymptotic stability of
steady states. Although food webs could in principle also persist in non-
steady states, the population densities should at least be stationary on the
scale of decades. Thus, we ask what features should be included in a model
to describe this stable stationarity.

The advantage of the GM approach is, that it can be applied simultaneously
to large families of similar systems. In Gross & Feudel (2006) the Jacobian
for steady states in a food web of arbitrary size and topology and with
arbitrary nonlinear predator-prey interactions has been derived. Effectively
this GM provides a parameterization of all possible steady states in a large
class of food webs. Thereby it allows us to ask in which types of webs stability
is likely.

The parameters identified by GM fall into two basic classes: *Scale parame-
ters* determine the topology and turnover of the biomass fluxes. *Exponent
parameters* measure the local nonlinearity of the functions in the model. For
mononomial functions the corresponding exponent parameter is the expo-
nent of the monomial. For instance, a linear function would correspond to a
parameter value of one, a quadratic functions to a value of two, and a square
root to a value of 0.5. However, we do not restrict the functional forms
in the model to monomials. For general functions, the exponent parameter
measure the sensitivity of a process to a variable and is closely related to the
curvature of the function in the steady state.

To reduce the number of parameters in the model, we assume that for all
species except top predators natural mortality can be neglected in compari-
son to predation. Moreover, we focus on the case of passive prey switching:
Predators preying on multiple species, consume each of them indiscrimi-
nately, without any preference. But, their diet depends on prey availability
as well as their ability to capture the prey.

Even with the simplifications described above the number of parameters in
the food web GM is still relatively high. This is a direct consequence of the
complexity of the problem (we parameterize every steady state in a large class
of food webs) and therefore cannot be avoided. Although we are thus faced
with having to explore a large parameter space, the numerical performance of
GM enables us to consider ensembles of a large number of randomly chosen
sample parameter sets. The realistic ranges from which the parameters have
to be chosen, are known from the GM and basic biological reasoning. Under

these conditions well-founded statistical conclusions can be drawn.

In order to obtain credible results we restrict the investigation to realistic food web topologies. These topologies are generated by the niche model (Williams & Martinez , 2000), which is based on ecological reasoning regarding the prey that can possibly be devoured by a given species of predators. We only consider topologies that consist of a single connected component. Moreover, double links, self links (cannibalism), and circular trophic relationships (e.g. through parasitism) are avoided. The timescale of biomass turnover for the species is chosen according to an allometric scaling relationship.

One notable difference between many random matrix models and the GM lies in the diagonal entries of the Jacobian, which are particularly important for stability. In many random matrix models these terms are assumed to be -1 (for instance May (1972)). The negative diagonal entries mean, that without interactions between the components, the system has to be stable. By contrast, the GM shows that diagonal entries for all species except primary producers and top predators should be positive under realistic conditions (see supporting material).

To assess the dependence of the stability on basic parameters we generate a sample of 10^8 food webs with 10 species each. In this sample the basic parameters are drawn randomly from a uniform distribution. We estimate the impact of the individual parameters on stability by computing the correlation between parameter values and the stability. The results of this sensitivity analysis are shown in Fig. 1. The prey-dependence of the predation, γ, and the exponent of closure, μ, correlate positively with stability. This corresponds to the well known fact, that low saturation of predators (Brose et al. , 2006) and nonlinear mortality of the top-predators promote stability. By contrast, the sensitivity of primary production on the number of primary producers, ϕ, and the sensitivity of predation on the density of the predator, ψ, are negatively correlated with stability. This confirms that stability is increased if primary production is strongly limited by external factors such as nutrient availability, or if the predator-dependence of predation is reduced, for instance in ratio-dependent predation. The total range of timescales t_{scale} as well as the total range of niche values n_{range} do not correlate with stability. However, the average difference in the niche value of predator and prey, n_{diff}, has a stabilizing effect, confirming that time scale-separation in the individual predator-prey interactions promotes stability (Brose et al. , 2006). Finally, our analysis confirms that the number of links is negatively correlated with stability. It thus shows that increasing connectivity *in general* corresponds to decreasing stability.

Repeating the analysis described above for food webs of 20 species yields a similar result (Fig. 1). The main difference is that the relative importance
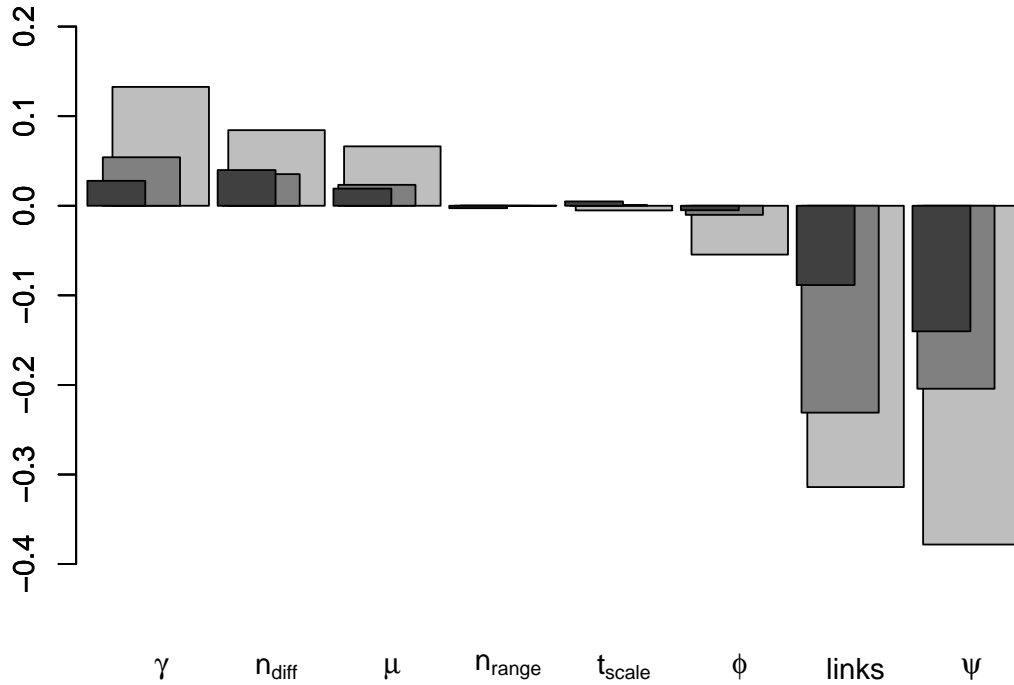
Figure 1: Correlation of food web parameters with stability. Shown is data from 10^8 randomly generated food webs with 10 species (light grey) and 20 species (dark grey). Error bars are on the scale of the line width. High sensitivity of predation to prey abundance γ, large scale separation between predator and its prey n_{diff}, and high exponents of closure μ promote stability. By contrast, high sensitivity of primary production to the number of producers, ϕ, a large number of links, and a high sensitivity of predation to the number of predators, ψ, have a destabilizing effect. The total range of niche values, n_{range}, and the total range of time scales, t_{scale}, spanned by the food web have little effect on stability.
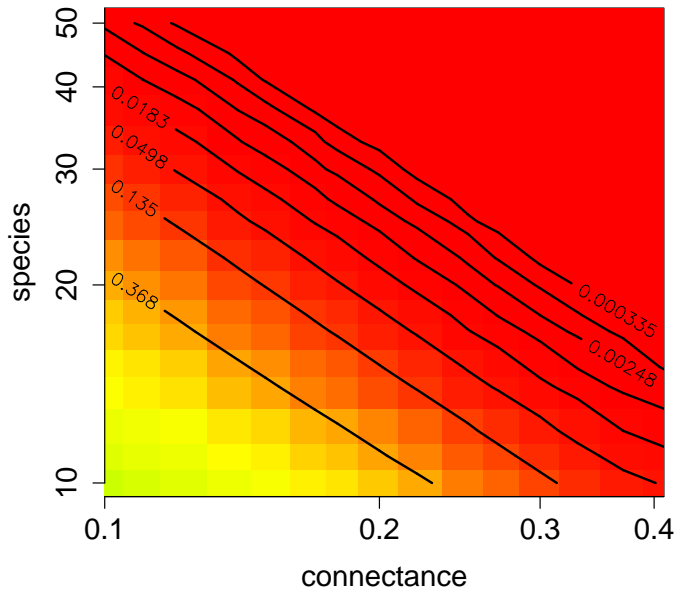
Figure 2: Double-logarithmic histogram of the stability of niche model food webs, depending on the number of species N and the connectance c. The fraction of stable webs found in a bin is color coded. The shape of the surface in the histogram is further highlighted by logarithmically spaced level lines. The level lines follow the power law $N = c^{-p}$, with $p = 0.9$.

of the total number of links is increased, which is reasonable for a larger web. Also repeating the sensitivity analysis with pyramidal food webs yields similar results (not shown). In the following we set the basic parameters to realistic values (see methods) and focus on the topology.

Let us start by investigating the relationship between number of species, N, the number of links, L, and the stability in more detail. For this purpose we measure the number of links in terms of the *connectance* $C = L/(N(N-1))$, which is related to the fraction of potential links that are realized in a given topology. We generate samples with random niche model topologies in such a way that the number of species and the connectance forms a discrete logarithmic lattice. From these samples we compute the density of stable webs (the probability of randomly drawing a stable food web) for given values of N and C. Figure 2 shows a double logarithmic plot in which the density is color coded. In total the figure contains data from more than 5 billion

webs. As expected the density of stable webs decreases with increasing N and C. Note however, that iso-stability lines are almost perfectly straight, corresponding to a power law with an exponent $p = 0.9$.

We have repeated the analysis described above several times with different basic parameters. The scaling exponent p depends on the choices of parameters and is therefore not universal. However, we have obtained power-law scaling in every case.

Having explored the basic relationship between connectance and stability, let us now move on to the investigation of weak links. It has been criticized that many competing definitions of weak links are used in the literature (Berlow et al. , 2004). Since we can scale the biomass flux in the web without changing the stability, weak links cannot be identified based on the absolute biomass flux alone. What we mean by weak links is that certain connections are much weaker than other *comparable* links. The notion of weak links is therefore connected to the coefficient of variation (CV) of link strength (Jansen & Kokkoris , 2003; Navarrete & Berlow , 2006). Moreover, we have to take into account that the biomass flux in higher trophic levels is much lower than in lower trophic levels because of allometric scaling. We therefore have to normalize the biomass flux appropriately before computing the CV. In the following we measure the presence of weak links as the CV of all predative biomass fluxes normalized individually by the total growth rate received by the respective predator. An alternative, prey-centric, measure is to use the CV of the biomass fluxes normalized by the the total loss rate of the respective prey.

To explore the impact of weak links, we generate a large ensemble of food webs in which all link strength are drawn from a uniform distribution. In Fig. 3 we plot the fraction of stable webs, that are generated in this way as a function of observed CV in the webs.

In very small food webs (e.g. $N = 5$, not shown) there are large jumps of stability as a function of CV. These jumps appear since a given web topology can only yield CVs in a certain range; If we vary the CV new topologies become available, which can have different stability properties. In small webs the number of possible topologies is relatively small. Therefore, a notable jump in the stability is observed as soon as the CV enters the range of a new topology. By contrast, in larger webs the number of topologies is combinatorially large. Therefore the stability as a function of the CV becomes a smooth curve approximately at $N = 10$.

In small and intermediate webs ($N < 30$) the stability of the web increases with increasing CV (see Fig. 3), confirming the stabilizing effect of weak links reported in the literature (e.g. McCann (1998)). However, in larger webs with $N > 30$ species this relationship is reversed: now increasing the CV
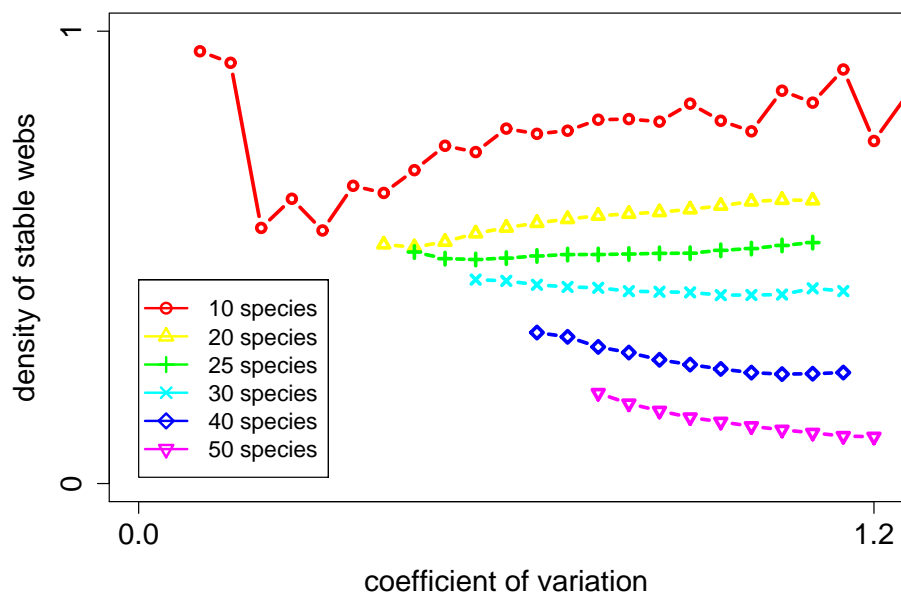
Figure 3: Dependence of stability on the weak links. The density of weak links is measured in terms of the coefficient of variation normalized to total loss of the respective predator species. In small food webs an increasing link variability corresponds to an increase in stability. However, in larger webs the opposite is the case: increasing variability decreases the stability.

decreases stability.

Repeating the study with the alternative prey-centric measure for weak links proposed above yields a slightly different result. In this case the overall trend is that high CV corresponds to low stability, regardless of web size. However, in small webs there is a local stability maximum at intermediate CVs, so that increasing the CV is stabilizing in a certain range. In larger webs this maximum becomes less pronounced and eventually disappears. Therefore, also with the alternative measure, we find that increasing link variability decreases stability in large food webs.

The results presented above suggest that the specific topologies play a significant role for the stability of food web. In principle the approach of GM could be used for an exhaustive search for stabilizing properties, such as specific patterns or motives. Since this search exceeds the scope of this Letter, let us focus on one particular result: We investigate whether the effect of links can depend on the position of a species in the food web. For this purpose we generate an ensemble of food webs with fixed *connectivity* $k = L/N$. We then take each individual web and assign a rank parameter p to each species according to its trophic position. The parameter p is normalized to the interval [0,1], so that the most basal species in a web always corresponds to $p = 0$ while the most apical species corresponds to $p = 1$. For all species with a given rank parameter we can then compute a) the correlation between stability and the number of predators preying on the species, and b) the correlation between stability and the number of prey species consumed by the species. The results of this analysis are shown in Fig. 4.

Figure 4 A shows the effect of the number of predators on stability as a function of the rank parameter. For species with low rank ($p < 0.25$) the number of predators correlates negatively with stability, indicating that increasing the number of predators preying on these species has generally an destabilizing effect on the system. Likewise the correlation is negative for species with high rank ($p > 0.75$). However, there is a large intermediate region ($0.25 < p < 0.75$) in which the correlation is positive. This shows that, for a given number of links, the stability is increased if predators prey mainly on species of intermediate trophic position.

The correlation of stability with the the number of prey species is shown in Fig. 4 B. For species with small rank parameters ($p < 0.719$) the number of prey species correlates negatively with stability, while a positive correlation is found for species with a high rank parameter ($p > 0.719$). This indicates that, for a given number of links, it advantageous to have generalist predators at the top of the food web and specialist predators below. Interestingly, the rank parameter $p = 0.719$ at which the crossover from negative to positive correlation takes place is independent of the number of species in the web or
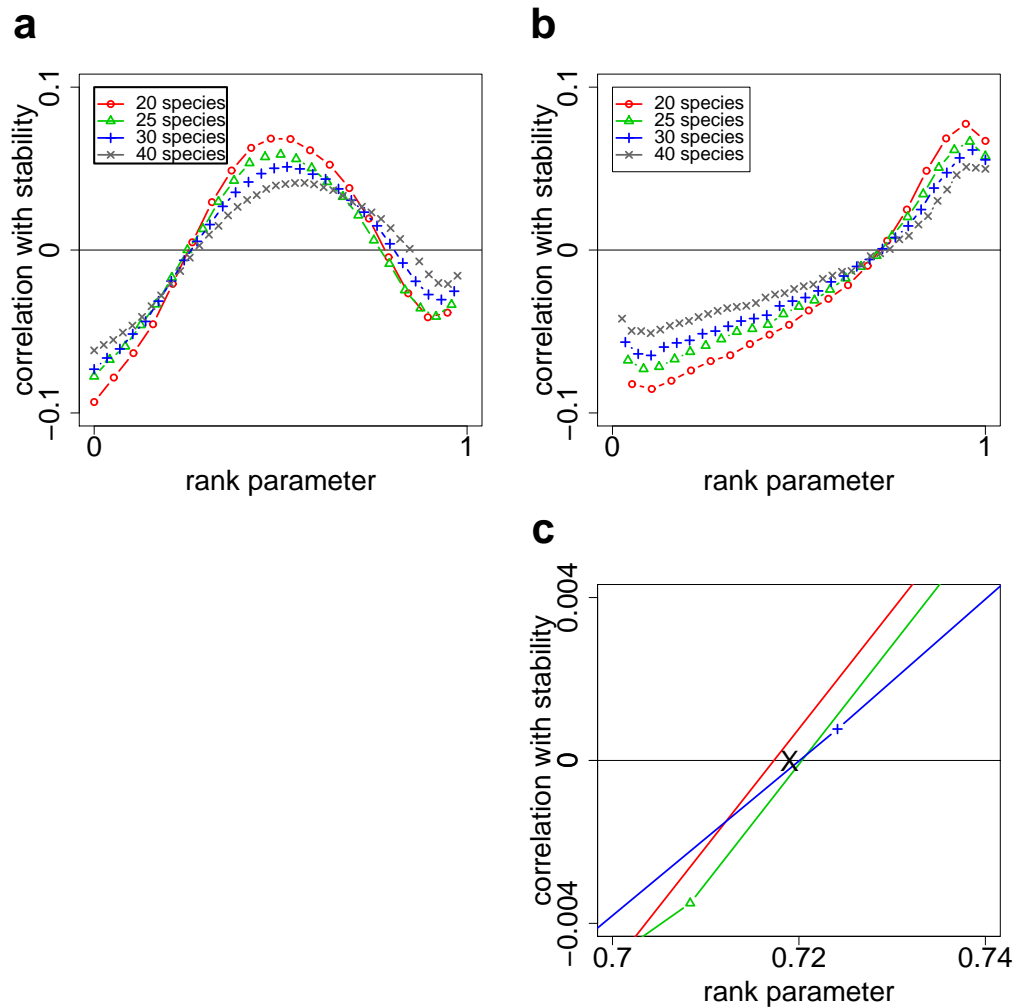
Figure 4: Effect of the distribution of links within the food web. a) The correlation of the number of predators preying on a species with stability, depending on the position of the species in the web (rank). Stability is enhanced if most species prey on intermediate consumers, characterized by rank parameters around 0.5. The correlation of stability with the number of prey species (b) shows that generalist predators preying on specialist enhance the stability. Note that all curves intersect in one point of vanishing correlation at a rank parameter of approx. 0.719 (c).

the connectivity. In additional investigations (not shown) we have confirmed that the location of the crossover point does not depend on the absolute number of links or species or on details of the predator-prey interaction. Based on these results we believe that the crossover point is a *universal feature.*

In this paper we have investigated the impact of different parameters on the asymptotic stability of steady states in food webs. While it was often pointed out that food webs can persist in non-stationary states, there is growing evidence that May's stability-complexity relationship also holds for non-stationary dynamics (Sinha & Sinha , 2005). In particular, population cycles or external forcing are averaged out if we consider the food webs on longer timescales. On these timescales the dynamics is effectively stationary. In this paper we have specifically focused on the question, which properties of natural food webs have to taken into account, to reproduce the astonishing stability in large model food webs.

A likely, though controversial, explanation why real world food webs are stable is that they have evolved for stability. However, this explanation does not answer the question addressed in this paper; Even if food webs have evolved for stability, one would still like to know what are the features that have evolved in order to protect them and possibly utilize them in bio-mimetic technical networks.

Our analysis shows that the presence of weak trophic links alone is only stabilizing in relatively small food webs. In larger food webs increasing the coefficient of variation of normalized link strength destabilizes the food web. Instead, our results point to another topological feature: For a given number of links it is advantageous if species with a high trophic position feed on many different prey species, while intermediate consumers are fed upon by multiple predators. This corresponds for instance to generalist top-predators preying on intermediate specialist predators – a pattern that is obvious for instance in the empirical data reported in Neutel et al.   (2002, 2007). Moreover, this insight is consistent with, but more general than, the stabilizing effect of top-predators that couple several distinct energy channels (Rooney et all. , 2006).

Our results have been obtained with a new method that allows us to base our conclusions on a large ensemble of individual food webs. In the present work this ensemble consisted of several billion individual webs. Using the same framework it is possible to analyze the effect of many other mechanism that have been proposed as explanations for stability, such as active prey switching, cannibalism or the presence of trophic loops. In order to solve the enigma of the stability of natural food webs further studies are clearly necessary. We believe that the approach proposed here will continue to contribute

to this ongoing effort.

Methods

Food web generation.

Following Williams & Martinez (2000), each species S_i is assigned a niche value n_i, randomly drawn from an uniform distribution within the interval [0,1]. A specie's rate of biomass turnover α_i is chosen according to the allometric scaling relation $\alpha_i = t_{\text{scale}}{}^{n_i}$. A species S_i consumes all species S_j with a niche value $n_j \in \left[c_i - \frac{r_i}{2}, c_i + \frac{r_i}{2}\right]$, where the feeding range r_i is drawn randomly from a beta distribution within an interval $[0, n_i]$ and the center of the range c_i is drawn uniformly from the interval $\left[\frac{r_i}{2}, n_i - \frac{r_i}{2}\right]$. All species which don't feed on another species are assumed to be primary producers. In most computations we chose similar link strength l_{ij} with small variations drawn from a Gaussian distribution. These variations are necessary to avoid degenerate cases. The standard deviation of the distribution is 10% of the mean links strength. Only in the investigation of weak links (Fig. 3) the link strength is drawn from a uniform distribution with arbitrary range. Webs that decompose into unconnected components are rejected.

Stability analysis.

We consider a food web as stable if all eigenvalues of the corresponding Jacobian are smaller than -10^{-6}. As shown by Gross & Feudel (2006), the diagonal elements of a food web's Jacobian can be written as

$$J_{i,i} = \alpha_i \left[\widetilde{\rho}_i \phi_i + \rho_i \psi_i - \widetilde{\sigma}_i \mu_i - \sigma_i \left(\sum_{m=1}^{N} \beta_{m,i} \lambda_{m,i} \left[(\gamma_m - 1)\chi_{m,i} + 1 \right] \right) \right] \quad (1)$$

and the non-diagonal elements as

$$J_{j,i} = \alpha_n \left[\rho_j \gamma_j \chi_{j,i} \lambda_{j,i} - \sigma_j \left(\beta_{i,j} \psi_i + \sum_{m=1}^{N} \beta_{m,j} \lambda_{m,i} (\gamma_m - 1)\chi_{m,i} \right) \right] \quad (2)$$

The parameter contained in these equations are given in Tab. 1

Correlation coefficients.

To asses the impact of the parameters on stability we compute the correlation of the parameter values with stability in an ensemble of size N. The

Table 1: List of model parameters

Parameter	Interpretation	Value	Range
α_i	turnover rate of species i	$t_{\text{scale}}{}^{n_i}$	[0.008,1]
$\beta_{i,j}$	contribution of predation by i to loss rate of species j	$l_{ij}/\sum_k l_{kj}$	[0,1]
γ_i	nonlineatity of predation with respect to prey density	0.95	[0.5,1.5]
$\lambda_{i,j}$	exponent of prey switching	1 (passive switching)	-
μ_i	exponent of closure	1	[1,2]
n_i	niche value of species i	-	[0,1]
ρ_i	fraction of growth gained by predation	0 (producers)	-
		1 (consumers)	-
$\widetilde{\rho}_i$	fraction of growth gained by production	$1 - \rho_i$	-
σ_i	fraction of mortality by predation	0 (top predators)	-
		1 (others)	-
$\widetilde{\sigma}_i$	fraction of non-predative mortality	$1 - \sigma_i$	-
t_{scale}	total time scale separation	0.008	[0,1]
ϕ_i	nonlinearity of primary production	0.5	[0,1]
$\chi_{i,j}$	contribution of species i to the prey of j	$l_{ij}/\sum_k l_{ik}$	[0,1]
ψ_i	nonlineatity of predation with respect to predator density	1	[0.5,1.5]

correlation coefficient is given by

$$\text{cor} = \frac{\sum_{n=1}^{N_s} \bar{X}_n - \frac{Ns}{N} \sum_{n=1}^{N} X_n}{\sigma_X \sigma_S / N} \tag{3}$$

where X_n and $\bar{X}_n$ are the parameter values in the stable webs and in the entire ensemble, respectively, and N_s is the number of stable webs. The quantity σ_{x} denotes the standard deviation of the parameters and σ_{s} denotes the standard deviation of the stability s_i, with $s_i = 1$ for stable and $s_i = 0$ for unstable webs.

Supplementary Information
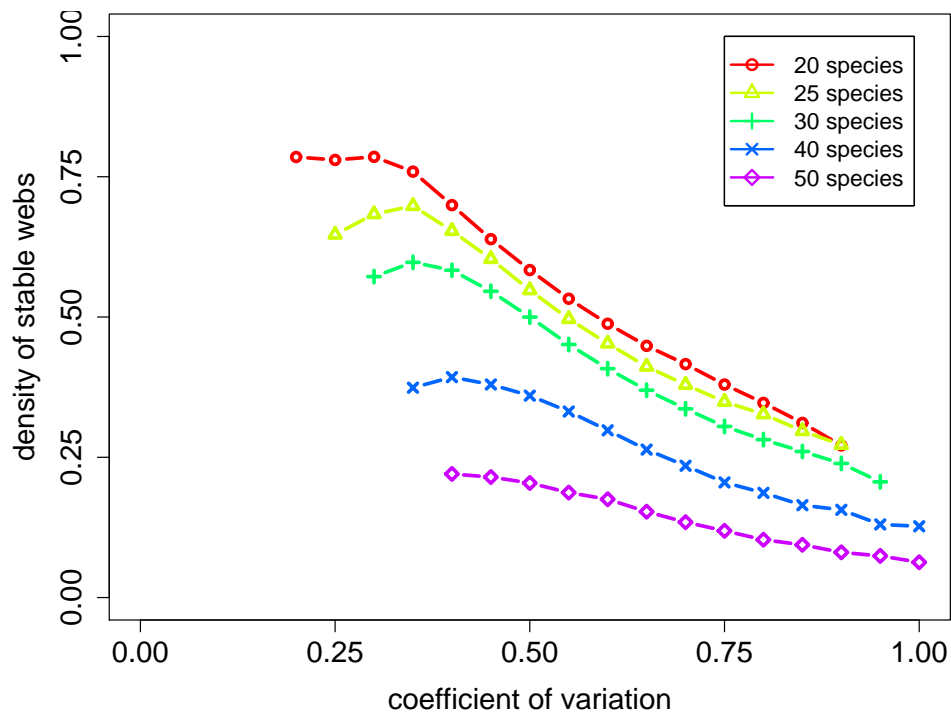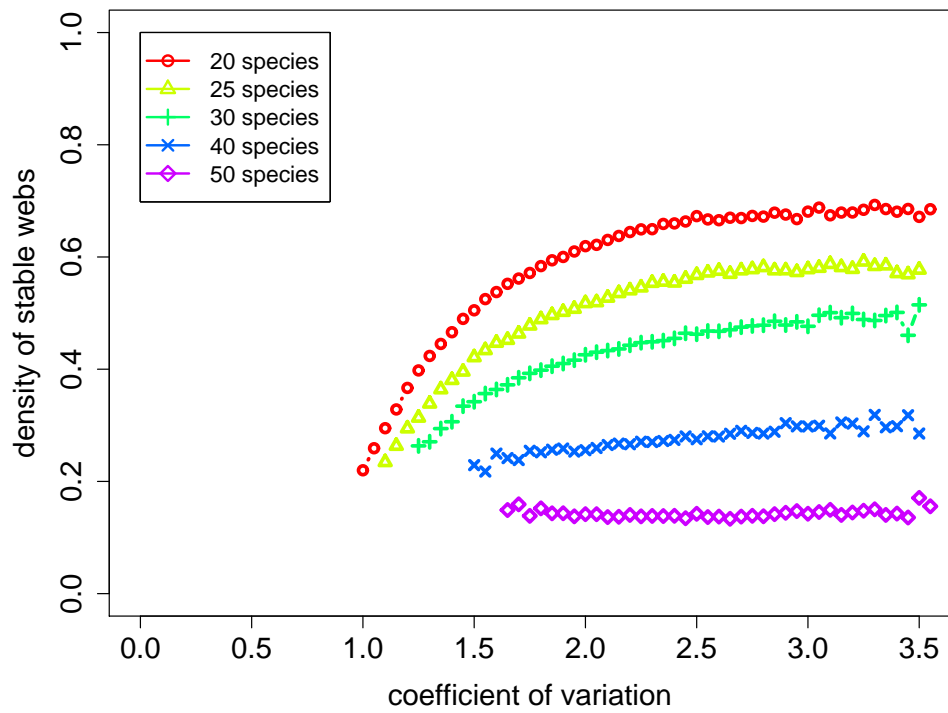

Supplementary Figure 1: Dependence of stability on the weak links. The density of weak links is measured in terms of the coefficient of variation normalized to total gain of the respective prey species. In large webs, an increase in link variability always corresponds to an decrease in stability, whereas in smaller webs one find a stability maximum at intermediate coefficients.
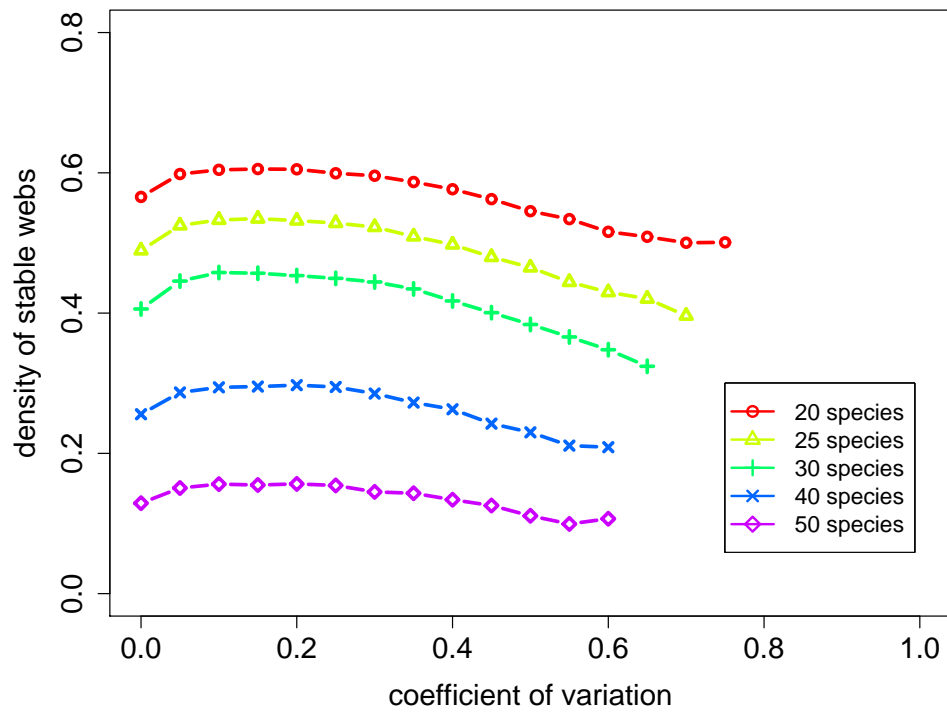
Supplementary Figure 2: Dependence of stability on the weak links. Here density of weak links is measured in terms of energy flow between the species. This measure gives a stability maximum for intermediate coefficients, in all observed web sizes.
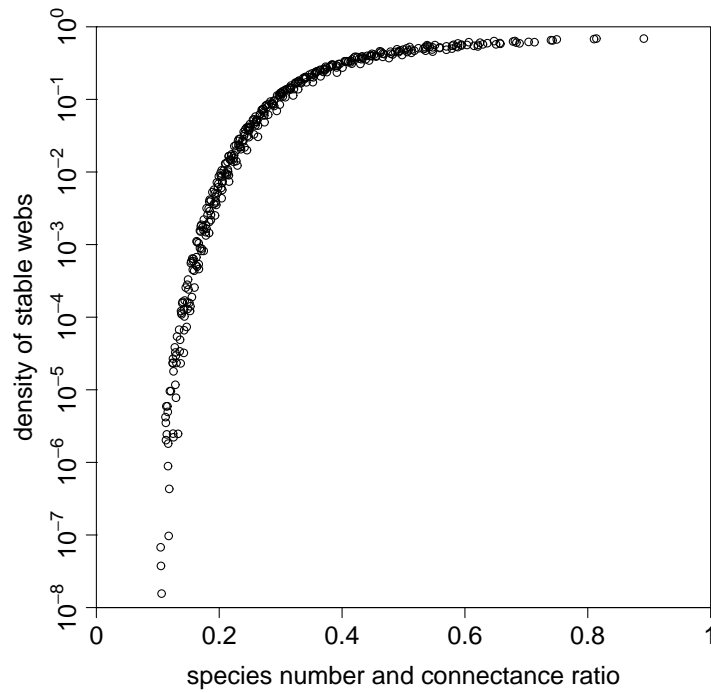
Supplementary Figure 3: Dependence of stability on the weak links. Here density of weak links is measured in terms of entries in the Jacobian matrix. For this measure we find in according to common knowledge a stabilizing effect of weak links.

Supplementary Figure 4: Dependence of density of stable webs on the ratio of species number and connectance r_{CN}:

$$r_{CN} = \frac{1}{C^s \cdot N} \tag{1}$$

where s is the slope of the stability isoclines (see Fig. 2 in the main part). We find an asymptotic decline of stability in the low stability range, whereas the ratio of stable webs becomes one for $r_{CN} = 1$, which corresponds to two species predator prey food web.

Chapter 3

General discussion

The results provided in this thesis contribute to the understanding of population dynamics and the underlying mechanisms. In particular species interaction by predation and competition on different levels of abstraction are studied. First, both types of interaction are investigated separately in basic systems, consisting of few species. Using such elementary systems we are able to study non-stationary dynamics and provide an detailed insight into the underlying mechanisms. Finally, we proceed to complex food webs, consisting of up to 50 different species, linked by an multitude of species interactions. To study a large ensemble of different food webs, on that level of complexity, we focus on the study of fix points. As a result, we present several different food web properties with a significant impact on stability.

Predator-prey cycles in experiment

In a first step, to close the gap between theory and field observations, we have presented exceptionally long predator-prey oscillation in an experimental chemostat system (Chapter I). We show, in opposite to recent experiments or field studies, that these predator-prey cycles can be maintained for more than 50 cycles without spatial structure, immigration or external force. Thereby, we confirm theoretical findings, which predict persistent cycles. However, in contrast to theoretical predictions, we note a strong variability in the observed dynamics and shifting cyclic regimes on short time scales. The system undergoes sudden changes between periods where pronounced oscillations of predator and prey are strongly phase locked and periods where this locking seems to be lost. The transition between these regimes arises spontaneous and without external influence. The reasons for these sudden regime shifts remain unlcear. As the experimental conditions were kept homogeneous, we assume that the observed variabilities in the dynamics are

at least to some extend system inherent and therefore might be inherent in other biological system, too. On that account, short time observations may lead to wrong assumptions and we suggest that for any interpretation of observational results the length of the observation period needs to be taken in account. In conclusion, we find for the measured time series, that the predicted population dynamics from theory are barely applicable for exact predictions, but describe average dynamics over a long period of time.

Analysis of ecological signals with common wavelet methods

For an detailed evaluation of recorded time series and to overcome the problems of background noise and system inherent variabilities in the dynamics, we propose the application of wavelet methods for a data analysis (Chapter I). We confirm, that these methods are a convenient approach to identify non-stationary population dynamics in ecological time series as they approach provide a time and frequency resolved measure of power and phase of population cycles. Furthermore, interactions between different signals are revealed. Most notably, a time resolved measure of the correlation between two non-stationary signals allows to distinguish between time intervals of phase-locked and non-phase-locked dynamics. For a clear classification of the species interaction we have applied a correlation threshold which distinguishes regular oscillations from irregular random patterns. We assume, that this correlation coefficient could be used to detect a relation between two populations in more complex systems. However this measure gives no information about the type of interaction and to overcome that problem, we developed a method which uses the phase information, provided by the wavelet method, to determine species interactions by a phase difference signature.

Evaluation of species interaction by the phase difference signature

Specific species interactions commonly lead to a specific phase difference between the interacting populations, and therefore, the phase difference signal in turn contain information about the type of interaction. Here we use wavelet methods to extract such a phase difference signal and its distribution from two non-stationary time series (Chapter I). For the experimental predator-prey time series we find a phase difference locked to a value around 0.5π. Repeating the analysis for a time series of egg-bearing predators and predator egg-ratio, we find again cyclic dynamics which are correlated to the prey availability. The abundance of egg-bearing predators follow the prey cycles with a phase difference of 0.17π, whereas the egg ratio precedes the prey signal, resulting in a negative phase difference of about -0.14π. For

a classification of the experimental system we compare this phase difference signature with results from different predator prey models. Thereby, we find a typical phase difference signature for predator-prey cycles which varies only marginally within the used systems and furthermore follows intuitive expectations (Chapter I). Nevertheless, subtle differences in the signature allow an estimation of the predator age structure. We find that the phase signature of the experimental time series correspond to a signature of a predator-prey system with a stage structured predator. As the phase signature is extremely robust, this method also could give insight into larger systems, consisting of more species. Furthermore, we assume that it could be able to detect other types of species interactions. Here, a systematic evaluation of the method with different model systems would be necessary.

Phytoplankton dynamics in an one-dimensional water column

For the study of interspecies competition we focus on the population dynamics in phytoplankton communities (Chapter II). We used a mathematical model to simulate nutrient and light limited phytoplankton growth over a one-dimensional vertical water column. To understand the background mechanisms and dynamics in such a system, independent of competitive effects, we performed a comprehensive research of a one species system. Recent theoretical investigations found in such systems two possible globally attracting fixed points, depending on system parameters. First, if a strong limitation by light keeps the phytoplankton biomass near the surface, one find a stable phytoplankton maximum in the upper layers. Second, a shortage in nutrient can lead to a deep phytoplankton maximum. However, in recent field observations (Venrick , 1993; Holm-Hansen & Hewes , 2004), deep or upper phytoplankton maxima were observed under similar environmental conditions. We assume, that this contradiction between theory and observation, could be caused by mechanisms in real ecosystems, which were not reflected in the theory. In particular an upper mixed layer could be such a mechanism (Chapter II). To mimic a realistic aquatic environment, we included a strong mixing in the upper and weak mixing in the deep layers of the water body. This one-dimensional inhomogeneous mixed system give rise to complex, non-trivial dynamics. We find, that the turbulent mixing in the upper layer can stabilise an initial upper phytoplankton maximum, even if the environmental conditions would favour a phytoplankton maximum in the depth, which gives rise to bistability between a deep and a upper phytoplankton maximum, in a certain range of parameters. In summary the minor extension of the model significantly changed the phytoplankton dynamics, and therefore may also influence phytoplankton competition significantly.

Competition in a phytoplankton community

In order to investigate the phytoplankton competition under the influence of
an upper mixed layer we extend the model system (see above) by a second
phytoplankton species, differently adapted to light and nutrient availability.
We find that with the increased number of phytoplankton species the range of
bistability between deep and upper chlorophyll maxima becomes considerably
larger, as differently adapted species can keep a stable maximum in different
parameter ranges (Chapter II). We show that the presence of different mix-
ing regimes and the inhomogeneous resource distribution over depth lead to
new phenomena in the competition of phytoplankton species, as the species
composition strongly correlates with the spatial patterning. The bistability
distributions over depth, generated by the upper mixed layer, is now also a
bistibility between different phytoplankton compositions. Therefore, the phy-
toplankton competition outcome becomes depend on initial conditions and
external disturbances, which may initiate a shift between the opposite stable
states. Moreover, we show that the presence of an upper mixed layer alter
the phytoplankton dynamics and strongly influence the interspecies compe-
tition in transient states. Finally, the upper mixed layer strongly increase
the range of species coexistence and therefore could be a mechanism which
give rise to additional niches in aquatic ecosystems. To obtain an insight into
the complex mechanisms of competition in such an environment, we present
a graphical approach, which can be seen as an extension of the graphical
method developed by Tilman (1980, 1982). Thereby, one can predict the
outcome of species competition depending on the import of resources into
the system, the nutrient uptake rates and growth kinetics of the involved
species (Chapter II). Using this approach, we show that, even in the two
species case, the competition outcome in the modelled system is non-trivial
and depends on a multitude of different factors.

Species in complex food webs

Although the investigation of species interactions in basic systems provides
insights into important mechanisms, the dynamics in large, complex systems
can be differ from these findings. Therefore, to understand the dynamics in
real ecosystems it is necessary to study systems with an equal level of com-
plexity. However, high complexity usually impedes a comprehensive study
and understanding of the systems functioning. Numerical constraints limit
simulative studies in the number of realised instances and the size of the web
under consideration. Furthermore, the relation between underlying mecha-

nisms and observed dynamics may be hidden by the complexity of the system. Therefore, we restrict our research of large food webs to the analysis of local stability. Thereby, we are able to utilize generalized modelling, a novel numerical approach for the analysis of stability in families of nonlinear rate equations (Gross & Feudel , 2006), to study several billion instances of food webs of up to 50 species with nonlinear interactions (Chapter III).

In agreement with preceding research (May , 1971, 1972), we find a low density of stable webs in complex systems, consisting of many species and species interactions, while smaller food webs are likely to be stable. To assess the dependence of stability on the model parameters we applied a sensitivity analysis and computed the correlation between parameter values and food web stability. We find a high correlation of the exponent of closure, and the prey-dependence of the predation, with stability, which corresponds to the known fact, that low saturation of predators and nonlinear mortality of the top-predators promote stability. By contrast, the sensitivity of primary production on the number of primary producers, and the sensitivity of predation on the density of predators, are negatively correlated with stability. These findings confirm that stability is increased if primary production is strongly limited by external factors such as nutrient availability, and if the predator-dependence of predation is reduced, for instance in a ratio-dependent predation. Furthermore, we show that a high scale-separation between predator and prey promotes stability. In summary, the sensitivity analysis reveals that food web stability strongly depend on certain physiological parameters, and thus strongly depend on the present species and species properties.

The findings of the sensitivity analysis are in agreement with common knowledge or follow intuitive explanations and therefore reconfirm the efficiency of the generalised modelling approach. In a second step, we used this method to scrutinise the effect of weak species interactions which is commonly assumed to be a stabilising. Here we used a normalised measure of the variation of interspecies biomass fluxes (Chapter III) to analyse the correlation of weak links with stability in a large ensemble of food webs with randomly distributed link strength. Thereby we confirmed a stabilising effect of weak links for small webs with less than 25 species. However, we find a contrary effect for large food webs consisting of more than 30 species. We show, despite the stabilising effect of weak links for small food webs, that weak links destabilise food webs, which are of a size, comparable to typical food webs found in nature. Thereby, we show, that results given by the analysis of small systems are not necessarily valid in larger systems.

By a comprehensive study of topological properties and their correlation to food web stability we revealed that the effect of certain species interactions can depend on the trophic position where it take place (Chapter III). We

show that the number of consumed prey species is positively correlated with stability for species in a high trophic position, but negatively correlated for species in a low or intermediate trophic position. Furthermore, also the numbers of predators, preying on a species, is differently correlated with stability in different trophic positions. We find for prey species in low as well as in high trophic positions, that the number of different predators is negatively correlated with stability, but by contrast, there is a stabilising effect if a high number of predator species prey on intermediate prey species. These findings indicate, that generalists at the top and specialists at the bottom of the food web should favour food web stability, a pattern which in fact can be found in empirical data (Neutel et al. , 2002, 2007).

In this thesis different approaches to study population dynamics were applied. First, predation was studied in an experimental system (Chapter I). Here, one is able to observe real species interactions, but is restricted in the number of realised instances and in the choice of the system. It was shown, that, even in basic systems, the measured times series can differ from theoretical predictions. Therefore, experiments or field observations are essential to prove hypotheses from theory. In the second part of this work, interspecies competition was studied in a model system (Chapter II). Modelling allows to compare different adjustable scenarios and to reveal underlying mechanisms. However, numerical constraints limit the size and the complexity of the investigated systems. For an analysis of larger systems, the generalised modelling approach was applied (Chapter III). Here, the investigation is restricted to the analysis of local stability. It was shown, that findings can depend on the size of the systems. Therefore, the study of large systems in theory is an essential tool do understand large system in nature. In summary, each the applied approaches provide an insight into population dynamics on a certain scale of abstraction and complexity. For a comprehensive understanding of the population dynamics in real ecosystems, it is necessary to study systems on all this different scales of abstraction and finally, to bring these findings into one comprehensive context.

Scientific summary

The subject of this thesis is the investigation of ecological systems and in particular population dynamics and species interaction. It is structured in three chapters. In the first two chapters, the two most important types of species interaction, predation and competition, are studied separately. Finally, in chapter three we study species interactions in complex food webs.

First, the dynamics of two interacting predator and prey species are studied in an experimental chemostat system. We provide a long-time measurement of 50 persistent predator-prey cycles, which is a five-fold increase over the previously known maximum number of oscillations. However, even though the experiment was not perturbed by external influences the observed signals undergo marked transitions in character. To reveal the underlying dynamics we performed a comprehensive time series analysis on the basis of established wavelet methods. We provide time resolved information on the frequency and the amplitude of the cycles and the correlation between the signals. Furthermore, the phase differences between all measured time series are compactly encoded in a single polar phase histogram, providing a fingerprint for the temporal succession of the community. These results, which are supported by numerical simulations, establish the phase signature as a robust measure for the identification of species interactions in dynamical systems and demonstrate the potential for perpetual coexistence of predator and prey populations in a cyclic dynamic regime.

Second, interspecies competition is studied by means of an advection-reaction-diffusion model of a phytoplankton community in a vertical water column. In extension to recent work, the model includes an upper mixed layer, a common phenomenon in aquatic systems. We show that the presence of an upper mixed layer can lead to bistability. Furthermore we show that that mixed layer generally promotes phytoplankton coexistence, but can, in the oscillatory regime, also lead to a subtle competitive exclusion phenomenon. Finally, we present a novel graphical approach for deducing the competition outcome in such a system.

In the third part of this thesis we use generalised modelling, a novel numer-

ical approach for the analysis of the stability in families of nonlinear rate equations, to study the stability of complex food webs. We generated realistic food web topologies by means of the niche model, which is based on ecological reasoning regarding the prey that can possibly be devoured by a given species of predators. Thereby, we were able to study several billion instances of food webs of up to 50 species with nonlinear interactions. The results confirm a negative correlation of food web complexity with stability. Furthermore, we analyse the influence of topological properties and model parameters on food web stability. Finally, we show that weak species interactions have a destabilising effect on large food webs.

In summary this thesis studies population dynamics on different scales of abstraction. It shows, advantages and problems of the applied approaches and points to the necessity to combine these findings for an understanding of real ecosystems.

Bibliography

Abbott M.R., K.L. Denman T.M. Powell P.J. Richerson, R.C. Richards and C.R. Goldman. (1984) Mixing and the Dynamics of the Deep Chlorophyll Maximum in Lake Tahoe. *Limnology and Oceanography* **29**, 862-878.

Abrams P.A. and Roth J. (1994) The responses of unstable food chains to enrichment. *Ecology* **75**, 1118-1130.

Anderson G.C. (1969) Subsurface chlorophyll maximum in the northeast Pacific Ocean. *Limnology and Oceanography* **14**, 386-391.

Aristegui J., Barton E.D., Montero M.F., Garcia-Munoz M. and J. Escanez. (2003) Organic carbon distribution and water column respiration in the NW Africa-Canaries Coastal Transition Zone. *Aquatic Microbial Ecology* **33**, 289-301.

Armstrong R.A. and McGehee (1980) Competitive Exclusion *The American Naturalist* **115**, 151-170.

Bandrivskyy A., Bernjak A., McClintock P. and Stefanovska A. (2003) Wavelet phase coherence analysis: Application to skin temperature and blood flow. *Cardiovascular Engeneering* **4**, 89-9.

Beckmann A. and Hense I. (2007) Beneath the surface: Characteristics of oceanic ecosystems under weak mixing conditions - A theoretical investigation. *Progress In Oceanography* **75**, 771-796.

L. Becks, F. M. Hilker, H. Malchow, K. Jürgens and H. Arndt (2005) Experimental demonstration of chaos in a microbial food web. *Nature* **435**, 1226-1229.

E. Beninca, J. Huisman, R. Heerkloss, K. D. J"ohnk, P. Branco1, E. H. Van Nes, M. Scheffer and S. P. Ellner (2008) Chaos in a long-term experiment with a plankton community. *Nature* **451**, 822-825.

Berlow E.L., Neutel A.M., Cohen J.E., de Ruiter P.C., Ebenman B., Emmerson M., Fox J.W., Jansen V.A.A, Jones J.I., Kokkoris G.D., Logofet D.O., McKane A.J., Montoya J.M. and Petchey O. (2004) *Journal of Animal Ecology* **73**, 585-598.

A.A. Berryman (2002) Population cycles (Oxford University Press, New York, 2002). book

Birch D.A., Tsang Y.K. and Young W.R. (2007) Bounding biomass in the Fisher equation. *Physical Review E* **75**, 066304-14.

Blasius B., Huppert A. and Stone L. (1999) Complex dynamics and phase synchronization in spatially extended ecological systems *Nature* **399**, 354-359.

Huppert A., Blasius B. and Stone L. (2002) A model of phytoplankton blooms. *The American Naturalist* **159**, 156-171.

Huppert A., Blasius B., Olinkya R. and Stone L. (2005) A model for seasonal phytoplankton blooms. *Journal of Theoretical Biology* **236**, 276-290.

Bopp L., Monfray P., Aumont O., Dufresne J.L., Le Treut H., Madec G., Terray L. and Orr J.C. (2001) Potential impact of climate change on marine export production. *Global Biogeochemical Cycles* **15**, 81-100.

Law C.S., Boyd W.P., Watson A.J., Gall M., Downing K., Frew R., Rintoul S., Pickmere S. and Pridmore R. (2000) A mesoscale phytoplankton bloom in the polar Southern Ocean stimulated by iron fertilization. *Nature* **407**, 695-701.

Britton N. F. and Timm U. (1993) Effects of competition and shading in planktonic communities. *Journal of Mathematical Biology* **31**, 655-673.

Brose U., Williams R.J. and Martinez N.D. (2006) Allometric scaling enhances stability in complex food webs *Ecology Letters,* **9**, 1228-1236.

Cantrell R.S. and Cosner C. (2001) Spatial Heterogeneity and Critical Patch Size: Area Effects via Diffusion in Closed Environments. *Journal of theoretical Biology* **209**, 161-171.

Cazelles, B. and Stone, L. (2003) Detection of imperfect population synchrony in a uncertain world. *Journal of Animal Ecology* **72**, 953-968.

Cazelles, B., Chavezs, M., Berteaux, D., Menard, F., Vik, J.O., Jenouvrier, S. and Stenseth, N.C. (2008) Wavelet analyses of ecological time series. *Oecologia* **156**, 287-304.

Cohen J.E. and Newman C.M. (1985) When will a large complex system be stable? *Journal of theoretical Biology* **113**, 153-156.

Cullen J.J. (1982) The deep chlorophyll maximum: comparing vertical profiles of chlorophyll a. *Canadian Journal of Fisheries and Aquatic Sciences* **39**, 791-803.

Transient and oscillations in continuous culture. (1983) In M. Bazin *Mathematics in Microbiology* Academic press, 1983.

Daubechies, I. (1992) Ten Lectures on Wavelets, Society for Industrial and Applied Mathematics, 1992. book

Deuser W.G. (1987) Variability of hydrography and particle flux: Transient and long-term relationships. *Mitteilungen aus dem Geologischen-Palaeontologischen Institut der Universitt Hamburg* **62**, 179-193.

Diehl S. (2002) Phytoplankton, light, and nutrients in a gradient of mixing depth: theory *Ecology* **83**, 386-98.

Ellner S.P., McCauley E., Kendall B.E., Briggs C.J., Hosseini P.R., Wood S.N., Janssen A., Sabelis M.W., Turchin P., Nisbet R.M. and Murdoch W.W. (2001) Habitat structure and population persistence in an experimental community. *Nature* **412**, 538-543

Elton C. and Nicholson M. (1942) The Ten-Year Cycle in Numbers of the Lynx in Canada *The Journal of Animal Ecology* **11**, 215-244.

Elton C.S. *The ecology of invasions by animals and plants* John Wiley and Sons Inc., New York 1958

Emmerson M.C. and Raffaelli D. (2004) Predatorprey body size, interaction strength and the stability of a real food web *Journal of Animal Ecology* **73**, 399-409.

Falkowski P., Scholes R.J., Boyle E., Canadell J., Canfield D., Elser J., Gruber N., Hibbard K., Hogberg P., Linder S., Mackenzie F.T., Moore B., Pedersen T., Rosenthal Y., Seitzinger S., Smetacek V. and Steffen W. (2000) The Global Carbon Cycle: A Test of Our Knowledge of Earth as a System. *Science* **290**, 291-296.

Fennel K. and Boss E. (2003) Subsurface maxima of phytoplankton and chlorophyll: Steady-state solutions from a simple model *Limnology and Oceanography* **48**, 1521-1534.

Fibonacci (1202) *Liber Abaci*

Finnigan T.D., Luther D.S. and Lukas R. (2002) Observations of enhanced diapycnal mixing near the Hawaiian ridge. *Journal of Physical Oceanography* bf 32, 2988-3002.

Fussmann, G.F., S.P. Ellner, K.W. Shertzer, N.G. Hairston Jr. (2000) Crossing the Hopf bifurcation in a live predator-prey system. *Science* **290**, 1358-1360.

Garcia-Domingo J.L. and Saldaña J. (2008) Effects of heterogeneous interaction strengths on food web complexity *Oikos* **117**, 336-343.

Gause G.F. (1934) *The struggle for existence.* Williams and Wilkens, Baltimore, 1934 book

Gilpin M.E. (1972) Enriched predator-prey systems: theoretical stability. *Science* **177**, 902-904

Grenfell, B.T., Bjornstad, O.N. and Kappey, J. (2001) Travelling waves and spatial hierarchies in measles epidemics. *Nature* **414**, 716-723.

Grinnel J. (1904) The origin and the distribution of the chestnut-backed chickadee. *Auk* **21**, 364-383.

Grinnel J. (1917) The niche-relationship of the california thrasher *Auk* **34**, 427-434.

Gross T. and Feudel U. (2006) Generalized models as a universal approach to the analysis of nonlinear dynamical systems *Physical Review E* **73**, 016205-1-14.

Guillard R.R.L., Lorenzen C.J. (1972) Yellow-green algae with chlorophyllide c. *J Phycol* **8**, 15-24.

Hanna R. Onzo A. Lingeman R. Yaninek J.S. and Sabelis M.W. (2005) Seasonal cycles and persistence in an acarine predator-prey system on cassava in Africa *Popul Ecol* **47**, 107117.

Hardin G. (1960) The competitive exclusion principle *Science* **131**, 1292-1298.

Haydon D. (1994) Pivotal assumptions determining the relationship between stability and complexity: an analytical synthesis of the stability-complexity debate. *The American naturalist* **144**, 14-29.

Haydon D. (2000) Maximally Stable Model Ecosystems Can Be Highly Connected (2000) *Ecology* **81**, 2631-2636.

Hodges B.A. and Rudnick D.L. (2004) Simple models of steady deep maxima in chlorophyll and biomass *Deep sea research* **51**, 599-1015.

Holm-Hansen O. and Hewes C.D. (2004) Deepchlorophyll-a maxima (DCMs) in Antarctic waters I. Relationships between DCMs and the physical, chemical, and optical conditions in the upper water column. *Polar Biology* **27**, 699-710.

M. Holoyak and S.P. Lawler. (1996) Persistence of an extinction-prone predator-prey interaction through metapopulation dynamics. Ecology 77: 1867-1879.

Hodges B.A. and Rudnick D.L. (2004) Simple models of steady deep maxima in chlorophyll and biomass. *Deep Sea Research I* **51**, 999-1015.

Huffaker C.B., Shea K.P. and Herman S.G. (1963) Experimental studies on predation III: Complex dispersion and levels of food in acarine predator-prey interaction. *Hilgardia* **34**, 305-330.

Huisman J. and Weissing F.J. (1995) Competition for nutrients and light in a mixed water column: a theoretical analysis *The American Naturalist* **146**, 536-564.

Huisman J. and Weissing F.J. (1999) Biodiversity of plankton by species oscillation and chaos *Nature* **402**, 407-410.

Huisman J., van Oostveen P. and Weissing F.J. (1999b) Critical depth and critical turbulence: two different mechanisms for development of phytoplankton blooms. *Limnology and Oceanography* **44**, 1781-1787.

Huisman J., van Oostveen P. and Weissing F.J. (1999) Species dynamics in phytoplankton blooms: incomplete mixing and competition for light. *The American Naturalist* **154**, 46-48.

Huisman J., Arrays E., U. and Sommeijer B. (2002) How do sinking Phytoplankton species manage to persist? *The American Naturalist* **2002**, 245-254.

Huisman J., Arrayas M., Ebert U. and Sommeijer B. (2002) Changes in Turbulent mixing shift competition for light between phytoplankton species. *The American Naturalist* **159**, 245-254.

Huisman J., Thi N.N.P., Karl D.M. and Sommeijer B. (2006) Reduced mixing generates oscillations and chaos in the oceanic deep chlorophyll maximum *Science* **439**, 322-325.

Hutchinson G.E. (1961) The paradox of the plankton *American Naturalist* **95**, 137-145.

Jansen V.A.A. and Kokkoris G.D. (D) Complexity and stability revisited *Ecology Letters* **6**, 408-502.

Jamart B.M., Winter D.F., Banse K., Anderson G.C. and Lam R.K. (1977) A theoretical study of phytoplankton growth and nutrient distribution in the Pacific Ocean off the northwestern U.S. coast. *Deep Sea Research* **24**, 753-773.

Jonsson T., Karlsson P. and Jonsson A. (2006) Food web structure affects the extinction risk of species in ecological communities *Ecological Modelling* **199**, 93-106.

Kaiser, G.: A friendly guide to wavelets, Birkhuser 1994

B. E. Kendall, J. Predergast, O.N. Bjornstad. (1998) The macroecology of population dynamics: Taxonomic and biogeographic patterns in population cycles. Ecology Letters 1: 160-164.

Kendall B.E., Briggs C.J., Murdoch W.W., Turchin P., Ellner S.P., McCauley E., Nisbet R.H. and Wood S.N. (1999) *Ecology* **80**, 1789-1805.

Keitt T.H. (2008) Coherent ecological dynamics induced by large-scale disturbance. *Nature* **454**, 331-334.

Kierstead H. and Slobodkin L. B. (1953) The size of water masses containing plankton bloom. *Journal of Marine Research* **12**, 141147.

Kirk J.T.O. (1994) *Light and Photosynthesis in Aquatic Ecosystems.* Cambridge University Press.

King A.W. and Pimm S.L. (1983) Complexity, diversity, and stability: a reconciliation of theoretical and empirical results *The American Naturalist* **122**, 229-239.

Kirk K.L. (1998) Enrichment can stabilize population dynamics: Autotoxins and density dependence. *Ecology* **79**, 2456-2462.

Klausmeier C.A. and Litchman E. (2001) Algal games: The vertical distribution of phytoplankton in poorly mixed water columns *Limnology and Oceanography* **2001**, 1998-2007.

Kondo M. (2003) Foraging adaptation and the relationship between food-web complexity and stability *Science* **299**, 1388-1391.

Lau, K.M. and Wen, H. (1995) Climatic signal detecting using wavelet transform: how to make a time series sing. *Bull Am Meteorol Soc* **76**, 2391-2402.

Levin S.A. (1970) Community equilibria and stability, and an Extension of the Competitive Exclusion Principle. *The American Naturalist* **104**, 413-423.

Levin S.A. *Fragile dominion* Perseus Books, Reading, Massachusetts, 1999

Levins R. (1979) Coexistence in a variable environment. *Am. Nat.* **114**, 765-783.

Lewis M.R., Harrison W.G., Oakey N.S., Hebert D. and Platt T. (1986) Vertical nitrate fluxes in the oligotrophic ocean. *Science* **234**, 870-873.

Lodtka A.J. *Elements of physical biology* Williams and Wilkins, Baltimore, 1925

Luckinbill L.S. (1974) The effect of space and enrichment on a predator-prey system. *Ecology* **55**, 1142-1147.

Matondkar P.S.G., Nair K.K.C. and Ansari Z.A. (2005) Biological Characteristics of Central Indian Basin Waters During the Southern Summer. *Marine Georesources and Geotechnology* **23**, 299-314.

May R.M. (1971) Stability in multispecies community models *Mathematical biosciences* **12**, 59-79.

May R.M. (1972) Will a large complex system be stable? *Nature* **238**, 413-414.

May R.M. (1987) Chaos and the dynamics of biological populations. *Proceedings of the Royal Society of London* **413**, 27-44.

May R.M., Levin S.A. and Sugihara G. (2008) Ecology for bankers *Nature* **451**, 893895.

Malthus T.R. (1826) *An Essay on the Principle of Population*, Roworth, London

McAllister C.D., LeBrasseur R.J. and Parson T.R. (1972) Stability of enriched aquatic ecosystems *Science* **175**, 562-564.

McArthur R. (1955) Fluctuations of animal populations and a measure of community stability *Ecology* **36**, 533-536.

McCann K.S., Hastings A. and Huxel G.R. (1998) Weak trophic interactions and the balance of nature *Nature* **395**, 794-798.

McCann K.S. (2000) The diversitystability debate *Nature* **405**, 228-233.

McCauley E. and Murdoch W.W. (1990) Predator-prey dynamics in environments rich and poor in nutrients *Nature* **343**, 455-461.

McCauley E., Nisbet R.M., Murdoch W.W., de Roos A.M. and Gurneyk W.S.C. Large-amplitude cycles of *Daphnia* and its algal prey in enriched environments *Nature* **402**, 653-656.

A.J. McKane and T.J. Newman. (2005) Predator-prey cycles from resonant amplification of demographic stochasticity *Physical Review Letters* **94** 218102.

Maraun, D. and Kurths, J. (2004) Cross wavelet analysis: significance testing and pitfalls *Nonlinear Processes in Geophysics* **11**, 505-514.

Montoya J.M., Pimm S.L. and Sol R.V. (2002) Ecological networks and their fragility *Nature* **442**, 259-264.

Naegli C. (1874) - cited in Harper, J.L. (1974) A centenary in population biology, *Nature* **252**, 526-527.

Navarrete S.A. and Berlow E.L. (2006) Variable interaction strengths stabilize marine community pattern *Ecology Letters* **9**, 526-536.

Neuhauser C. (2001) Mathematical challenges in spatial ecology. *Notices of the American Mathematical Society* **48**, 1304-1314.

Neutel A., Heesterbeek J. A. P. and de Ruiter P. C. (2002) Stability in Real Food Webs: Weak Links in Long Loops *Science* **296**, 11201123 (2002).

Neutel A.M., Heesterbeek J.A.P., van de Koppel J., Hoenderboom G., Vos A., Kaldeway C., Berendse F. and de Ruiter F. (2007) Reconciling complexity with stability in naturally assembling food webs *Nature* **449**, 599602 .

Nicholson A.J. (1957) The self-adjustment of populations to change. *Cold Spring Harbor Symposium on Quantitative Biology* **22**, 153-173.

Okubo, A. and Levin S.A. (2001) *Diffusion and Ecological Problems.* Springer. book

Padisk J., Reynolds C.S. and Sommer U. (1993) The intermediate disturbance hypothesis in phytoplankton ecology. *Hydrobiologia* **249**, 1-199.

Pascual M. and Caswell H. (1997) From the cell cycles to population cycles in phytoplankton nutrient interactions. *Ecology* **78**, 897-912.

Radach G., and Maier-Reimer E. (1975) The vertical structure of phytoplankton growth dynamics; a mathematical model. *Memoires Societe Royale des Sciences de Liege* **7(6)**, 113-146.

Raven J. A. and Falkowski P. G. (1999) Oceanic sinks for atmospheric CO2. *Plant, Cell and Environment* **22**, 741-755.

Richardson P.J., Armstrong R., Goldman C.R. (1970) Contemporaneous disequilibrium: a new hypothesis to explain the paradox of the plankton. *Proceedings of the National Academy of Sciences of the United States of America* **67**, 1710-1714.

Riley G. A., Stommel H. and Bumpus D. F. (1949) Quantitative ecology of the plankton of the Western North Atlantic. *Bulletin of the Bingham Oceanographic Collection* **12**, 1-169.

Rooney N., McCann K. S., Gellner G. and Moore J. C. (2006) *Nature* **442**, 265269.

Rosenzeig M.L. (1971) Paradox of enrichment: Destabilization of exploitation ecosystems in ecological time. *Science* **171**, 385-387.

Rosenzweig M.L. (1977) Aspects of biological exploitation. *Quarterly review of biologys* **52**, 371-380

Rosenzweig M.L. (1995) *Species diversity in space and time* Cambridge University Press, Cambridge 1995.

J. L. Sarmiento, Slater R., Barber R., Bopp L., Doney S.C., Hirst A.C., Kleypas J., Matear R., Mikolajewicz U. and Monfray P. (2004) Response of ocean ecosystems to climate warming. *Global Biogeochemical Cycles* **18**:GB3003, doi:10.1029/2003GB002134.

Shertzer K.W., Ellner S.P., Fussman G.F. and Hairston N.G. (2002) Predator-Prey Cycles in an Aquatic Microcosm: Testing Hypotheses of Mechanism *Journal of Animal Ecology* **71**, 802-815.

Shigesada, N., and A. Okubo. (1981) Effects of competition and shading in planktonic communities. *Journal of Mathematical Biology* **12**, 311-326.

Sinha S. and Sinha S. (2005) Evidence of universality for the May-Wigner stability theorem for random networks with local dynamics *Physical Review E* **71**, 0209024.

Skellam J.G. (1951) Random Dispersal in Theoretical Populations. *Biometrika* **38**, 196-218.

Smyth W.D., Moum J.N. and Caldwell D.R. (2001) The efficiency of mixing in turbulent patches: inferences from direct simulations and microstructure observations. *Journal of Physical Oceanography* **31**, 1969-1992.

Sommer U. (1985) Comparison between steady state and non-steady state competition: experiments with natural phytoplankton. *Limnology and Oceanography* **V**, p1-pN.

Speirs D.C. and Gurney W.S.C. (2001) Population persistence. in rivers and estuaries. *Ecology* **82**, 1219-1237.

Steele, J.H. and C.S. Yentsch (1960) The vertical distribution of chlorophyll. *Journal of the Marine Biological Association of the United Kingdom* **39**, 217-226.

Steele J.H. and Henderson E.W. (1981) A simple plankton model *The American Naturalist* **117**, 676-691.

Steele H.J. and Henderson E.W. (1992) The role of predation in plankton models. *Journal of Plankton Research* **14**, 157-172.

Steuer R., Gross T., Selbig R. and Blasius B. (2006) Journal of the Marine Biological Association of the United Kingdom. *Proceedings of the National Academy of Science of the United States* **103**, 1186811873.

Straube, A.V. and Pikovsky A. (2007) Mixing-induced global modes in open active flow. *Physical Review Letters DOI*, 10.1103/PhysRevLett.99.184503

Sverdrup H. U. (1953) On conditions for the vernal blooming of phytoplankton. *Journal du Conseil* **18**, 287-295.

Pham Thi N.N., Huisman J. and Sommeijer B.P. (2005) Simulation of three-dimensional phytoplankton dynamics: competition in light-limited environments. *Journal of Computational and Applied Mathematics* **174**, 83-96.

Tilman, D. (1980) Resources: a graphical-mechanistic approach to competition and predation. *The American Naturalist* **116**, 362-93.

Tilman D. (1982) Resource competition and community structure. New York: Princeton Univ. Press. book

Tilman D. and Wedin D. (1991) Oscillations and chaos in the dynamics of perennial grasses. *Nature* **353**, 653-655.

Tilman D. and Kareiva P. M. (1997) Spatial Ecology: The Role of Space in Population Dynamics and Interspecific Interactions. New York: Princeton Univ. Press. book

Tittel J., Bissinger V., Zippel B., Gaedke U., Bell E., Lorke A. and N. Kamjunke. (2003) Mixotrophs combine resource use to outcompete specialists: Implications for aquatic food webs *Proceeding of the National Academy of Science of the United States* **100**,12776-12781.

Torrence C. and Compo C. (1998) A Practical Guide to Wavelet Analysis. *Bulletin of the American Meteorological Society* **70**, 61-78.

Turchin P. and Ellner S.P. (2000) Living on the edge of chaos: Population dynamics of fennoscandian voles. *Ecology* **81**, 3099-3166.

Turchin. (2003) Complex Population Dynamics. todo

Turpin D.H. (1988) Physiological mechanisms in phytoplankton resource competition. In: Sandgren, C. D. (ed.) Growth and reproductive strategies of freshwater phytoplankton. Cambridge Univ. Press, Cambridge:316-368. book

Uchida S., Drossle B. and Brose U. (2007) The structure of food webs with adaptive behaviour *Ecological Modelling* **206**, 263-276.

Utida S. (1957) Cyclic fluctuations of population density intrinsic to the host-parasite system. *Ecology*, **38**, 442-449.

Varela R.A., A. Cruzado, J. Tintore and E.G. Ladona. (1992) Modelling the deep-chlorophyll maximum: A coupled physical-biological approach. *Journal of Marine Research* **50**, 441-463.

Venrick E.L. (1993) Phytoplankton seasonatity in the central North Pacific: The endless summer reconsidered. *Limnology and Oceanography.* **38**, 1135-1149.

Verhulst P.F. (1838) Notice sur la loi que la population poursuit dans son accroissement. *Correspondance mathmatique et physique* **10**, 113-121.

Volterra V. (1926) Fluctuations in the Abundhance of a Species considered Mathematically. *Nature* **118**, 558-560.

Volterra V. (1928) Variations and fluctuations of the number of individuals in animal species living together *J. Cons. Cons. Int. Explor. Mer.* **3**, 3-51. todo

Weston K., Fernand L., Mills D.K., Delahunty R. and Brown J. (2005) Primary production in the deep chlorophyll maximum of the central North Sea. *Journal of Plankton Research* **27**, 909-922.

Williams R.J. and Martinez N.D. (2000) Simple rules yield complex food webs *Nature* **404**, 180-183.

T. Yoshida, Jones L.E., Ellner S.P., Fussmann G.F. and N. G. Hairston Jr. (2003) Rapid evolution drives ecological dynamics in a predator prey system. *Nature*, **424**, 303-306.

Yoshida T., Ellner S.P., Jones L.E., Bohannan B.J.M., Lenski R.E. and Hairston N. G. (2007) Cryptic population dynamics: rapid evolution masks trophic interactions. *PLoS Biology* **5**, 1868-1879.

Yoshiyama K., and H. Nakajima. (2002) Catastrophic Transition in Vertical Distributions of Phytoplankton: Alternative Equilibria in a Water Column. *Journal of Theoretical Biology* **216**, 397-408.

Yoshiyama K., and H. Nakajima. (2006) Catastrophic shifts in vertical distributions of phytoplankton. The existence of a bifurcation set. *Journal of Mathematical Biology* **52**, 235-276.

Acknowledgement

I would like to thank my supervisor Prof. Dr. Bernd Blasius for his support and the possibility to work in his group.

Thanks to all members of his Theoretical Ecology and Complex Systems group for all the discussion, the multitude of advises and the nice time in Potsdam. Special thanks to Nina for the provided knowledge about Linux.

Moreover I'd like to thank the members of the nonlinear dynamics group in Postdam for the provided knowledge about time series analysis.

Thanks to the work group Ecology and Ecosystem Modelling in Potsdam, which gave me the possibility to keep in touch with Biology. Special thanks to Thomas and Edith for all the Chemostat things.

Very special thanks to Thilo Gross for all the useful help and support he gave me. I really appreciate the inspiring discussions and his advices.

Also, I would like to thank all members of his Dynamics of Biological Networks group in Dresden. It's nice to work here.

Finally I really would like to thanks my family for all the support and possibilities